THE
PHYSICAL REVIEW
A Journal of Experimental and Theoretical Physics Established by E. L. Nichols in 1893
VOL. 51, NO. 2 JANUARY 15, 1937 SECOND SERIES

Electric and Magnetic Focusing in Mass Spectroscopy

A. J. DEMPSTER
University of Chicago, Chicago, Illinois
(Received October 7, 1936)

The theory of a mass spectrograph is described. The instrument is arranged so that an electric field forms near the entrance to the magnetic field a real image of the entrance slit with rays of one velocity. The velocity dispersion produced by the electric field is counterbalanced by the velocity dispersion in the magnetic field.

IN mass spectrographs of high resolving power, great advantages are obtained by focusing a beam of charged atoms which not only diverges in direction but also contains particles with slightly different velocities. If focusing methods are not used, the selection of a sufficiently narrow bundle and a sufficiently restricted velocity range implies a very great loss of intensity.

In this paper the theory of one type of mass spectrograph is discussed in which an electric field forms a real image of the entrance slit with rays of one velocity near the entrance to a magnetic field, and in which the velocity dispersion produced by the electric field is counterbalanced by the velocity dispersion in the magnetic field.

CHARGED PARTICLES IN A CYLINDRICAL CONDENSER

Let us consider a charged particle passing from the slit S (Fig. 1) into an electric field at a distance l' from S, and at a radial distance y_1 from the circular orbit AB to which SA is tangent at A. If the field is due to a potential V applied to two cylinders of radius r_1 and r_2, its value at any radius r is c/r where $c=\log_e r_2/r_1$. Let v_0 be the velocity required for the circular orbit of radius a ($v_0^2(m/a)=c(e/a)$; $v_0^2=(e/m)c$), and consider a particle with a velocity $v_1=v_0(1+\beta)$, making an angle α with SA and entering the condenser at y_1 ($y_1=\alpha l'$). Here its energy $\frac{1}{2}mv^2$ is less than $\frac{1}{2}mv_1^2$ by the work done in moving the particle through a distance y_1 against the electric force. This potential energy is $y_1e(c/a)$ or $mv_0^2(y_1/a)$ so that $\frac{1}{2}mv^2=\frac{1}{2}mv_0^2(1+2\beta)-mv_0^2(y_1/a)$ or $v=v_0(1+\beta-(y_1/a))$.

The orbit has been calculated by R. Herzog[1] as a special case of a general theory in which electric and magnetic fields both act on the particle. The calculations may be considerably shortened if the equations of motion in polar coordinates $d^2r/dt^2-r(d\phi/dt)^2=-k^2/r$, where $k^2=(m/e)\times c=(m/e)\log_e r_2/r_1$ and $r^2d\phi/dt=A$ where A is a constant for each orbit, are transformed into an equation between $1/r$ and ϕ.[2] Setting $u=1/r$ we have $dr/dt=(-1/u^2)(du/d\phi)(d\phi/dt)=-A(du/d\phi)$ and $(d^2r/dt^2)=-A(d/dt)du/d\phi=-Au^2(d^2u/d\phi^2)$, so that the equation of motion is $(d^2u/d\phi^2)+u=(k^2/A^2)(1/u)$. We are interested in small devia-

[1] R. Herzog, Zeits. f. Physik **89**, 447–473 (1934).
[2] The author is indebted to Professor W. Bartky for pointing out the advantages of this transformation in this problem. The resulting equation was also used by Hughes and Rojansky (reference 3) for different initial conditions.

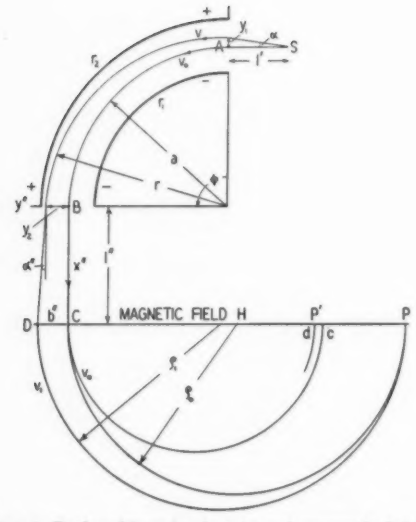

FIG. 1. Paths of ions in electric and magnetic fields.

tions from the circular orbit $u=1/a$ for which $A=ka=av_0$. For the general orbit discussed above $A=(a+y)^2\dot{\phi}=(a+y_1)v=av_0(1+\beta)$.

Setting $u=1/a(1+z)$, where z is small, we have the following equation for z, $d^2z/d\phi^2=-2z-2\beta$, which gives $z=-\beta+P\cos\sqrt{2}\phi+Q\sin\sqrt{2}\phi$. One initial condition $\phi=0$, $u_0=1/a(1-(y_1/a))$ gives $P=-(y_1/a)+\beta$ and the other

$$\left.\frac{du}{d\phi}\right|_0=\frac{-1}{r^2}\frac{dr}{dt}\cdot\frac{dt}{d\phi}\bigg|_0=\frac{-1}{A}\left.\frac{dr}{dt}\right|_0=-\frac{\alpha}{v_0}$$

gives $Q=-(\alpha/\sqrt{2})$, so that to a first approximation, the equation of the orbit in the electric field is $u=1/r=1/a\{1-\beta+(\beta-(y_1/a))\cos\sqrt{2}\phi-(\alpha/\sqrt{2})\sin\sqrt{2}\phi\}$. The special case discussed by Hughes and Rojansky[3] may be deduced by putting $y_1=0$, i.e. $l'=0$; then $r=a$ for $\phi=0$ and $\phi=\pi/\sqrt{2}$ showing that a divergent beam at $\phi=0$ is brought to a focus at $\phi=127°$.

We are interested in the more general case in which $l'\neq 0$ and in which the rays after being deviated through an angle ϕ leave the electric field and come to a focus at a distance l''. At the angle ϕ,

$$r=a+y_2=a\{1+(\alpha/2)\sin\sqrt{2}\phi+\beta(1-\cos\phi)+(y_1/a)\cos\sqrt{2}\phi\}$$

and the angle α'' with the tangent BC to the circular orbit is given by $\alpha''=(1/a)dr/d\phi|_\phi=\alpha\cos\sqrt{2}\phi+\sqrt{2}(\beta-(y_1/a))\sin\sqrt{2}\phi$. In rectilinear coordinates, with the axis x'' in the direction BC and the y'' coordinate at right angles, the equation of the path is $y''=y_2+\alpha''x''$. Putting $y_1=al'$, and substituting the values of y_2 and α'' and collecting terms,

$$y''=\alpha\{l'\cos\sqrt{2}\phi+(\alpha/\sqrt{2})\sin\sqrt{2}\phi+x''(\cos\sqrt{2}\phi-\sqrt{2}(l'/a)\sin\sqrt{2}\phi)\}+\beta a\{1-\cos\sqrt{2}\phi+(x''/a)\sqrt{2}\sin\sqrt{2}\phi\}.$$

At a value of $x''=l''$ which makes the first bracket zero, the value of y'' is independent of the angle α at which the rays originally entered the condenser. A divergent bundle of one velocity is therefore brought to a focus at l''. The relation between l' and l'' for which this occurs is:

$$(l'+l'')\cos\sqrt{2}\phi+(a/\sqrt{2})\sin\sqrt{2}\phi-(\sqrt{2}/a)l'l''\sin\sqrt{2}\phi=0$$

or $l'l''-(l'+l'')(a/\sqrt{2})\cot\sqrt{2}\phi-(a^2/2)=0$, as deduced by Herzog (Eq. (25)). This may be written $(l'-g)(l''-g)=f^2$, where $f=(a/\sqrt{2})\times(1/\sin\sqrt{2}\phi)$, $g=(a/\sqrt{2})\cot\sqrt{2}\phi$, in analogy with the formulae of geometrical optics.

The velocity dispersion is given by the second bracket in the above equation for the path after leaving the condenser. At $x''=l''$ let the value of y'' be b''. Then

$$b''=\beta a\{1-\cos\sqrt{2}\phi+(l''/a)\sqrt{2}\sin\sqrt{2}\phi\}=a\beta\{1+(l''-g)1/f\}=a\beta\{1+f/(l'-g)\}\quad\text{(Herzog, Eq. (34)).}$$

FOCUSING CONDITION

For the paths of charged particles in a magnetic field analogous expressions may be deduced for the corresponding distances l' and l'' (See Herzog, reference 1, p. 459). However in the mass spectrograph to which the present paper refers very simple relations hold, as the angle of deviation is 180°, and both l' and l'' are zero. With these semicircular orbits two velocities v_0 and $v_1=v_0(1+\beta)$ will unite[4] at P (Fig. 1) if they enter the field H at two points C and D where $PC=2\rho_0=2mv_0/eH$ and $PD=2\rho_1=2mv_1/eH$ so that $DC=2\beta\rho_0$. If the velocity dispersion produced by the electric field is equal to CD, that

[3] A. L. Hughes and V. Rojansky, Phys. Rev. **34**, 284 (1929).

[4] A. J. Dempster, Phys. Rev. **20**, 638 (1922).

is if $2\rho_0 = a(1+f/(l'-g))$, the rays of different velocity will enter the magnetic field at the proper points to be united at P. In this way the velocity dispersion produced by the electric field is counterbalanced by the dispersion in the magnetic field, and a divergent beam entering at S containing particles of slightly different velocities is brought to a focus at P. For example, if $a = 8.48$ cm, $\phi = 90°$, and $l' = 1$ cm, then $f = 7.55$ cm, $g = -4.57$ cm and ρ_0 must be 10 cm giving $l'' = 5.66$ cm.

This focusing condition can be filled exactly only by one radius of curvature ρ_0. If different ions of the same energy are used, the curvature in the electrostatic field will be the same for all, but in the magnetic field the paths will have different radii of curvature. For ions that do not follow the path for perfect focus, the image width dc increases with their distance from P. A simple geometrical computation shows that $dc/DC = PP'/PC$. Thus with a diaphragm at C of 2 mm opening the image width of an infinitely narrow slit would be increased to 0.1 mm at a distance of 1 cm from P. For the qualitative analysis of elements this widening of the image is not disturbing, and for exact comparisons of atomic weights by the method of doublets, the doublets may be always brought to the position of exact focus.

The observations made with an apparatus constructed on these principles will be described in a later paper.

JANUARY 15, 1937 PHYSICAL REVIEW VOLUME 51

Electron and Negative Ion Mobilities in Oxygen, Air, Nitrous Oxide and Ammonia

RUSSELL A. NIELSEN AND NORRIS E. BRADBURY
Department of Physics, Stanford University, California

(Received November 13, 1936)

The electrical shutter method for measuring electron mobilities in gases has been extended to include experiments in oxygen, air, nitrous oxide and ammonia. The experimental data support the hypothesis that collisions of low energy electrons with molecules of these gases may be inelastic. Such collisions cause excitation of vibrational levels, electronic levels, or dissociation of the molecule. The results are compared with experiments reported elsewhere on negative ion formation in these gases. In general the onset of negative ion formation is accompanied by inelastic collisions which result in a marked increase in the electron drift velocity. Negative ion mobilities in these gases have been measured in the same apparatus by an adaptation of the Rutherford alternating current method. The ions were formed by electron attachment in an auxiliary field and their mobility determined at various ages. The probable character of the ions is discussed after comparing the experimental results with those predicted by the Langevin theory.

A. ELECTRON MOBILITIES

AN electrical shutter method for measuring the drift velocities of electrons in gases has been described in previous communications.[1, 2] The results heretofore obtained have been restricted to gases in which the electrons remained free. By working at somewhat reduced pressures, however, it is possible to extend the method to take data in gases in which negative ions are formed by electron attachment. Under these circumstances there appears a negative ion background current upon which is superimposed the electron current to be measured. For gases in which the probability of electron attachment at a collision is of the order of 10^{-4} to 10^{-6}, the background current can be reduced sufficiently to permit accurate measurement of the electron current maxima by restricting the pressure to values between 2 and 10 mm. In the present experiments the electrons were emitted from a photoelectric surface in the same apparatus employed in the measurements on hydrogen[1] using, however, the constant potential and varying frequency method of measurement.[2]

[1] N. E. Bradbury and R. A. Nielsen, Phys. Rev. **49**, 388 (1936).
[2] R. A. Nielsen, Phys. Rev. **50**, 950 (1936).

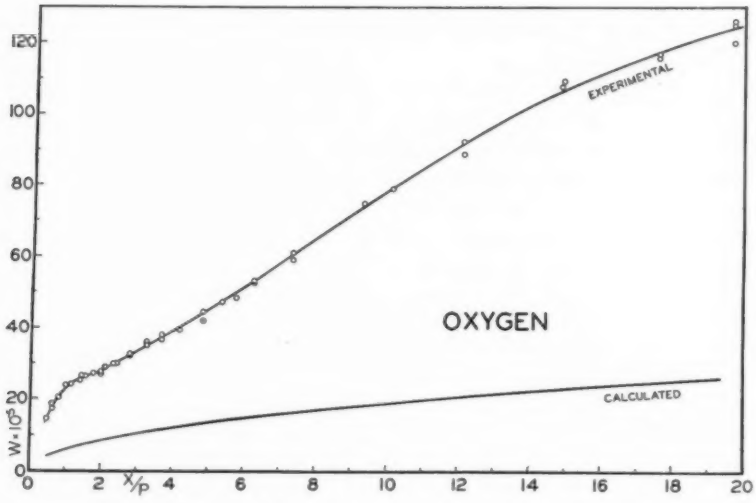

FIG. 1. Electron drift velocity in oxygen as a function of X/p.

Oxygen

Oxygen was obtained from a commercial tank of the gas and all condensable impurities were removed by passage through traps immersed in liquid nitrogen. The experimental data are reproduced in Fig. 1, together with a curve calculated on the basis of Brüche's[3] values for the collision cross section and Townsend and Bailey's[4] values for the mean energy of the electrons. It is seen that the experimental values are considerably greater than the theoretical and, as in the case of hydrogen and nitrogen, this may be ascribed to the presence of inelastic collisions. For values of $X/p<2$, where the average electron energy is less than one volt, these inelastic collisions occur in the excitation of vibrational levels. At an X/p of about 2, a marked point of inflection is observed in the experimental curve. This is undoubtedly due to the increased possibility of excitation of the $^1\Sigma$ state of O_2 whose energy is 1.62 volts above the ground state. Electrons of this energy are available in consequence of their distribution about their mean energy of one volt. Support for this hypothesis is to be found in the experiments on negative ion formation in oxygen.[5] The probability of electron attachment at a collision in this gas, at first decreases with X/p and then undergoes a rapid rise beginning at approximately an X/p of 2. This rise as well as the increase in drift velocity at this point may be ascribed to the increase in number of low energy electrons following collisions in which the $^1\Sigma$ state is excited.

Air

Samples of air employed in these measurements were purified by passage through traps immersed in liquid air. The experimental results are shown in Fig. 2. It is of interest to note that Blanc's law[6] is obeyed for the drift velocity of electrons in air inasmuch as values calculated from the experimental drift velocities in nitrogen and oxygen agree closely with those found experimentally. This is, of course, true only in this instance because the mean energy as a function of X/p as well as the distribution function of electron velocities, appear to be nearly the same for the two gases. The strong inflection at $X/p=2$ in oxygen may also be noticed in the curve for air.

Nitrous oxide

Nitrous oxide was obtained from a commercial cylinder of the gas stated to be of high purity.

[3] E. Brüche, Ergeb. d. exakt. Naturwiss. **8**, 185 (1929).
[4] J. S. Townsend and V. A. Bailey, Phil. Mag. **42**, 873 (1921).
[5] N. E. Bradbury, Phys. Rev. **44**, 883 (1933).
[6] L. B. Loeb, Phys. Rev. **32**, 81 (1928).

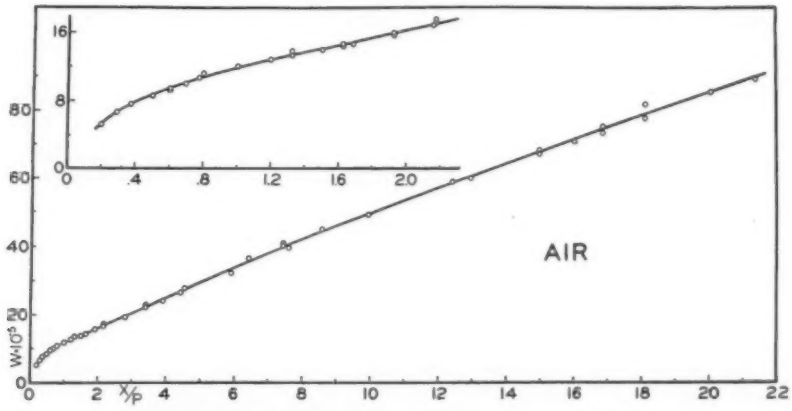

FIG. 2. Electron drift velocity in air as a function of X/p.

The gas was subjected to fractional distillation at reduced pressure at liquid-air temperatures, and the middle fractions only retained for use. The experimental data are presented in Fig. 3. While measurements have been made of the cross section of N_2O as a function of electron energy,[7] the results do not extend to sufficiently low energies to permit the calculation of a theoretical curve. It is of interest to compare the curve of Fig. 3 with what is known of negative ion formation in this gas.[8] Negative ions are not formed in N_2O by low energy electrons. At an X/p of 2, however, negative ions begin to appear which are ascribed to the dissociation reaction

$$N_2O+e\rightarrow N_2+O^-.$$

It is thus not surprising to find evidence of the dissociation in the drift velocity curve where it takes the form of an increasingly rapid rise at an $X/p\sim 0.6$.

Ammonia

Ammonia was obtained from a commercial cylinder of the anhydrous gas. The gas was liquefied over metallic sodium and fractionated at low pressure with liquid air and solid CO_2. The experimental data are shown in Fig. 4. At $X/p\sim 8$, a rapid increase in drift velocity is observed. This is without doubt to be ascribed to the same process which causes the onset of negative ion formation[9] in this gas at approximately this same value of X/p. This process has been suggested to be one of dissociation of NH_3 by electron impact with the initial formation of NH^-. The behavior of the drift velocity at lower values of X/p is remarkable for its linearity. Inasmuch as the variation of drift velocity with X/p for constant cross section and in the absence of inelastic collisions, is as $(X/p)^{\frac{1}{2}}$, this must mean a cross section for collision in NH_3 which increases at least as rapidly as the inverse square root of the electron energy.

B. Negative Ion Mobilities

In order to measure negative ion mobilities, the electrical connections to the experimental apparatus were changed so as to permit the use of

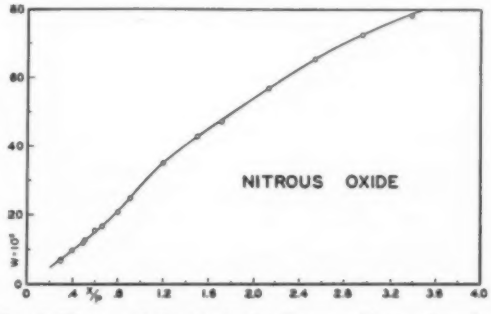

FIG. 3. Electron drift velocity in nitrous oxide as a function of X/p.

[7] V. A. Bailey and J. B. Rudd, Phil. Mag. **14**, 1033 (1932).
[8] N. E. Bradbury and H. E. Tatel, J. Chem. Phys. **2**, 835 (1934).
[9] N. E. Bradbury, J. Chem. Phys. **2**, 827 (1934).

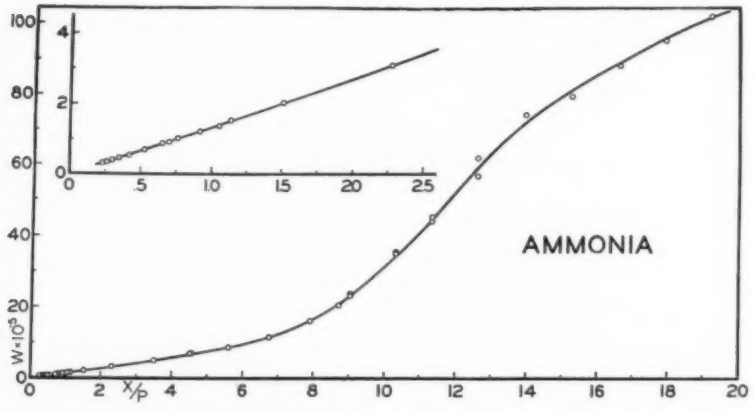

FIG. 4. Electron drift velocity in ammonia as a function of X/p.

the Franck and Pohl modification of the Rutherford alternating current method.[10] This was done in the following way: a steady auxiliary field was applied between the emitting surface and the lower grid which was of sufficient strength to insure the formation of negative ions in NH_3 and N_2O. Between alternate wires of this grid was maintained a high frequency alternating field, the magnitude of whose potential was sufficiently high to sweep from the current stream all electrons, but to permit the passage of negative ions. A square wave alternating potential was applied between this grid and the collecting electrode. This square wave was produced by commutation and had a variable frequency between 20 and 400 cycles/second. The second grid had no function, and was kept at a potential appropriate to its position in the field by connecting it to the surrounding guard ring. The wave form and frequency were determined by a cathode-ray oscillograph permanently connected to the apparatus.

The precautions to be observed in the use of this method have been pointed out by Loeb.[11] In particular, if the strength of the auxiliary field in which the ions are formed is not equal to that of the measuring field, interpenetration of fields will result, and the distance actually traveled by the ions in the measured time will not be the distance between the grid and the collector. Accordingly, the higher the ratio of auxiliary to main field, the shorter the effective distance, and therefore the greater the *apparent* mobility. For this reason, measurements of the mobility must be made as a function of the ratio $R=F_a/F_m$, where F_a and F_m refer to the auxiliary and the main field strength, respectively. The actual value of the mobility is then obtained by extrapolation to unity. It may be pointed out that in the experiments reported here, the distance between grid and collector was 80 mm and the grid spacing 1 mm. The use of such a relatively long distance tends to decrease the effect of field interpenetration on the measured value of the mobility.

The character of the experimental data obtained is shown in Fig. 5 in which the current is plotted as a function of frequency. Although the intercept of the current curve with the axis is not perfectly sharp, the extrapolation of the curve to the axis may be carried out with difficulty and is theoretically justified by the form of the current curve. The mobility may then be calculated from the expression $k=d^2/VT$, where V is the potential carrying ions across the field, d the distance through which the ions move, and T the time of application of V. The mobility may then be reduced to standard conditions by the expression $k_{20°}=k(p/760)(293/T)$.

As, expected, the experimental values of k are dependent upon the ratio R of the field strengths on both sides of the grid. The values of the mobility obtained in oxygen as a function of R are plotted in Fig. 6. The variation is seen to be

[10] Franck and Pohl, Ver. der Deut. Phys. Ges. **9**, 69 (1907).
[11] L. B. Loeb, J. Frank. Inst. **196**, 771 (1923).

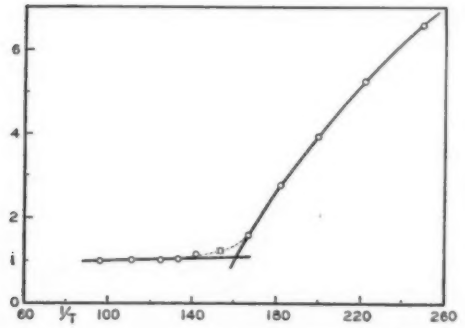

FIG. 5. Electrometer current as a function of the frequency of the square wave alternating potential.

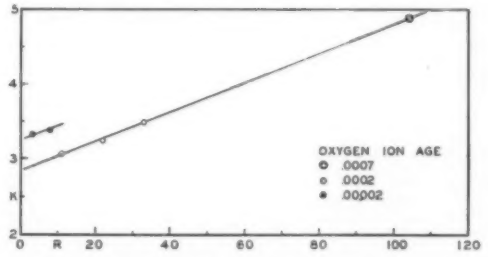

FIG. 6. Mobility of negative ions in oxygen as a function of the ratio of auxiliary to main field strength.

linear and may be extrapolated to $R=1$ to obtain the true value of the mobility. Actually, since the mobility of the ion may vary with its age, this procedure must be justified. In O_2, ions of the same age were measured with R varying from 10 to 40. It will be noticed that these lie on a straight line which may be extrapolated to $R=1$ as well as to higher values. It will also be noticed that the point for $R=104$ lies on this line, although this ion is considerably older. Furthermore, points below $R=10$ which correspond to very short ion ages also lie upon a straight line whose slope is substantially the same as the first. From this data alone, however, it cannot be said that the actual variation of k with R is linear from $40<R<100$, for within this age range a decrease in mobility with age may occur. In these experiments, in general, an increase in R may be associated with an increase in the age of the ion. If the mobility of the negative ion in oxygen remained approximately constant between the ages 0.0002 to 0.0007 second, corresponding to $20<R<104$, then the linear extrapolation to high R is obviously justified. If, however, at the *oldest* age ($R=104$) the true mobility has decreased below that corresponding to $R\sim20$, the actual mobility *vs.* R curve must be concave upwards. In the particular case of negative ions in air the ion of shortest age corresponds to the highest value of R. If the extrapolated curve deviated from linearity by being only very slightly concave upwards, one would be led to a value for the mobility of the negative ion in *air* which *increases* with age. Inasmuch as such a behavior is contrary to all previous experience, linear extrapolation in the reduction of data taken by this method seems justified.

Oxygen

The experimental results for the mobility of the negative ion in O_2 are presented in Fig. 7. The mobility is seen to be a function of ion age with a value of 3.3 cm²/volt sec. for the fastest ion, and to decrease with age to a value of 2.85 for the oldest ion measured. In order to provide a uniform age scale, which can be compared with other experiments, the actual ion ages in the gas at the pressure of the experiment have been recomputed to ages corresponding to atmospheric pressure and 20°C. The values for k obtained in this experiment are much higher than those ordinarily given, and undoubtedly do not refer to the so-called "normal" mobility in this gas. However, ions with a mobility greater than the "normal" have been reported by one of the authors,[12] who found that in oxygen of high purity but at atmospheric pressure and ion ages of 0.05″, a transient mobility of 2.65 was observed which shortly decreased to 2.47 and lower. The older ion in the present experiments probably corresponds to an earlier phase of the 2.65 mobility ion previously reported. The meaning of these values with regard to the character of the ion will be considered separately

Air

The results for the mobility of the negative ion in air are presented in Fig. 7. Due to the low coefficient at attachment in this gas it was impossible to obtain sufficient ion currents under conditions which simultaneously gave short ion ages. Consequently the fastest ion observed had a mobility of 2.8 which appeared to decrease

[12] N. E. Bradbury, Phys. Rev. **40**, 508 (1932).

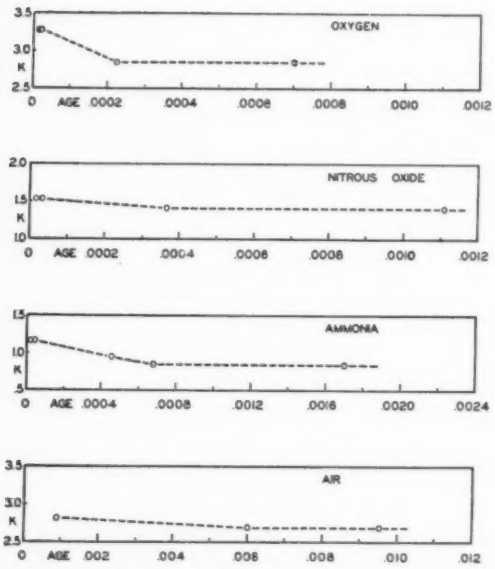

FIG. 7. Negative ion mobilities in oxygen, nitrous oxide, ammonia, and air, as a function of ion age, in seconds.

slowly with age up to 0.01″. This ion is probably of the same character as the ion of similar mobility and age in O_2 since it is known that nitrogen molecules do not attach electrons.

Nitrous oxide

The mobility of negative ions in N_2O are presented in Fig. 7. Since negative ions in this gas are apparently not formed by direct attachment, the ions measured were those formed in an auxiliary field with $X/p>2$. It is seen that the mobility decreases with age from a value of 1.5 to 1.4. This older value is almost exactly the same as that obtained by Loeb.[13]

Ammonia

The mobility of negative ions in NH_3 decrease rapidly with age for short ages, dropping from a value of 1.15 to 0.85 in less than 0.001 second. The value for the older ion is in good agreement with that of 0.87 given by Loeb.[14]

Discussion of Results

Various theories have been presented giving the dependence of ion mobility upon the physical constants of the ion and the gas through which it moves. The Langevin[15] theory assumes hard spherical ions of diameter σ, which experience an inverse 5th power law of attraction with neutral molecules resulting from dielectric forces. Hassé and Cook[16] have presented a theory which supposes an inverse 5th power law of attraction superimposed upon the dielectric forces together with an inverse 9th power law of repulsion. This latter equation does not require the use of an ion-molecule collision radius. However, since the coefficients of the inverse powers are not known with accuracy, and furthermore, since calculations by the two theories lead to substantially the same results, the Langevin theory will be used in this discussion. This theory has been used very successfully by Powell and Brata[17] to explain the mobility of positive alkali ions in the rare gases.

The Langevin theory gives the mobility to be of the form

$$k=\frac{A}{[\rho(D-1)]^{\frac{1}{2}}}\left(\frac{m+M}{M}\right)^{\frac{1}{2}},$$

where M is the mass of the ion, m the mass of the gas molecule, ρ the gas density, and D the dielectric constant of the gas, A is a function of a quantity λ where

$$\lambda^2=(8\pi p\sigma^4)/((D-1)e^2),$$

in which p is the pressure, σ the sum of the radii of ion and molecule, and e the electronic charge. A as a function of λ may be obtained from a table given by Hassé.[18] The values of σ used in these calculations will be those taken from viscosity measurements.

If values are substituted in the above equation corresponding to a *monomolecular* ion in O_2 using the value of σ given by Jeans[19] of 3.6×10^{-8} cm, one obtains a value of 3.46 for the mobility at 20°C. This corresponds remarkably well with the experimental value of 3.3 and serves to suggest the hypothesis that the *ion actually measured at these short times is* O_2^-. If, instead of the ion

[13] L. B. Loeb, Phil. Mag. **43**, 229 (1922).
[14] L. B. Loeb, Proc. Nat. Acad. Sci. **12**, 617 (1926).
[15] W. P. Langevin, Ann. chim. phys. **8**, 238 (1905).
[16] H. R. Hassé and W. R. Cook, Phil. Mag. **12**, 554 (1931).
[17] C. F. Powell and L. Brata, Proc. Roy. Soc. **A138**, 117 (1932).
[18] H. R. Hassé, Phil. Mag. **1**, 139 (1926).
[19] J. H. Jeans, *Dynamical Theory of Gases* (Cambridge University Press, London, 1925), p. 327.

O_2^-, the mass and approximate radius corresponding to a bimolecular oxygen ion is substituted, the value of 2.94 is obtained for the mobility. In this calculation, the value of A is relatively insensitive to changes in σ and the factor $((m+M)/M)^{\frac{1}{2}}$ plays the important role. The relative difference between this value and that calculated for a monomolecular ion is nearly the same difference as observed experimentally. Thus it is suggested from this data that within the first 2×10^{-4} second, *the addition product to the initial monomolecular negative ion in O_2 is a molecule whose molecular weight is between 15 and 35.* This suggests either H_2O or O_2. Subsequent ions have lower mobilities due either to the attachment of further molecules of impurity or the transfer of charge to some bulky impurity molecule inevitably present in the most stringently purified gas. Under such circumstances the factor A plays an increasingly important role, and the mass factor a lesser one.

Similar calculations may be carried out for air. If an ion be assumed of the same mass and radius which leads to a value of 2.94 in O_2, a value of 2.88 is obtained for the mobility of such an ion in air. This is slightly lower than its mobility in O_2 and is in accord with the experimental results of 2.85 in O_2 compared to 2.8 in air. It is therefore suggested that the same ion was observed in both cases, and that the failure to observe a faster ion in air was due to the greater ion ages studied.

In N_2O the original ion formed may be O^-. Assuming this to be so, the calculated value for the mobility is 2.73. This is much higher than the experimental value for the shortest ion ages measured, and therefore such an ion must lose its identity within 10^{-5} second. Using the molecular weight corresponding to the ion $(NO)_2^-$, a value for the mobility of 1.85 is obtained. It must be pointed out that the value of σ for this ion is very uncertain; great reliance cannot therefore be placed upon the calculated value for the mobility. It may be said, however, that the ion at an age of 10^{-5} second apparently has a mass at least that of $(NO)_2$, and increases its mass and diameter but little thereafter.

It has been suggested that in the process of negative ion formation in NH_3 the initial process is the dissociation of the molecule with the formation of NH^-. Although values of σ are not available for this molecule, the high value of the dielectric constant makes A insensitive to variations in σ, and the mass factor plays the dominant role. If an approximate value of 5×10^{-8} cm can be assigned to σ, one finds the mobility of an hypothetical NH^- ion to be 1.25. This is not substantially higher than the fastest mobility observed. If one employs a mass corresponding to $(NH+NH_3)^-$ one calculates a mobility of 1.06 which is obtained experimentally at an age of approximately 2×10^{-4} second. From the shape of the graph, a mobility of 1.25 for extremely short times seems probable. This ion apparently rapidly picks up an additional molecule and in less than 0.001″ reaches a stable value of 0.85 which is characteristic of ions in even impure ammonia.

JANUARY 15, 1937 PHYSICAL REVIEW VOLUME 51

The Development and Performance of an Electrostatic Generator Operating Under High Air Pressure

R. G. Herb, D. B. Parkinson and D. W. Kerst
University of Wisconsin, Madison, Wisconsin

(Received October 22, 1936)

A belt type electrostatic generator has been developed which operates in a steel tank, 5½ feet in diameter and 20 feet long, under an air pressure of 100 lb./in.². The generator is provided with a high potential electrode system of a new design which serves both to give a high breakdown potential and to furnish a satisfactory potential distribution along the charging belts and the accelerating tube. The maximum potential of the generator is about 2500 kv and the highest steady potential at which reliable data have been obtained is 2160 kv. An evacuated tube for acceleration of ions has been developed which withstands the highest generator potential. The apparatus has been successfully used in experiments on atomic disintegration.

Introduction

A FEW years ago an electrostatic generator of the Van de Graaff type was developed at this laboratory in which the apparatus was operated in a steel tank under high air pressure.[1] Because of the small size of the enclosing tank, the usable potential of this generator was limited to about 400 kv but its numerous advantages indicated the desirability of further development.

During the past year a second electrostatic generator has been constructed utilizing higher pressure and larger dimensions and has been successfully used in disintegration experiments. Although the generator is of the same type as the small generator referred to above, the increased dimensions of the new apparatus presented certain problems in the design of a satisfactory high potential electrode system; and for their solution a new type of electrode has been developed. This paper describes the development and performance of the large electrostatic generator, and because of the importance of the high potential electrode system for successful operation of the generator, considerable space is devoted to a description of its design.

Design of Pressure Tank

From a consideration of the performance of electrostatic generators of the Van de Graaff type developed here and at other laboratories, it was expected that the peak voltage of the proposed generator would be approximately proportional to the diameter of the enclosing tank, assuming a fixed air pressure and sufficient tank length. From this consideration, a tank having a very large diameter would be desirable but for convenience in operation and low cost of construction, it was decided to install the generator in one of the regular research rooms available at this laboratory. To satisfy this condition the tank diameter was chosen to be $5\frac{1}{2}$ feet and, by making what seemed a reasonable assumption as to the lengths necessary for charging belts and the accelerating tube, the necessary tank length was determined to be 20 feet. The tank[2] was designed for a working pressure of 100 lb./in.^{2}, thus giving a total pressure almost twice as high as that used for the small generator referred to above.

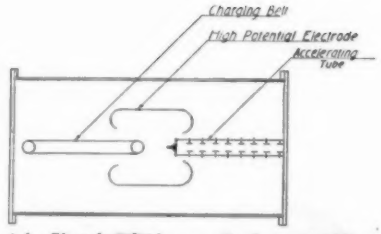

FIG. 1A. Sketch of the small electrostatic generator developed at the laboratory. Because of the short length of the accelerating tube and the comparatively large diameters of the steel tank and the high potential electrode, the tube operates satisfactorily without shielding.

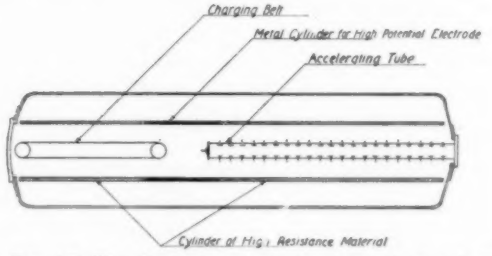

FIG. 1B. The electrode system shown in this sketch, if experimentally realizable, would be ideal for the large generator both to give a breakdown potential and to provide a satisfactory potential distribution along the charging belts and the accelerating tube. Cylinders of high resistance material were thought, however, to be impractical.

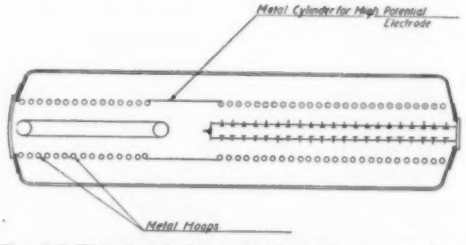

FIG. 1C. This sketch shows the electrode system adopted for the large generator. The hoop system was thought to provide the closest practical approach to the theoretically ideal arrangement shown in B.

Design of High Potential Electrode System

A length of about 11 feet was considered necessary for the accelerating tube to assure satisfactory performance at the maximum potential expected of the generator. Because of the great length of accelerating tube compared with the $2\frac{3}{4}$-foot radius of the surrounding tank, a

[1] R. G. Herb, D. B. Parkinson and D. W. Kerst, R. S. I. 6, 261 (1935).

[2] We are indebted to The Chicago Bridge and Iron Works from whom the tank was purchased for their generous cooperation in working out the details of its construction.

high potential electrode similar to that used on the small pressure generator (*A*, Fig. 1) would be unsatisfactory, since it provides no shielding for the accelerating tube and a corona discharge would surely take place between high potential sections of the tube and the wall of the tank. Another reason for departing from the usual electrode design is given by a consideration of the inner electrode system which will give a potential distribution most nearly like the potential distribution given by two concentric cylinders infinite in length. Perhaps the closest approach to this ideal potential distribution would be given by an arrangement as shown in *B*, Fig. 1, with a conducting cylinder which is at the highest potential being continued at both ends by a cylinder of high resistance material down which a leakage current flows to give a gradual drop in potential. Such an arrangement, if experimentally realizable, would probably give a breakdown potential close to the breakdown potential between cylinders of infinite length, but cylinders of high resistance material were thought to be impractical and the arrangement *C*, Fig. 1, was considered the best practical way to secure good potential distribution. The conducting hoops as shown in *C*, Fig. 1, must be insulated from one another with provision, however, for a small current from hoop to hoop which can be provided by a system of corona points or resistors of very high ohmage. With this arrangement the potential, which is highest on the main electrode of *C*, Fig. 1, will decrease from both ends of the electrode by a number of discrete steps and will reach ground potential at both ends of the enclosing tank.

In order to decide on the radius of the inner electrode system, use was made of the relation that, for concentric cylinders of infinite length, the radius of the inner cylinder should be given by $r=R/e$ for maximum breakdown potential, where R is the fixed radius of the outer cylinder and e is the base of the natural logarithmic system. This relation would determine a radius of 12.2 inches for the inner electrode system of the large electrostatic generator, but since the breakdown voltage is a slowly varying function of r in the region of optimum r, the radius of the inner electrode system was chosen to be $14\frac{7}{8}$ inches. This larger value of the radius was chosen so as to give ample room for charging belts and a power plant for the ion source.

Simple calculations were made in order to determine reasonable values for the diameter of the tubing from which the hoops were to be made and the air gap between the hoops, assuming the hoops to be made of round metal tubing bent into a circular form. Taking into account only the axial field, these calculations showed that for a generator potential of 3 MV the air gap between hoops could be safely made less than one-half the tubing diameter without danger of sparking from hoop to hoop. To allow for the added effect of the radial field, the ratio of tubing diameter to air gap was finally chosen to be 1.2. With this ratio determined to eliminate axial sparking, the absolute diameter of the tubing for the hoops was chosen partly from a consideration of the size most likely to give a high radial breakdown potential, but principally for convenience of construction. It seemed reasonable to assume that the breakdown potential should improve as

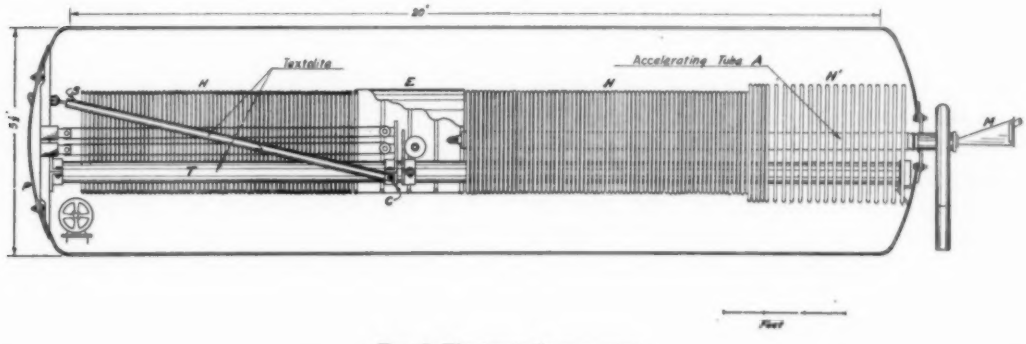

FIG. 2. Electrostatic generator.

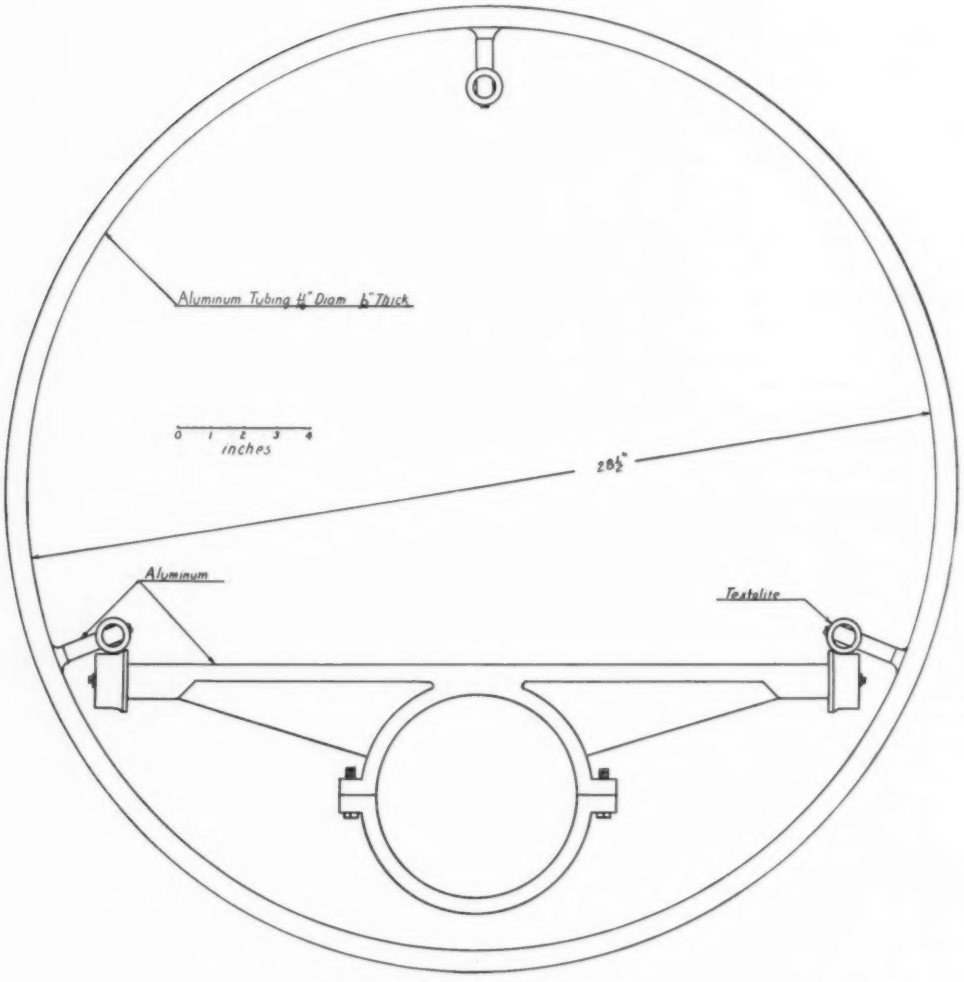

FIG. 3. Aluminum hoop and support.

the hoop tubing diameter and air gap become smaller, with their ratio held constant, since in the limit, with the hoop system degenerated into a system of closely spaced rings of fine wire, the potential distribution out a short distance from the system would be much like the potential distribution given by ideal cylinders of high resistance material. To best fulfill the conditions outlined above, of convenience of construction and high radial breakdown potential, the hoop tubing was chosen to have an outside diameter of $\frac{11}{16}$ inches and the hoops were spaced to have an air gap of $\frac{9}{16}$ inches.

DETAILS OF CONSTRUCTION OF HIGH POTENTIAL ELECTRODE SYSTEM

In Fig. 2, the general arrangement of the high potential electrode system is shown, but to avoid confusion, many of the details are not included in the diagram. Mechanical support for all inner apparatus is provided by the textolite tube T which has a 6-inch outside diameter and a $\frac{1}{4}$-inch wall thickness, and extends along the entire length of the tank. For additional rigidity, two textolite tension members S with a $2\frac{1}{2}$-inch outside diameter and a $\frac{1}{4}$-inch wall thickness run parallel to each other from opposite sides of the

aluminum casting C to an angle iron support at the end of the tank. These two textolite tubes are spaced $17\frac{1}{2}$ inches apart, from center to center, leaving sufficient free space for the charging belts.

The hoops are made from straight aluminum tubing, half-hard, $\frac{11}{16}$-inch outside diameter and $\frac{1}{32}$-inch wall thickness, bent into accurate circles and soldered with Kester aluminum solder. Each hoop is provided with 3 soldered studs as shown in Fig. 3 and by means of three small textolite tubes, the hoops are connected into rigid cylindrical sections with a total of 4 sections of hoops H of Fig. 2. As a frame work for electrode E, Fig. 2, five aluminum hoops of the same size as those described above were mounted on 3 textolite tubes to form a section 30 inches long and over this frame, light weight galvanized sheet steel was bent and soldered.

To support electrode E and the four hoop sections, aluminum castings fitted with Bakelite rollers, as shown in Fig. 3, are clamped to the large textolite tube T, Fig. 2. Eighteen of these castings are used, spaced evenly along the entire length of the textolite tube. The four hoop sections and electrode E rest on these rollers and are ordinarily pinned together to form a rigid system with uniform hoop spacing. In order to have all apparatus inside the hoop system and the electrode easily accessible for adjustment or repair, the hoop section H', Fig. 2, was made sufficiently large so that the smaller system H can be telescoped into it. Thus by unpinning the system H, Fig. 2, in the proper place and telescoping it into section H', a space four feet long is left uncovered wherever needed and is easily accessible. Section H' is ordinarily clamped to the end of the tank but may be unclamped, and if the smaller hoop section has been telescoped inside, section H' may be made to rest on it and may then be rolled out to have the inner apparatus at this end of the tank uncovered and accessible.

Each hoop is equipped with a needle point and a plate mounted so as to form a corona system with the corona gaps set at about $\frac{1}{2}$ inch and with the needles turned so as to be negative. As all electrical contacts of the hoop system and electrode E with the inner apparatus are made automatically, the system can frequently be unpinned, an adjustment made on apparatus inside, and the system repinned, ready for operation in 3 or 4 minutes. The 3-foot opening in the end of the tank which may be covered by plate P, Fig. 2, provides room for an operator to enter the tank, and when inside, an operator with rubber soled shoes can walk without difficulty alongside of the inner electrode system on the sloping wall of the tank.

Charging Belts and Pulleys

The two charging belts are each 13 inches wide and are made of rubberized fabric of the type used in hospitals for sheeting, with the splice formed by vulcanizing. Pulleys for the charging belts are made of steel tubing 3 inches in diameter and 14 inches long with steel end plugs brazed into place and turned down to form shafts. The pulleys have no crowning except for a 1° taper at the ends along a distance of $\frac{1}{2}$ inch. A one horsepower d.c. motor is used for each belt and the speed of the charging belt pulleys is about 3600 r.p.m. The needle system for charging the belts (not shown in Fig. 2) is similar to that used on the small pressure generator developed at this laboratory except that the pulleys in the high potential electrode are insulated from the electrode and can therefore be used as inductor plates for feeding negative charge to the outgoing belts.

Accelerating Tube

Experience with an accelerating tube made up in short sections from straight glass cylinders

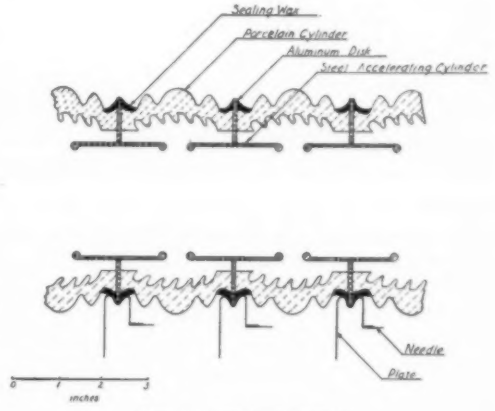

Fig. 4. Accelerating tube.

FIG. 5. Interior view of the generator showing the accelerating tube and the hoop system.

showed that the most serious factor limiting the voltage is a flash-over along the inner glass surface. Porcelain cylinders were therefore designed, corrugated inside and outside as shown in Fig. 4. A single porcelain section with electrodes as shown in the diagram withstood a potential of 100 kv satisfactorily. For the accelerating tube of the large generator 54 porcelain cylinders and metal electrodes were waxed together as shown in Fig. 4 using red sealing wax (American Express No. 2). The accelerating tube is supported inside the generator by heavy piano wire cradles at intervals of 15 inches along its entire length (Fig. 5) and sufficient flexibility to prevent strains and cracking is provided by a sylphon bellows and gimbal ring joint just next to the end plate of the tank. This tube has caused very little trouble due to leaks and when first mounted in the tank, it pumped down to a pressure of 2×10^{-6} mm Hg.

While testing the performance of a single porcelain section in the small pressure generator, trouble was experienced with sparking along the external surface of the porcelain. This sparking occurred only when the porcelain section was evacuated and was practically unaffected by increasing the air pressure outside the section. Apparently charges on the inner surface of the porcelain caused irregular gradients on the external surface and consequent flash-over. This external sparking was later eliminated by wrapping a fine mesh brass gauze around the metal disk at each end of the porcelain cylinder. The explanation of this behavior is probably as follows: points on the fine mesh gauze cause a small corona current through the air close to the surface of the porcelain which prevents the development of high potential gradients. Further tests showed that the gauze could be replaced by three needle points spaced evenly around the metal disk at the end of each porcelain cylinder. The accelerating tube was therefore equipped with a corona system as shown in Fig. 4 and Fig. 5 which serves two separate purposes. First, it gives a uniform potential drop from section to section along the entire length of the tube; and second, the corona current along the surface of each porcelain cylinder prevents the development of high gradients on the surface and thus prevents sparking. By a simple system of automatic contacts, the accelerating tube is connected electrically to the surrounding hoop system at intervals of 15 inches. Over the period of a few months during which the generator has been in operation, the accelerating tube has performed satisfactorily at all generator potentials.

PRODUCTION, FOCUSING AND MAGNETIC ANALYSIS OF POSITIVE IONS

Power for the ion source is provided by a 500-watt, 125-volt, self-excited a.c. generator driven from the inner pulley of the lower charging belt. By means of an RCA 866 rectifier tube and an 83 rectifier tube with the necessary transformers and condensers, d.c. potentials are supplied at 3000 volts and at 200 volts to run an ion source similar to that used by Tuve, Hafstad and Dahl. The rectifier tubes have operated without trouble with the air pressure in the tank up to 100 lb. and electric light bulbs of the ordinary type have also withstood the pressure satisfactorily except for one or two failures.

Focusing is accomplished by an adjustable corona gap across the first section of the accelerating tube. With the accelerating cylinders as shown in Fig. 4, no satisfactory focus could be obtained and the fluorescent spots formed by the ions on a quartz plate at the end of the magnetic analyzer were poorly defined. As these accelerating cylinders have a length of $2\frac{1}{8}$ inches and an inside diameter of about $2\frac{1}{4}$ inches, it

seemed probable that cylinders having a smaller inside diameter compared to their length would give better results. The first six accelerating cylinders at the high potential end of the tube were therefore made with the same length of $2\frac{1}{8}$ inches but were reduced to a diameter of one inch. After making this change, the ion beam has been well focused and, generally, by adjusting the corona gap across the first section of the tube, the fluorescent spots formed by the ions at the end of the magnetic analyzer can be brought down to a diameter of about 3 mm. In the brass box M of Fig. 2, the ion beam is separated into its mass spectrum by means of an electromagnet, and the ions to be studied are shot into the target chamber.

Hydrogen pressure in the ion source, filament heating current for the ion source, and the corona gap for ion focusing can all be adjusted from outside the tank by controls working through packing glands. A window in the wall of the tank and a mirror properly placed inside the tank enable operators to read meters inside the high potential electrode. The pumping system for evacuation of the accelerating tube consists of three brass diffusion pumps using Apiezon oil, and a Cenco Hypervac. The diffusion pumps are of the same type as those used for the high voltage work at the Department of Terrestrial Magnetism of the Carnegie Institute of Washington and were made up from drawings generously furnished by Dr. M. A. Tuve.

Measurement of Voltage

Voltage is measured by means of a generating voltmeter mounted on the side of the tank with the sectored spinning disk flush with the wall, in an opening just opposite the high potential electrode. The alternating current generated by the spinning disk is rectified by means of a commutator and measured with a Leeds and Northrup galvanometer, sensitivity 2.99×10^{-10} amp./mm. A calibration of this voltmeter was made in the following way. With the small electrostatic generator which had been carefully calibrated by a method recently described in *The Physical Review*,[3] a series of runs were taken on the gamma-rays emitted by lithium bombarded by protons. Using two thick targets of pure evaporated lithium and two thin targets, nine separate runs were taken giving values for the peak of the gamma-ray resonance varying from 433 kv to 450 kv with an average at about 440 kv. This value of the resonance voltage agrees with the results of Hafstad, Heydenburg and Tuve, recently reported.[4] With the large generator, four runs were then taken on the gamma-rays from lithium bombarded by protons using both thick and thin targets, and by assuming that the average value thus determined for the resonance peak was at a potential of 440 kv, the sensitivity of the generating voltmeter was determined.

The generating voltmeter was shown to have a linear scale by a study of the deflections of the proton beam and the hydrogen diatomic ion beam in the magnetic analyzer. With the voltage at V_1, the magnetic field was adjusted to bring the proton beam through a $\frac{3}{16}$-inch hole into the target chamber where it impinged on a glass plate and formed a fluorescent spot. Then, with the magnetic field held constant, the voltage was lowered until the diatomic ions entered the target chamber. If V_2 is this second voltage, its value, provided the voltmeter is linear, should be given by $V_2=V_1/2$. By choosing a number of values for V_1, the voltmeter was shown to be linear to within about 5 percent over the entire voltage range of the generator. A more accurate check was not possible because the spots formed by the ion beams at the time these tests were made were at some voltages larger than the $\frac{3}{16}$-inch defining hole at the entrance to the target chamber.

Additional Apparatus

Compressor

Air is delivered to the tank up to the required pressure by a Quincy compressor, air-cooled, with a capacity of about 20 cubic feet per minute. For drying ingoing air, a steel cylinder filled with sodium hydroxide sticks is connected into the pipe line.

[3] R. G. Herb, D. B. Parkinson and D. W. Kerst, Phys. Rev. **48**, 118 (1935).

[4] L. R. Hafstad, N. P. Heydenburg and M. A. Tuve, Phys. Rev. **49**, 866 (1936).

Cooling System

An air blast from a vacuum cleaner blower provides cooling for the ion source. The blower is mounted on grounded angle iron supports near the motors which drive the charging belts, and the textolite tube *T*, Fig. 2, serves as a pipe line to deliver air to the ion source.

Upper Voltage Limit of Generator

With the tank at atmospheric pressure, the highest usable generator voltage is generally about 500 kv although the peak voltage is not sharply defined and often the generator can be held above 600 kv for short periods of time. As the air pressure is increased, the upper voltage limit becomes even less sharply defined than at low pressures so that a study of peak voltages as a function of pressure is not very satisfactory. Experience over a period of a few months, during which considerable data have been taken on proton induced reactions, definitely shows that the maximum usable potential of the generator does not increase linearly with air pressure. For a short period of time, the generator has been held at 2500 kv but up to the present time the highest potential at which reliable data have been obtained is 2160 kv. This maximum usable potential could probably be increased somewhat by a careful overhauling and a thorough cleaning of the apparatus.[5]

During the first high voltage trials with the tank at high pressure, the potential was limited to about 1.7 MV by sparking along the textolite tubes *S*, Fig. 2. The sparking distance along these tubes is about 7 feet whereas the radial distance from the high potential electrode to the wall of the tank is only 18 inches. Sparking such as this, along the surface of insulators, has also been experienced in the small generator and in all cases an increase of air pressure gave no improvement in the sparking potential. This behavior indicates that on long insulators irregular surface charges accumulate which may give a sufficiently high gradient at some point to initiate a discharge. The surface discharges along the textolite tubes, *S*, were eliminated by a corona system similar to that used on the accelerating tube to prevent accumulation of charges. Strips of fine brass gauze about $\frac{1}{4}$ inch wide were wrapped around the tubes at intervals of $2\frac{1}{2}$ inches, and at intervals of 15 inches, the gauze systems were connected to the surrounding hoops. Although these gauze systems draw very little current (probably less than 5 microamperes), they have successfully eliminated surface sparking.

Trouble has also been caused by surface sparking down the charging belts when large charging currents are being used at high potentials, but these can be avoided by keeping the charging current below about 200 microamperes when working at high generator potentials. As this current limitation is not serious for work with positive ions, no effort has been made to increase the usable charging current, but to adapt a generator of this type to high voltage x-ray production for which currents of several milliamperes are needed, further development work would be necessary.

After eliminating the surface sparking along the belts and the textolite supports, the upper voltage limit was determined by radial sparking between the high potential electrode and the wall of the tank with the sparks generally occurring at the ends of the electrode.

Voltage Control

Charge is put on the belts by a kenotron rectifier set and thus, by varying the resistance in the primary of the kenotron transformer, the generator voltage can be changed. When taking a run during which a steady generator potential is desired at some particular value, changes will occasionally occur so that the kenotron voltage must be varied to bring the electrostatic generator

[5] Some increase in the potential of an electrostatic generator can be obtained by the addition of CCl_4 vapor to the air. This effect was noticed by one of us (R. G. H.) three years ago while working with the small electrostatic generator and was then studied in considerable detail. A saturated vapor pressure of CCl_4 in air at atmospheric pressure was found to give a breakdown potential of about 1.7 times the breakdown potential of ordinary air. These results with air at atmospheric pressure were verified later by two different observers using an apparatus consisting of an adjustable sphere gap in a small pressure tank. A thorough investigation was then made using CCl_4 vapor in air at several different pressures up to a maximum of 75 lb. Publication was delayed because it was intended to look for similar effects caused by other vapors but details of the work will be published soon. In a recent issue of Compte rendus **202**, 291 (1936), Joliot, Feldenkrais and Lazard report the discovery of this effect. They find that an electrostatic generator operated in air containing a high vapor pressure of CCl_4 gives a maximum potential twice as high as when operated in ordinary air.

back to the desired potential. Recently a control has been devised utilizing corona current from the high potential electrode and an amplifying system for automatically varying the kenotron voltage to keep the electrostatic generator at a constant potential. Generally during a run, the automatic control keeps the voltage of the generator constant to within about 1 percent and often to 0.5 percent. As improvements are still being made in the amplifying circuit, a complete description of the apparatus will be postponed until a later time.

High frequency fluctuations of the generator voltage cannot be detected with the generating voltmeter because of the long period of the galvanometer used. A study of high frequency fluctuations was therefore made utilizing corona current to a needle sticking through a hole in the wall of the tank. The only periodic voltage fluctuation detected had a magnitude of about 0.5 percent and as its frequency was the same as that of the charging belts, it was probably caused by the splice in the belts.

Discussion

As the success of the electrostatic generator described in this paper, both for development of high potential and for utilization of that high potential, depends to a large extent on the arrangement of the inner electrode system, a brief discussion will be given of the advantages of this electrode design. The hoop system gives a uniform, axial field along the accelerating tube and along the belts. The distance provided for the tube and the belts is great compared with the radial distance from the high potential electrode to the wall of the tank and therefore when the generator is at its maximum potential, the field inside the hoop system is far below the breakdown value. Metal castings and wires inside the hoop system cause no trouble if kept approximately parallel to the plane of the hoops and the accelerating tube with its metal electrodes and its corona system is operating under ideal conditions. As the high potential electrode (*E*, Fig. 2) may be left open at both ends, the space available for charging belts and the accelerating tube is limited only by the diameter of the cylinder.

A similar system could be used for an electrostatic generator in a large room at atmospheric pressure or in an upright pressure tank. Instead of the usual sphere mounted on insulating supports, a cylindrical column of hoops could be used, capped by a hemisphere. Ample room would then be available inside the hoop system for supports, belts and accelerating tubes.

From a consideration of the performance of the two generators developed at this laboratory it would seem that to obtain a further increase in potential an increase in the dimensions of the apparatus would be the safest way to proceed. Higher pressures might also give considerable improvement but the nonlinear increase of usable potential with pressure up to a pressure of 100 lb. makes the effectiveness of still higher pressure difficult to predict.

We wish to express our indebtedness to the late Professor C. E. Mendenhall and to Professor H. B. Wahlin for advice and generous support. We also wish to express our appreciation to Mr. J. P. Foerst and Mr. J. A. Johnson for their work on the construction of apparatus and to Mr. J. L. McKibben for valuable work in the development of the generator. We are indebted to the Wisconsin Alumni Research Foundation and the Bowman Cancer Foundation for generous financial assistance.

On the Capture of Orbital Electrons by Nuclei

C. MØLLER
Universitetets Institut for Teoretisk Fysik, Copenhagen, Denmark
(Received November 9, 1936)

ACCORDING to the theory of β decay put forward by Fermi[1] a nucleus of charge Z can, provided the process is energetically possible, be transformed into a nucleus of charge $Z-1$ in two different ways: by the emission of a positron or by the absorption of an orbital electron. In a paper to appear shortly.[2] I have calculated the probability of the latter process and have found that for heavy elements the capture of a K electron is in most cases much more probable than the emission of a positron. The total probability per second for the emission of a positron is in the case of "allowed" transitions given by

$$\lambda^+ = |M|^2 G^2 \kappa F(Z, W_0), \qquad \kappa = \frac{4(2\rho)^{2S} mc^2}{\Gamma(3+2S)^2 \hbar};$$
$$S = (1-(Z\alpha)^2)^{\frac{1}{2}} - 1. \quad (1)$$

Here $\alpha(=1/137)$ is the fine structure constant, ρ is the radius of the nucleus divided by $\hbar/mc$, m is the mass of the electron and W_0 is the energy difference between the initial nucleus of charge Z and the final nucleus of charge $Z-1$, mc^2 being taken as unit energy. $F(Z, W_0)$ is a function of Z and W_0, whose form depends on what assumption is made about the interaction between heavy and light particles. If we take the (0, 0) interaction proposed in Fermi's original paper and put $Z=82.2$ we get for different values of W_0 the F values given in the second column of Table I. The corresponding F values for the case of the (0, 1) interaction proposed by Konopinski and Uhlenbeck[3] are given in the fourth column. G in (1) is a dimensionless constant related to the universal constant g in Fermi's theory. To account for the decay periods found experimentally of the ordinary β-ray emitters we must put

$G=1.1\times10^{-12}$ in the case of (0, 0) interactions,
$G=0.1\times10^{-12}$ in the case of (0, 1) interactions. (2)

$|M|$ in (1) is the matrix element of the Fermi theory, a quantity which by definition cannot be larger than unity. The experimental data on the decay constants and on the upper limits of the ordinary β-ray spectra show that the matrix elements $|M|$ for heavy nuclei are in general several times smaller than the matrix elements of the light elements.

For the probability per second of a K electron being absorbed by the nucleus we found the expression

$$\lambda_K = |M|^2 G^2 \kappa F_K(Z, W_0) \quad (3)$$

for "allowed" transitions, where F_K in the case of (0, 0) interactions is given by

$$F_K = \pi\Gamma(3+2S)(Z\alpha)^{3+2S}(W_0+1)^2.$$

For (0, 1) interaction the factor $(W_0+1)^2$ is replaced by $(W_0+1)^4$. The values of F_K for $Z=82.2$ and for the two kinds of interactions are given in the third and fifth columns of Table I. It can be seen that F_K is certainly considerably larger than F so that the probability of the capture of a K electron is much larger than the probability of the emission of a positron.

This result seems to be essential for the interpretation of the experiments of Cork and Lawrence[4] who bombarded platinum with deuterons and found that among other things a radioactive substance was found which emitted positrons. They assumed that $_{78}Pt^{192}$ is trans-

TABLE I. *Values of $F(Z, W_0)$ and of $F_K(Z, W_0)$.*

	(0, 0) INTERACTION		(0, 1) INTERACTION	
W_0	$F(Z=82.2)$	F_K	$F(Z=82.2)$	F_K
0	0	1.2	0	1.19
1	0	4.8	0	19.0
1.40	$<6\times10^{-4}$	6.8	$<10^{-5}$	39.4
2.29	0.02	12.9	0.008	139.3
3.20	0.25	21.0	0.38	369.9
4.11	1.2	31.0	3.8	810.6
5.03	3.9	43.2	20.7	1572
7.09	26.5	77.8	318.2	5092

[1] E. Fermi, Zeits. f. Physik **88**, 161 (1934).
[2] Physik. Zeits. Sowjetunion.
[3] E. J. Konopinski and G. E. Uhlenbeck, Phys. Rev. **48**, 7 (1935).
[4] J. M. Cork and E. O. Lawrence, Phys. Rev. **49**, 788 (1936).

formed by the bombardment into $_{78}Pt^{192}$, which can emit a positron and go over to $_{77}Ir^{192}$. The upper limit of the positron spectrum lies in the neighborhood of 2.1 MV, which corresponds to $W_0=5.1$. The decay period is 49 min. corresponding to a decay constant $\lambda=3.4\times10^{-4}$ sec.$^{-1}$.

For $Z=78$ and $W_0=5.1$ we get the following values for F and F_K (in the neighborhood of $Z=82.2$ F_K varies approximately as $Z^{3-2\times0.2}$ while F is practically constant)

$$\begin{aligned} F&=4.2, \quad F_k=37.8 \quad \text{for (0, 0) interaction} \\ F&=30.8, \quad F_k=1440 \quad \text{for (0, 1) interaction.} \end{aligned} \tag{4}$$

From (1) we get, using (2)

$$\begin{aligned} \lambda^+&=2.6\times10^{-4}|M|^2, \quad \text{(0, 0) interaction,} \\ \lambda^+&=3.1\times10^{-5}|M|^2, \quad \text{(0, 1) interaction.} \end{aligned}$$

Even if we give $|M|^2$ its maximum value of unity these values are smaller than the experimental decay constant $\lambda=3.4\times10^{-4}$, which shows that there must exist some other process, in addition to the positron emission, whereby $_{78}Pt^{193}$ can be transformed into $_{77}Ir^{193}$. If we take into account the possibility of a K electron being captured, we have $\lambda=\lambda^+ + \lambda_K$. Using (1), (2) and (3) we get for the two different types of interaction

$$\lambda=\lambda^+ + \lambda_K = \begin{cases} 26.2\times10^{-4}|M|^2 \\ 14.8\times10^{-4}|M|^2 \end{cases}$$

which can be brought into agreement with the experimental value by choosing a suitable value for $|M|^2$. This gives $|M|^2\sim\frac{1}{5}$ which is of the same order of magnitude as has been found for the matrix elements of other heavy elements.

While the total decay constant $\lambda^+ + \lambda_k$ is about the same for both types of interaction, the ratio $\lambda_k/\lambda^+ = F_K/F$ between the probabilities of the two processes depends very much on the assumption made about the interaction. As can be seen from (4) we have

$$\frac{\lambda_K}{\lambda^+}=\frac{F_K}{F}=\begin{cases} 9 & \text{for (0, 0) interaction,} \\ 47 & \text{for (0, 1) interaction.} \end{cases}$$

From a theoretical point of view it would therefore be of great value if this ratio could be determined experimentally. Since the capture of a K electron will always be followed by the emission of a quantum belonging to the characteristic x-ray spectrum of the element formed by the process, the ratio λ_K/λ^+ is equal to the ratio between the number of x-rays and the number of positrons emitted in a given time interval.

Finally in using the output of positrons after saturation has been obtained, to calculate the cross section for the formation of $_{78}Pt^{193}$ by the bombardment of $_{78}Pt^{192}$ with deuterons, we must take into account the fact that the number of active nuclei formed per second is $(F+F_K)/F$ times the number of positrons emitted per second. Allowing for the abundance of $_{78}Pt^{192}$ in platinum being smaller than 3 percent[5] we find from the data on the output of positrons given in the paper of Cork and Lawrence that this cross section is of the order of at least 10^{-26} cm^2 on the assumption of (0, 0) interaction. On the (0, 1) interaction assumption this cross section is even larger, being in fact of the order of 7×10^{-26} cm^2 at the lowest.

[5] B. Fuchs und H. Kopfermann, Naturwiss. **23**, 372 (1935).

A Study of Kinetic Energies of Atomic Ions Formed by Electron Impact in Nitric Oxide and Hydrogen Chloride

ELMO E. HANSON
Department of Physics, University of Minnesota, Minneapolis, Minnesota
(Received June 6, 1936)

A study was made of the kinetic energy of the atomic ions formed by electron impact in NO and HCl. Their energy distribution was measured as a function of the electron energies at impact, and their ionization potentials were determined. The most probable values of the heats of dissociation of the molecules and of the molecular ions were calculated. Negative ions possessing up to 2.5 volts kinetic energy were observed in NO, and the electron affinity of oxygen was calculated. Negative ions found in HCl had less than 0.5 volt energy. The following is a summary of the results and the probable processes:

PROBABLE PROCESS	KINETIC ENERGY OF IONS	HEAT OF DISSOCIATION
$NO^+ \rightarrow N^+ + O(^1D_2)$	0 to 6 VOLTS	
$NO^+ \rightarrow N + O^+$		9.3±0.2 VOLTS
$NO \rightarrow N + O$		5.3±0.2
$NO + e \rightarrow N + O^-$	1 to 2.5	ELECTRON AFFINITY OF O = 2.1±0.5
$HCl^+ \rightarrow H^+ + Cl(^2P)$	0 to 10	
$HCl^+(^2\Pi) \rightarrow H + Cl^+$		4.8±0.2
$HCl^+ \rightarrow H^+ + Cl$	2 to 6	EXCITATION ENERGY OF Cl ≦ 11.6
$HCl \rightarrow H + Cl$		4.7±0.2
$HCl \pm e \rightarrow H + Cl^-$	LESS THAN 0.5	ELECTRON AFFINITY OF Cl ≦ 4.0

INTRODUCTION

IT was predicted by the quantum mechanics[1–4] that in hydrogen positive ions which would have kinetic energies much greater than the normal thermal energies could be formed by dissociation following electron impact. This was experimentally verified by Bleakney and Tate[5, 6] and later by Lozier,[7] who made a detailed study of the phenomenon.

Tate and Lozier,[8] and Lozier[9–11] have shown that such ions are also formed in all the molecular gases which they studied. Besides hydrogen the gases which have been studied are N_2, CO and O_2. Furthermore, it was shown that when negative ions are formed as dissociation products, they also might have several volts energy.

The formation of high energy ions is interpreted as arising from a transition to an unstable electronic state of the molecule. When this occurs, dissociation takes place, and the molecular components fly apart with velocities determined by: (1) the energy absorbed by the normal molecule, (2) the final states of the dissociation products and (3) the masses of the products. Thus in the process, $AB^+ \rightarrow A^+ + B$, the kinetic energy of the ion, A^+, is[8]

$$V_F = M_B/(M_A + M_B)[V_i - (U_2 - U_1)]. \quad (1)$$

M_A and M_B are the masses of the component atoms A and B, respectively, V_i is the energy absorbed by the normal molecule in its transition to the unstable state (i.e., the "ionization potential"), and $(U_2 - U_1)$ is the difference in potential energy between the final and the initial states of the molecule. Since the above formula was derived simply from considerations of the conservation of energy and of momentum it is, therefore, also applicable to the case of negative ions.

The heat of dissociation of the normal molecule and of the molecular ion may be calculated[8] if $(U_2 - U_1)$ is determined from measurements of V_F and V_i, and if the masses and the excitation energy of the products are known. The heat of dissociation of the normal molecule is given by

[1] Heitler and London, Zeits. f. Physik **44**, 455 (1927).
[2] Burrau, Kgl. Dansk. Selsk. Math. Fys. **7**, 14 (1927).
[3] Morse and Stuekelberg, Phys. Rev. **33**, 932 (1929).
[4] Condon, Phys. Rev. **35**, 658 (1930).
[5] Bleakney and Tate, Phys. Rev. **35**, 658 (1930).
[6] Bleakney, Phys. Rev. **35**, 1180 (1930).
[7] Lozier, Phys. Rev. **36**, 1285 (1930).
[8] Tate and Lozier, Phys. Rev. **39**, 254 (1932).
[9] Lozier, Phys. Rev. **43**, 776 (1933).
[10] Lozier, Phys. Rev. **44**, 575 (1933).
[11] Lozier, Phys. Rev. **46**, 268 (1934).

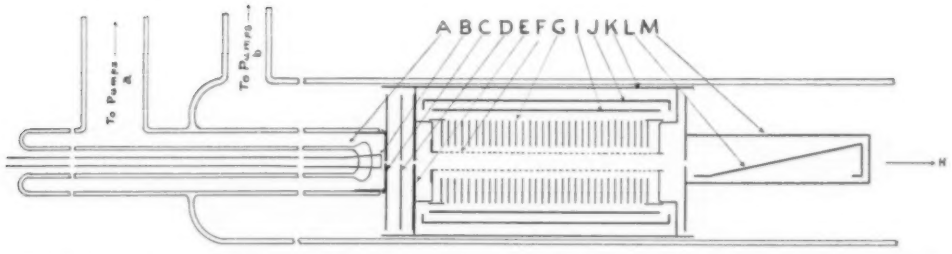

FIG. 1. The experimental tube. The filament chamber A is formed by closing the Pyrex tube with a snugly fitting spun copper cup. A 0.5 mm diameter hole in the center of this cup allows electrons to pass and be accelerated to the desired energy by controlled potentials placed between the disks C, D and E. After passing down the axis of the tube (in the direction of a collimating magnetic field H) these electrons are collected in the trap LM. The cylindrical wire gauze F is connected to E to give a field free region of ionization. The disks G allow only those ions to pass whose velocity is 98 percent perpendicular to the electron beam. The ions which qualify in direction of travel and which have sufficient energy to penetrate the differences of potential which may be placed between the elements F, G and I are collected on the cylinder I. J is a guard ring, while K is an electrical shield.

the formula,

$$D(AB) = (U_2 - U_1) - I_A - E,$$

where I_A is the ionization potential of atom A (assuming that A comes off charged) and E is the total excitation energy of the products. The heat of dissociation of the normal molecular ion, AB^+, is given by

$$D(AB^+) = (U_2 - U_1) - I_m - E, \qquad (2)$$

where I_m is the ionization potential of the molecular ion. Similarly, if negative ions having large kinetic energies are formed in the gas, the electron affinity of the atom may be calculated. Thus, if B^- ions having kinetic energy are formed, the electron affinity of B is

$$E(B) = D(AB) - (U_2 - U_1) - E. \qquad (3)$$

Thus, aside from showing the presence of unstable electronic levels in the ionized molecule, a study of the formation of high velocity ions by electron impact is valuable in that it gives values for heats of dissociation and electron affinities.

APPARATUS

The experimental tube, a modification of Tate and Lozier's apparatus,[8] was built entirely from copper, tungsten and Pyrex. Because NO and HCl are easily dissociated by a hot tungsten filament, it was necessary to employ differential pumping to maintain as low a pressure as possible around the filament while the pressure in the remainder of the tube was high enough to allow accurate measurements to be made. The leads a and b (Fig. 1) go to the same set of pumps; a difference in the rates of effusion through the two leads is effected by the difference in their diameters. A mercury cut-off in series with b can be used to lower its effusion rate still more.

In all cases the apparatus was baked out first in a quartz furnace at 800°C under a vacuum, and later in the Pyrex tube for thirty hours at 360°C.

The flow method was used to admit the gas to the apparatus, the pumps being run continuously while the gas leaked in through a capillary tube. The pressure behind the capillary was adjusted to give a working pressure in the experimental tube of about 5×10^{-5} mm of Hg.

The nitric oxide was prepared by the action of nitric acid on electrolytic copper and purified by being passed through water and over potassium hydroxide and by being fractionally distilled. A mass-spectrograph analysis by Dr. A. L. Vaughan showed the only measurable impurity was N_2O in concentration less than one percent.

The sample of hydrogen chloride was prepared by the action of H_2SO_4 on NaCl. It was dried over P_2O_5, and fractionally distilled in the usual manner. A mass-spectrograph analysis run in collaboration with Mr. A. O. Nier showed no measurable impurities.

A vacuum tube electrometer[12] was used to measure the ion currents. When used with an input resistor of 2.3×10^{10} ohms, the maximum

[12] Distad and Williams, Rev. Sci. Inst. **5**, 289 (1934).

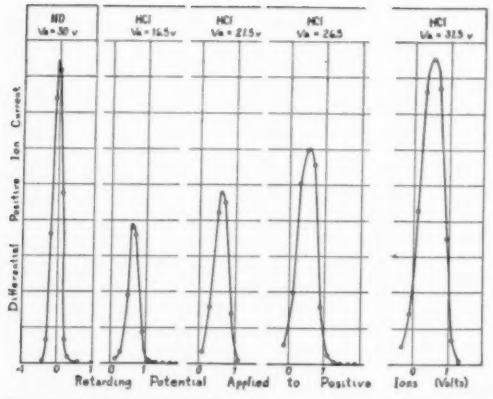

FIG. 2. Distribution in kinetic energy of molecular ions.

current sensitivity available was 3.3×10^{-16} amp./mm with random fluctuations of less than 2 mm.

METHOD

Two types of data were obtained: (1) the minimum electron energy V_i necessary to form an ion having a kinetic energy V_F, and (2) the kinetic energy distribution of ions for various electron energies.

The velocity distribution of the ions was found by the retarding potential method. The ions, in traversing the region from gauze to defining disks to collector, lost or gained an energy equal to the algebraic sum of the voltages applied between these elements. It was customary in the work on positive ions to apply a drawing out potential of 3 volts in the gauze-grid region, while this potential plus the retarding potential was applied in the opposite direction in the grid-collector region. With the electron energy fixed at some value V_a, the retarding potential V_R was changed in steps of ΔV_R and the corresponding change in positive ion current ΔI^+ was measured. ΔI^+ was, then, proportional to the number of ions having energies between $V_R-\Delta V_R/2$ and $V_R+\Delta V_R/2$. A plot of ΔI^+ *vs.* V_R gives the kinetic energy distribution of the ions. In practice ΔV_R was 0.4 volt for NO and 0.2 volt for HCl. To make it possible to utilize a high sensitivity in the amplifier, the potential drop across the input resistor was balanced by a potentiometer between the input grid and the positive end of the resistor. The sensitivity utilized in the amplifier was then 10^{-14} amp./mm.

When a retarding potential V_R will just prevent an ion from reaching the collector, the ion must have started from the electron beam with a kinetic energy equal to V_R unless there were other fields present or if there were a magnetic field present to curve the path of the ions. Since a magnetic field of 158 oersteds parallel to the tube axis was used, the ions must have started with an energy $(300b^2eH^2)/(8mC^2)$ volts[7] greater than the retarding potential. To measure the contact potentials and the space charge that might exist in the tube, use was made of the fact that the most abundant ions, the molecular ions, have only thermal velocities of a few hundredths of a volt. Velocity distribution curves of these ions are given in Fig. 2. Their maxima should within experimental error appear at $V_R=0$ volts; their measured position gives the value of the inherent potentials in the tube and therefore the

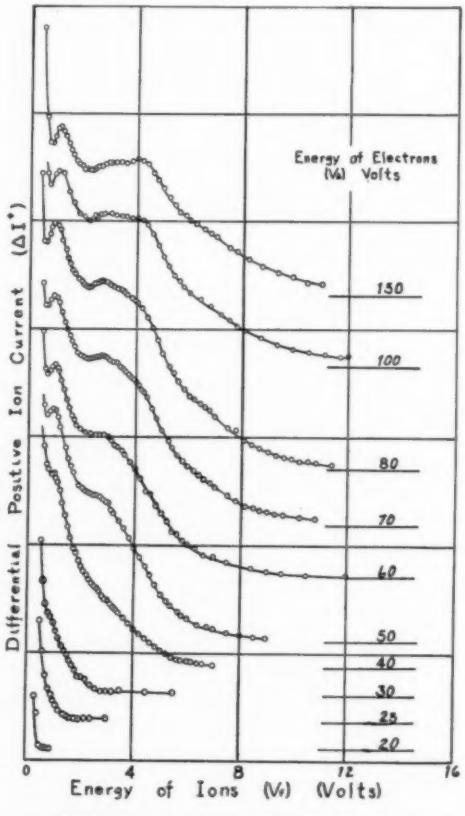

FIG. 3. Distribution in kinetic energy of positive ions formed in NO at various electron energies.

corrections to be applied to V_R. Space charge in the tube appeared to be negligible since the position of the maxima in Fig. 2 did not vary with pressure or electron current.

To measure the minimum electron energies V_i necessary to produce ions having kinetic energies V_F the following method was used: With the retarding potential set to give the desired V_F, the energy V_a of the electrons was varied and the ion currents were recorded. An upward break in the curve thus obtained gave the onset potential of the ion having the kinetic energy V_F. The voltage scale for the electrons was calibrated from the observed onset potential of the molecular ion and from the known ionization potential of the molecule. (Drawing-out potentials in the gauze-grid-collector regions served to sweep the molecular ions into the collector.) For the work on NO, Tate and Smith's value[13] of 9.5 volts was used for the ionization potential; for the work on HCl the ionization potential used was 12.9 volts from the work of A. O. Nier and the author.[14]

Negative ions were studied in much the same way as the positive ions. In addition the relative efficiency of formation of the total number of negative ions was measured as a function of the electron energy.

Results and Conclusions

Nitric oxide

The distribution in kinetic energy of the positive ions is given in Fig. 3. The increments in ion current have been reduced to the same pressure and electron current. As one might expect, the ions of higher velocity become relatively more abundant as the incident electron energy is increased. We note that the curves have two maxima, a broad maximum at about 3 volts kinetic energy, and a very sharp peak at about 1 volt. The sharp peak, which is present in all the curves above 30 volts electron energy, is probably due to ions formed by the dissociation of NO^+ (excited) from a flat repulsive potential energy curve. The ions in the broad peak must be due to a dissociation of NO^+ from a rather steep potential energy curve, there being a rise of about 10 volts in the Frank-Condon region.

[13] Tate and Smith, Phys. Rev. **39**, 270 (1932).
[14] Nier and Hanson, Phys. Rev. **48**, 477 (1935).

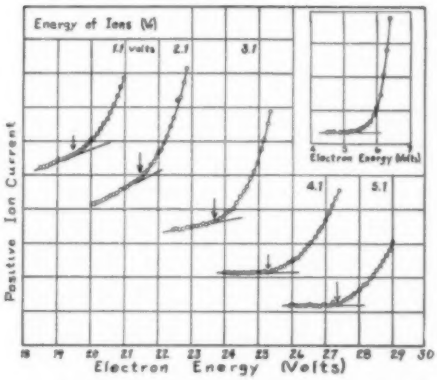

FIG. 4. Ionization potentials of positive ions having kinetic energy in NO.

In Fig. 4 we have a sample of the curves used to determine the onset potentials, V_i, of ions having kinetic energies, V_F. The curve in the inset is for the onset of NO^+, and it is used to calibrate the electron voltage scale. The mass-spectrograph studies of Hogness and Lunn,[15] and of Tate, Smith and Vaughan[16] have shown that both N^+ and O^+ are formed in NO. Vaughan[17] has also shown that the amount of O^+ formed was less than 5 percent of the N^+ formed. The upward breaks in the above curves were therefore assumed to be due to the onset of N^+ ions. This assumption gives good agreement with the experimental value of the slope of the V_i *vs.* V_F curve given in Fig. 5. From Eq. (1) we note that V_F is a linear function of V_i. The experimental values of these quantities are plotted in Fig. 5 and a straight line of the theoretical slope 16/30 is drawn through the points. The closed circles are from data taken earlier on another sample of gas. The intercept gives $(U_2-U_1)=21.7$ volts as the weighted mean. It is to be noted that Hogness and Lunn[15] and also Tate, Smith and Vaughan[16] give 22.0 volts for the ionization potential of N^+. One would expect the mass-spectrograph value to be higher inasmuch as the kinetic energy carried by the ions is not corrected for. To calculate the probable observational error, (U_2-U_1) was calculated for each of the 21 observations and the probable error obtained from the method of least squares. The value so

[15] Hogness and Lunn, Phys. Rev. **30**, 26 (1927).
[16] Tate, Smith and Vaughan, Phys. Rev. **48**, 525 (1935).
[17] Vaughan, Thesis, Univ. of Minn. (1934).

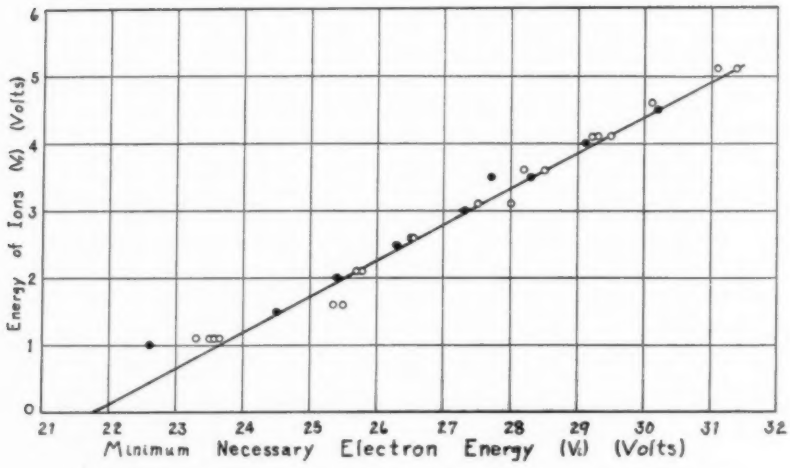

FIG. 5. Kinetic energies *vs.* ionization potentials of positive ions in NO.

obtained was ± 0.03 volt; however, it was felt that a safer estimate for the probable systematic error would be ± 0.2 volt.

If one assumes the process for forming these kinetic energy ions in NO to be $NO^+ \rightarrow N^+ + O$, the heat of dissociation of NO would be $D(NO) = 21.7 - 14.48 = 7.22$ volts, where 14.48 volts is the spectroscopic value for the ionization potential of atomic nitrogen. Kaplan,[18] however, has shown from band spectra that $D(NO) \leqq 6.1$ volts. We must therefore assume that one of the products is in an excited state. In Table I are given the possible states of excitation[19] of N^+ and O with the corresponding values of $D(NO)$. The only reasonable values for $D(NO)$ are those obtained from the combinations $N^+(^1D_2) + O(^3P_0)$ and $N^+(^3P_0) + O(^1D_2)$. From Lozier's work[10, 11] it appears that it is more probable for the uncharged dissociation product to be excited. Also if N^+ were excited, it would involve a double electron jump, which is perhaps unlikely.[20] The difference between the two possible values of $D(NO)$ is only 0.06 volt, which is well within our probable error.

Using our value of 5.27 volts for $D(NO)$, and the known value for $D(O_2)$ in the thermochemical equation,

$$(1/2)D(N_2) + (1/2)D(O_2) - 0.94 = D(NO),$$[21]

we obtain for $D(N_2)$ the value 7.32 volts. The latest value given by Kaplan[22, 23] from the band spectra is 7.4 volts, with which our value is in very good agreement.

A limit may be sent on $D(NO^+)$. The mass-spectrographic work mentioned above[15, 16] showed that O^+ was formed about one volt lower than N^+. For the process, $NO^+ \rightarrow N + O^+$, $(U_2 - U_1)$ should be less than the corresponding value for the process $NO^+ \rightarrow N^+ + O$ by the difference in the ionization potentials of N and O, i.e., by $14.48 - 13.55 = 0.93$ volt. Therefore, $(U_2 - U_1)$ for the first process above is $21.7 - 1.95 - 0.93 = 18.82$ volts, and $D(NO^+) = 18.82 - 9.5 = 9.3$ volts, where 9.5 is the ionization potential of NO.

TABLE I. *Possible states of excitation of N^+ and O and the corresponding heats of dissociation.*

State	N^+ Term Value (electron volts)	State	O Term Value (electron volts)	$D(NO)$ (electron volts)
$^3P_0$	0	$^3P_0$	0	7.22
$^3P_0$	0	$^1D_2$	1.95	5.27
$^3P_0$	0	$^1S_0$	5.27	3.05
$^1D_2$	1.89	$^3P_0$	0	5.33
$^1D_2$	1.89	$^1D_2$	1.95	3.48
$^1S_0$	4.03	$^3P_0$	0	3.19

[18] Kaplan, Phys. Rev. **37**, 1410 (1931).
[19] Bacher and Goudsmit, *Atomic Energy States* (McGraw-Hill Book Company, 1932).
[20] Mulliken, Phys. Rev. **46**, 144 (1934).
[21] Landolt Bornstein **2**, 1495 (1923).
[22] Kaplan, Phys. Rev. **45**, 898 (1934).
[23] Lozier, Phys. Rev. **46**, 268 (1934).

This value is independent of the ionization potential of NO since it was also used to calibrate the electron voltage scale. We can only set a limit on $D(NO^+)$ since r_e, the internuclear equilibrium distance, is not known.

Negative ions in NO

In Fig. 6 is given the relative efficiency of production of negative ions in NO. The shape of the curve and the position of the maxima agree in general with the curve given by Tate and Smith.[13] These ions, which have been identified as O^-,[16] have an appreciable amount of kinetic energy. The ionization potentials of the kinetic energy ions are given in Fig. 7. The currents that were measured were very small, which accounts for the points not falling very well on a smooth curve. In Fig. 8 is given the straight line of the theoretical slope 14/30 obtained by plotting V_1 *vs.* V_F. For values of V_F lower than 1.1 and greater than 2.1 volts, the points deviate consistently from a straight line. The intercept of the line gives $U_2-U_1=3.2$ volts, with a systematic error estimated to be less than ± 0.5 volt. If the process is $NO+e\rightarrow N+O^-$, the electron affinity of oxygen is $E(O)=D(NO)-3.2=2.1 \pm 0.5$ volt. This is in good agreement with Lozier's value[11] of 2.2 volts. It is not likely that the nitrogen atom comes off excited in the process since this would make the value of $E(O)$ greater than 4.4 volts. This would mean that in Lozier's experiment O^- would have to possess at least 2.2 volts excitation energy. The little that is known about excited states in negative ions seems to indicate that they are for the most part unstable.[11]

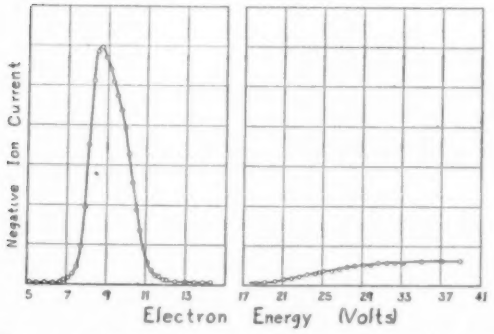

FIG. 6. Relative efficiency of formation of negative ions in NO.

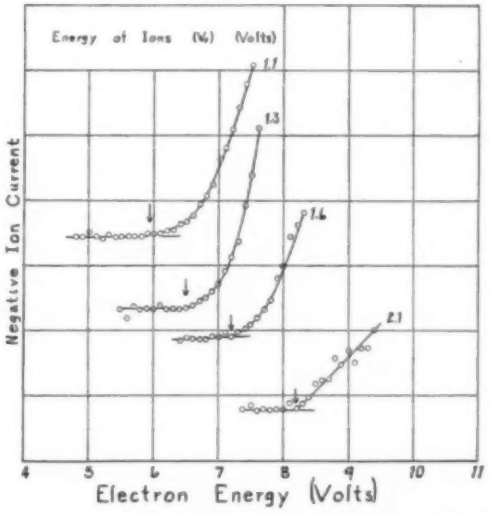

FIG. 7. Ionization potentials of negative ions having kinetic energy in NO.

By an empirical method of extrapolation, Glockler[24] has estimated the value of $E(O)$ to be 3.8 volts. To reconcile our value to this would require O^- to have 1.7 volts excitation energy, a value that seems high from the standpoint of stability. Since Glockler's extrapolation was rather long, the discrepancy is not as serious as it might appear.

HYDROGEN CHLORIDE

In Fig. 9 are given the kinetic energy distribution curves for positive ions in HCl. It is obvious that these ions are H^+ ions since from momentum and energy considerations neither HCl^+ nor Cl^+ could possess such velocities. That these ions were H^+ was confirmed by Nier and the author[14] by using a mass spectrograph. The most prominent features of the curves in Fig. 8 are the three sharp maxima that become evident above 40 volts electron energy. The sharpness of these peaks indicates that the repulsive potential energy curves which describe the dissociation process must be rather flat in the Franck-Condon region. The most likely process for the formation of the ions of the peaks is $HCl^{++}\rightarrow H^+ + Cl^+(^3P)$. To form an H^+ ion having 6 volts kinetic energy by this process would require 37 volts electron

[24] Glockler, Phys. Rev. **46**, 268 (1934).

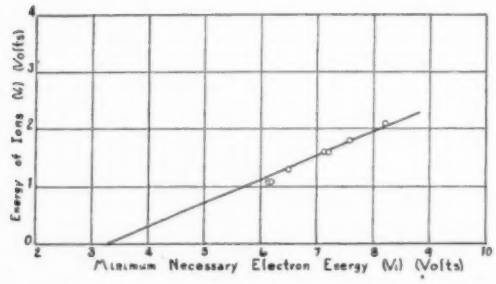

FIG. 8. Kinetic energy *vs.* ionization potentials of negative ions in NO.

energy, while if the Cl^+ were excited to the next energy level it would require 48.5 volts energy to form such an ion. To explain the triplet structure of the peaks we might assume that there exists for each J value of $Cl^+(^3P)$ an unstable potential energy curve. Since the separation in energy of the three peaks is much greater than the corresponding differences in the triplet levels of $Cl^+(^3P)$, the highest potential energy curve must be the steepest and the highest energy peak should be the broadest. It is of interest that this is true. Mulliken[25] has tentatively constructed such triplet repulsive potential energy curves for the process $HCl^+ \rightarrow H + Cl^+(^3P)$. The above data are evidence in favor of the existence of such states for the doubly charged molecular ion.

In Fig. 10 are given samples of the ionization potential curves for kinetic energy ions. In the inset is given the corresponding curve for the onset of HCl^+; it is used as a calibration curve for the electron voltage scale. The readings for these curves were staggered, the open circles being for one sequence of readings, while the closed circles are for another sequence. The negative slope of the base lines of these curves was probably due to negative ions from a small amount of NO which existed as an impurity in the tube. These small negative currents did not interfere with the measurement of the positions of the breaks in the ionization curves.

For the V_F *vs.* V_i graph of Fig. 11 the mean straight line was drawn with the theoretical slope 35/36. The intercept gives for $U_2 - U_1$ the value 18.35 volts. The appearance potential of H^+ ions in the mass-spectrograph[14] study was 18.6 ± 0.3 volts; this is higher as one would expect if all the H^+ ions carried some kinetic energy. From a calculation on the deviation of $U_2 - U_1$ from its mean for each individual observation on the basis of least squares the probable observational error is 0.002 volt; we feel

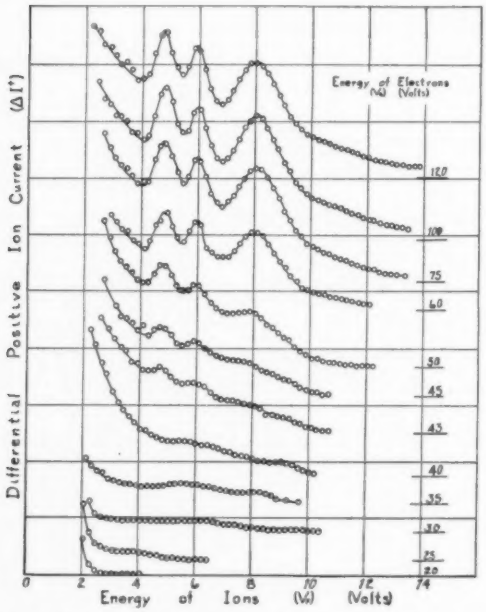

FIG. 9. Distribution in kinetic energy of positive ions formed in HCl.

[25] Mulliken, Rev. Mod. Phys. **4**, 6 (1932).

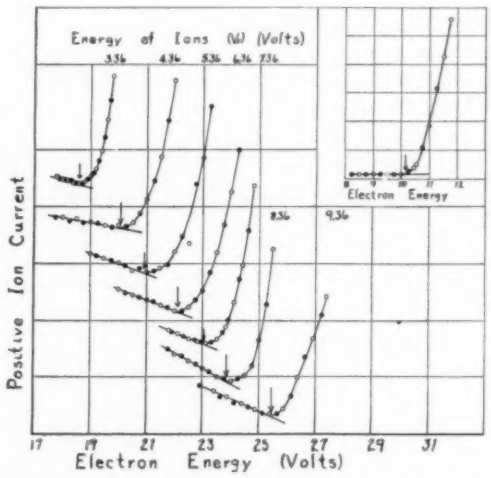

FIG. 10. Ionization potentials of positive ions having kinetic energy in HCl.

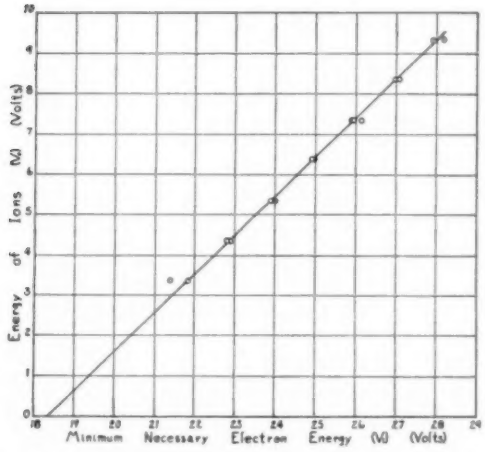

FIG. 11. Kinetic energies vs. ionization potentials of positive ions in HCl.

certain that the systematic error must be less than 0.2 volt.

Assuming that the process for the formation of these ions is $HCl^+ \rightarrow H^+ + Cl(^2P^0_{3/2})$, we get for $D(HCl)$ the value $18.35-13.54=4.8\pm0.2$ volts, which is 0.4 volt higher than the rather reliable chemical value.[26] The only other possible process would be $HCl^+ \rightarrow H^+ + Cl(^2P^0_{1/2})$; if we assume this process, $D(HCl)=4.7\pm0.2$ volts, which still does not agree within the probable error with the chemical value of 4.42 volts. The explanation for this may be that the ionization potential of HCl, upon which our value for U_2-U_1 depends, is actually lower than the value used. It should be pointed out that the values for the ionization potential of HCl given previous[27, 28] to the work of Nier and Hanson[14] would give for $D(HCl)$ a value 0.9 volt still higher.

The heat of dissociation of HCl^+ may be calculated. Two stable states for HCl^+ have been observed from band spectra,[29, 30] a $^2\Pi$ and a $^2\Sigma^+$ state. The $^2\Sigma^+$ state when dissociated gives $H^+ + Cl$; the $^2\Pi$ state is made up of $H + Cl^+$. Therefore, the horizontal asymptote of the $^2\Pi$ potential energy curve must lie below the

[26] Landolt Bornstein **2**, 1489 (1923); Frank, Trans. Faraday Soc. **21**, 536 (1926).
[27] Knipping, Zeits. f. Physik **7**, 328 (1921).
[28] McKaye, Phys. Rev. **24**, 319 (1925).
[29] Brice and Jenkins, Nature **123**, 944 (1929).
[30] Kulp, Zeits. f. Physik **67**, 7 (1931).

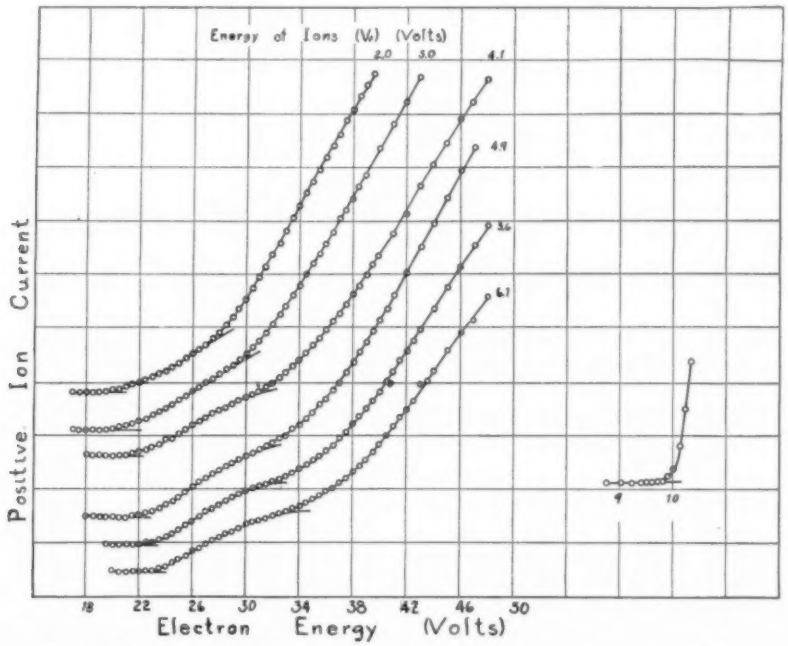

FIG. 12. The first and second ionization potentials of kinetic energy ions in HCl.

asymptote of the $^2\Sigma^+$ curve by the difference in the ionization potentials of atomic hydrogen and atomic chlorine, i.e., by 0.58 volt. Subtracting the ionization potential of HCl from $U_2-U_1-0.58$ we get $D(HCl^+\,^2\Pi)=4.76$ volts. This value is independent of the ionization potential of HCl since that quantity is contained in U_2-U_1 as an additive constant. Since r_e is nearly the same for $HCl^+(^2\Pi)$ as it is for HCl,[30] we can do more than set a limit on $D(HCl^+\,^2\Pi)$.

When the curves for the determination of the ionization potentials of high velocity H^+ ions were continued to higher electron energies, a second break was found in the curves. In Fig. 12 are given a few such curves. In Table II is given a summary of the results and the calculated values of U_2-U_1 for the process. Within experimental error U_2-U_1 is constant and equal to 29.5 volts in the region $V_F=3.0$ to 6.1 volts. This indicates that the process is $HCl^+\rightarrow H^++Cl$ (excited), where the excitation energy of Cl is 11.6 volts. We note that there are several energy levels in Cl near this value, notably the so called 4° level at 11.6 volts.[19] The excitation energy is too low to give the process $HCl^{++}\rightarrow H^++Cl^+$.

Negative ions in HCl

Negative ions, which have been identified as Cl^-,[14, 31] were observed. The kinetic energy of these ions was definitely less than 0.5 volt.

TABLE II. *The second ionization potentials of positive ions with kinetic energy in HCl.*

V_F	V_i(corrected)	$U_2-U_1=V_i-36/35V_F$
2.0 volts	30.3 volts	28.2 volts
3.0	32.5	29.4
4.1	33.6	29.4
4.9	34.5	29.45
5.6	35.4	29.6
6.1	35.9	29.6
7.1	38.1	30.8
8.2	38.8	30.3
9.5	40.8	31.3

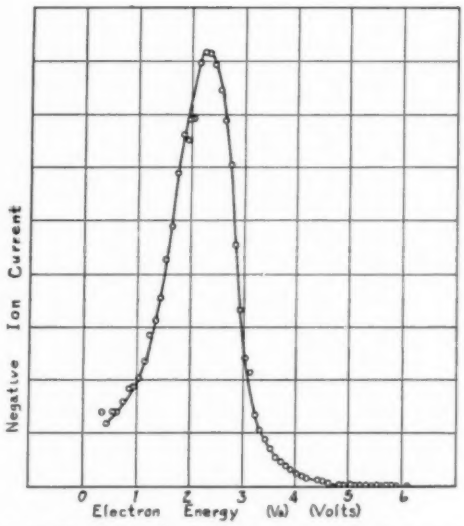

FIG. 13. Total negative ion current per unit electron current in HCl.

In Fig. 13 is given the relative efficiency of production of these ions. The curve exhibits the characteristic sharp peak usually observed for negative ions. Because the electron and the ion currents became very small in the region near an electron energy of zero, it was not possible to determine whether the relative efficiency became zero for $V_a>0$. When we extrapolate the symmetrical portion of the curve to zero efficiency, we get 0.4 volt for the onset potential. This makes the electron affinity of Cl equal to or greater than $D(HCl)-0.4=4.0$ volts. In view of our long extrapolation, the agreement with the value 3.7 volts cited by Glockler[24] is good.

The author wishes to express his gratitude to Professor John T. Tate, under whose direction the work was performed.

[31] Aston, *Isotopes* (Longmans Green & Co., 1924), p. 65.

On the Structure of the Nuclei Between Helium and Oxygen

E. FEENBERG* AND E. WIGNER†
University of Wisconsin, Madison, Wisconsin
(Received October 10, 1936)

In order to test the present assumptions on nuclear forces, the theory is applied to the nuclei in which the first p shell of protons and neutrons is being built up, i.e., to the nuclei with masses between 5 and 16. The Hartree-Fock approximation is used for the numerical calculations, but the more qualitative results are independent to a large degree of the approximations used. The angular momenta of the ground states appear to be given correctly by the theory. Although the wave functions used do not correspond to preformed alpha-particles, the first-order energies exhibit a marked four-shell structure. The experimental energy difference between the nuclear pairs $(N, N+1)$, $(N+1, N)$ may possibly be somewhat larger than the difference in the electrostatic energies. Support for the use of spin exchange (Heisenberg) forces to account for the singlet-triplet separation in the deuteron is found in the singlet-triplet separation inferred from the Li^6-He^6 normal state energy difference. However, the $B^{10}-Be^{10}$ and $N^{14}-C^{14}$ normal state differences do not fit the simple theory which is adequate for the singlet-triplet spacing in the two and six particle problems.

I. INTRODUCTION

IT is generally accepted now that the explanation of the binding energies and scattering properties of the nuclei n, H^1, H^2, H^3, He^3, He^4 requires several kinds of forces.[1] The forces which are generally assumed at present between a proton and a neutron ("between unlike particles") are: (1) a "Majorana force" involving an exchange P of the Cartesian coordinates of the two particles and (2) a "Heisenberg force" involving the product of a Cartesian coordinate exchange P and a spin coordinate exchange Q. The Heisenberg force has about $\frac{1}{4}$ the depth of the Majorana force and the same range of action. For all present calculations the exact dependence of the potential on distance seems to be relatively unimportant and we shall use, for the sake of convenience, the usual

$$(1-g)A_{rr}e^{-r^2/r_0^2}P=(1-g)A_{rr}e^{-\alpha r^2}P \quad (1a)$$

for the Majorana force and

$$gA_{rr}e^{-\alpha r^2}PQ \quad (1b)$$

for the Heisenberg force between unlike particles. Here $A_{rr}=72\ mc^2$, $r_0=2.25\cdot10^{-13}$ cm, $g=0.22$ and $\alpha=16$ if r is measured in units of $\hbar/c(Mm)^{\frac{1}{2}}=8.97\cdot10^{-13}$ cm.

The forces between like particles are less well known. Between pairs of protons and pairs of neutrons one assumes a potential with a depth $A_{pp}=41\ mc^2$ and the same width as between unlike particles.[1] This force is either assumed to involve an exchange P of the Cartesian coordinates

$$A_{pp}e^{-\alpha r^2}P \quad (2a)$$

or else the scalar product of their spin operators:

$$-\tfrac{1}{3}A_{pp}e^{-\alpha r^2}(\sigma_1\cdot\sigma_2). \quad (2b)$$

The latter possibility can be considered, because of Dirac's identity for antisymmetric wave functions[2]

$$-\tfrac{1}{3}(\sigma_1\cdot\sigma_2)=\tfrac{1}{3}+\tfrac{2}{3}P_{12}, \quad (3)$$

as the sum of an ordinary and an exchange force. It is undecided, at present, which of the two forms of interaction deserves preference. In fact it has been proposed[3] to assume interactions which would give equal attractions between pairs of like and unlike particles in the singlet state. We obtain a problem having this property by assuming for the interaction between like particles the same forces as between unlike particles:[4]

$$(1-g)A_{pp}e^{-\alpha r^2}P+gA_{rr}e^{-\alpha r^2}PQ. \quad (2c)$$

* Now at the Institute for Advanced Study.
† Now at Princeton University.
[1] E. Feenberg and J. K. Knipp, Phys. Rev. **48**, 906 (1935). E. Feenberg and S. S. Share, Phys. Rev. **50**, 253 (1936).
[2] Cf. P. A. M. Dirac, *Quantum Mechanics* (Oxford, 1935), §19, §61; J. H. Van Vleck, Phys. Rev. **48**, 367 (1935).
[3] G. Breit and E. U. Condon, private communications.
[4] The assumption that the forces between all kinds of particles are the same was first put forward by L. A. Young, Phys. Rev. **47**, 972 (1935).

For like particles the second part of this expression can be written, because of the antisymmetry of the wave function in the coordinates of the protons (or neutrons), as an ordinary repulsive force $-gA_{rr}e^{-\alpha r^2}$. We shall consider this "all forces equal model" because it is at least a useful approximation, the properties of which in some cases, can be discussed with greater ease[5] than the properties of a model with forces (2*a*) or (2*b*). In addition to the forces (2), there are between protons the electrostatic forces and also the ordinary spin-orbit and spin-spin interactions are generally assumed to exist. These latter interactions seem to play only a minor role in nuclear problems.

Of course, it is most probable that the interaction of the constituents of nuclei cannot be described at all rigorously by a Schrödinger equation, the variables of which are the Cartesian and spin coordinates of the protons and neutrons only. A similar description is impossible, strictly speaking, for the extranuclear electrons also. The cause of the interaction is probably some field in both cases—the electromagnetic field of light quanta in the second case and, perhaps, the electron-neutrino field in the first case. The elimination of the field variables is possible always in a certain approximation only and breaks down in a higher order approximation. This is manifested by the phenomena of spontaneous emission and line width for the extranuclear electrons and by the β disintegration, for example, in the case of nuclear constituents. Nevertheless, the usual Schrödinger equation gives a practically perfect description of atomic states and it may be hoped that a similar equation exists for the nuclear constituents also.

We shall attempt here to find experimental criteria which can be used to answer the following three questions:

(1) Whether or not the difference between proton-proton and neutron-neutron interaction is only the Coulomb force.

(2) Whether (2*a*), (2*b*) or (2*c*) is the more correct form for this interaction.

(3) Whether or not the assumption is correct that the neutron-proton interaction operator is a linear combination of Majorana and Heisenberg terms.

Before examining these questions we apply the Hartree-Fock approximation method to the light nuclei between and including Li^6 and O^{16} and perform the same calculation for the position of the terms arising from the lowest configuration which Slater[6] has made for atomic spectra.

[5] It is equivalent to "approximation (2)" of the paper of one of the present writers in this issue.

II. Hartree-Fock Calculations

It is well known that the Hartree-Fock method gives only very roughly correct solutions of the nuclear wave equation. This has been pointed out by Weizsäcker, Flügge and Heisenberg[7] for the older models (no interaction between like particles). It is true, however, also for the forces (1) and (2), though to a somewhat lesser degree. Bethe and Bacher[8] performed similar calculations for both light and heavy nuclei using the newer model with the result that the method gives practically no binding energy for the observed nuclear densities. Since the Schrödinger equation without doubt has solutions with much lower characteristic values at the same densities (conglomerates of slightly compressed alpha-particles), the result obtained by Bethe and Bacher must be interpreted as revealing the inaccuracy of the Hartree approximation in nuclear problems. Considering the great similarity between the nuclear and metallic wave equations and the importance of the correlation energy in the latter,[9] this is not surprising.

Table I. *Binding energies of elements with masses between 4 and 16.*

n_1		$n_2=0$	1	2	3	4	5	6
0	He	55	—	56				
1	Li		62	76	89			
2	Be			109	113	126		
3	B			110	125	147	153	
4	C				141	176	186	202
5	N					180	201	222
6	O						215	246

[6] Cf. E. U. Condon and G. Shortley, *The Theory of Atomic Spectra* (Cambridge, 1936). In the Hartree approximation the nuclei of the group He^6-O^{16} are obtained by successive additions to the p shell which is completed at O^{16}. This has been first pointed out by J. H. Bartlett, Nature **130**, 165 (1932). Cf. also his letter in the Phys. Rev. **41**, 370 (1932) and G. Gamow, Zeits. f. Physik **89**, 592 (1934) and especially W. M. Elsasser, J. de phys. **4**, 549 (1933); **5**, 389 and 635 (1934).

[7] C. F. v. Weizsäcker, Zeits. f. Physik **96**, 431 (1935); S. Flügge, p. 459; W. Heisenberg, p. 473.

[8] H. A. Bethe and R. F. Bacher, Rev. Mod. Phys. **8**, 82 (1936).

[9] It is more than half of the binding energy in Na.

Nevertheless, it can be expected that in the case of light nuclei the order of the terms will be given correctly by such a calculation. This is true for the corresponding atomic spectra[6] although the calculated ratios of the term differences show marked deviations from the experimental values.

Table I gives the elements with which we shall be concerned; n_1+2 is the number of protons, n_2+2 the number of neutrons. The figures in the table are the binding energies[10] in units of mc^2. As long as we neglect the Coulomb forces, the constitutions of elements symmetric with respect to the main diagonal of the table are identical. The theory of holes[11] gives us furthermore the constitution of a nucleus from its mirror image with respect to the other diagonal.

In this section we shall neglect the Heisenberg forces. This makes the Hamiltonian operate on the Cartesian coordinates only and both protons and neutrons will have a "multiplicity"; each resultant spin angular momentum will be a good quantum number. In addition to these, we have the total azimuthal quantum number. The possible terms for Be^9, for example, can be determined by combining every term of the configuration s^2p^2 of the protons with every term arising from the configuration s^2p^3 of the neutrons.[12] The former terms are ^1S, ^1D, ^3P, the latter ones ^2P, ^2D, ^4S. Taken together these two configurations yield for the whole nucleus the terms ^{12}P, ^{12}D, ^{14}S, ^{12}P, ^{12}D, ^{12}F, ^{12}S, ^{12}P, ^{12}D, ^{12}F, ^{12}G, ^{14}D, ^{32}S, ^{32}P, ^{32}D, ^{32}P, ^{32}D, ^{32}F, ^{34}P. The first index represents the multiplicity of the protons, the second the multiplicity of the neutrons. (The Heisenberg forces will introduce an interaction between proton spin and neutron spin and split many of these terms into several new ones.)

Since the number of terms is quite high, we first want a quick orientation as to which of the terms will be the lowest ones. It is clear that most of the terms just enumerated lie high in the continuous spectrum. We shall be interested in the low terms only.

For this first orientation, we shall assume the interaction between like particles to be the same as that between unlike particles. This amounts to assuming (1a) to be valid for all pairs of particles, since the interaction (1b) involving the spin is omitted in this section. We shall call this model the "equal orbital forces model." It does not constitute a good approximation to either (1a) and (2a) or to (1a) and (2b), but it is useful in obtaining a first orientation.

In the equal orbital forces model, the Hamiltonian is symmetric in all particles and acts on the Cartesian coordinates only. Four particles can be in the same orbit, namely two protons and two neutrons. Hence, not only those representations of the symmetric group will occur[13] which occur in atomic spectra, but we shall have representations with 1, 2 and also 3, 4 as addends. The representations play a very great role in the calculation of the potential energy, because the interaction operator contains a permutation of the particles.

The kinetic energy is the same for all wave functions arising from the same configuration.

If $\psi_1, \psi_2, \cdots \psi_s$ belong to a certain representation D of the symmetric (permutation) group of $n=n_1+n_2$ particles, we can calculate the matrix elements of the potential energy

$$V_{\kappa\kappa}=(\psi_\kappa(x_1\cdots x_n), \sum_{\alpha\beta} J(x_\alpha-x_\beta)P_{\alpha\beta}\psi_\kappa(x_1\cdots x_n)), \quad (4)$$

which is equal to

$$V_{\kappa\kappa}=\sum_{\alpha\beta}\sum_{\lambda} D(\alpha\beta)_{\lambda\kappa}(\psi_\kappa, J(x_\alpha-x_\beta)\psi_\lambda) \quad (5)$$

because of the relations

$$P_{\alpha\beta}\psi_\kappa(x_1\cdots x_n)+\sum_{\lambda} D(\alpha\beta)_{\lambda\kappa}\psi_\lambda(x_1\cdots x_n). \quad (6)$$

Only those terms will be great in the sum (5) for which $\kappa=\lambda$; in the other terms the positive and negative regions will about cancel each other. This canceling would be exact if the range of the forces were very long: in this case J could be taken out of the integral as a constant $J(0)$ and the remaining integral would vanish for $\kappa\neq\lambda$ and be 1 for $\kappa=\lambda$. The whole $V_{\kappa\kappa}$ is for very

[10] Computed from the mass values given by Bethe and Livingston at the Cornell Nuclear Conference, July, 1936. The C^{14} value is taken from a paper by T. W. Bonner (same conference).

[11] Cf. W. Heisenberg, Ann. d. Physik **10**, 888 (1931); G. Shortley, Phys. Rev. **43**, 451 (1933).

[12] Cf. reference 8, Table XIV for a complete list of terms.

[13] Cf. E. Wigner, *Gruppentheorie* etc. (Braunschweig, 1931), Chap. 13. The "all orbital forces equal" model is equivalent to approximation (1) of the paper mentioned in reference 5.

TABLE II. *The terms of a p^n configuration which correspond to a definite partition.*

p^2		p^3		
2 $S\ D$ 1/1	1+1 P −1/1	3 $F\ P$ 1/1	2+1 $D\ P$ 0/2	1+1+1 S −1/1

p^4				p^5			
4 $G\ D\ S$ 1/1	3+1 $F\ D\ P$ 1/3	2+2 $D\ S$ 0/2	2+1+1 P −1/3	4+1 $P\ D\ F$ 2/4	3+2 $G\ F\ D\ P$ 1/5	3+1+1 $D\ S$ 0/6	2+2+1 P −1/5

p^6				
4+2 $G\ F\ D\ D\ S$ 3/9	3+3 $F\ P$ 1/5	4+1+1 $F\ P$ 2/10	3+2+1 $D\ P$ 0/16	2+2+2 S −1/5

long range forces

$$V_{\kappa\kappa}=J(0)\sum_{\alpha\beta}D(\alpha\beta)_{\kappa\kappa}. \tag{7}$$

The last sum has to be extended over all $n(n-1)/2$ transpositions and is equal to $n(n-1)/2$ times the character $\chi(T)$ corresponding a transposition, divided by the dimension $\chi(E)=s$ of the representation:

$$V_{\kappa\kappa}=J(0)(n(n-1)/2)\chi(T)/\chi(E). \tag{8}$$

This expression is independent of the detailed shape of the wave function and depends only on the representation D to which the wave function belongs. The formulas for the characters of representations[14] show that it is greatest for that representation which contains as many 4's as possible and in addition to these only one other addend. The terms corresponding to this representation will be called the "low terms."

TABLE III. *Interaction energies between like particles.*

	p^2 or π^2			p^3 or π^3		
INTERACTION	^1S	^1D	^3P	^2P	^2D	^4S
(2*a*)	$L+2K$	$L-K$	$-L+3K$	$5K$	$3K$	$-3L+9K$
(2*b*)	$L+2K$	$L-K$	$(-L+3K)/3$	$L+2K$	L	$-L+3K$
ORDINARY FORCE	$L+2K$	$L-K$	$L-3K$	$3L-4K$	$3L-6K$	$3L-9K$

INTERACTION	p^4 or π^4	p^5 or π^5	p^6 or π^6
(2*a*)	ADD $-L+8K$ to p^2	$-2L+16K$	$-3L+24K$
(2*b*)	ADD $L+2K$ to p^2	$2L+4K$	$3L+6K$
ORDINARY FORCE	ADD $5L-10K$ to p^2	$10L-20K$	$15L-30K$

It is easy to determine the terms of a p^n configuration which correspond to a definite partition[15] and the result is given in Table II. The last row contains $\chi(T)/\chi(E)$. The four s particles form a closed shell and contribute the same amount of energy to every term of a configuration.

We proceed now to the secular equations, using (2*a*) and (2*b*) for the interaction between like particles. The kinetic energy has been omitted, because it is the same for all terms of the same configuration. In the calculation of the potential energy, the closed s shell has been omitted for the same reason and the wave function for the p particles only used. To illustrate, for Li^7 the configuration is $p\pi^2$, the Greek letter π corresponding to the neutron, p to the proton. First the wave functions for the different π^2 terms ^1S, ^1D, ^3P are written down. Then, for example, to calculate the ^2P term, wave functions with the azimuthal quantum number 1 are constructed from the proton wave function and the ^1S neutron function, and from the proton function and the ^1D neutron function. The spin functions can always be omitted when calculating in this way.

With this choice of wave functions, the interaction between like particles has only diagonal elements, these being the sum of the energies of the proton term and the neutron term used. The matrix elements for the proton-neutron

[14] I. Schur, Berl. Ber. (1908), p. 664. We found the following formula most suitable for the calculation of characters:

$$\{\lambda_1,\lambda_2,\cdots\lambda_\rho\}=\{\lambda_1-1,\lambda_2,\cdots,\lambda_\rho\}+\{\lambda_1,\lambda_2-1,\cdots\lambda_\rho\}+\cdots+\{\lambda_1,\lambda_2,\cdots\lambda_\rho-1\}.$$

Here the symbol $\{\lambda_1,\lambda_2,\cdots\lambda_\rho\}$ is the character of a permutation in the representation corresponding to the partition $\lambda_1+\lambda_2+\cdots+\lambda_\rho=n$. The left side gives the character of the representation of the permutation group of n elements, the right side contains characters of representations of the permutation group of $n-1$ elements. The formula holds for every permutation and can be used as a recursive formula. On the right side, all symbols must be omitted in which one number in the bracket is greater than the preceding. If the last figure in a bracket is a zero, it can be dropped. Thus, e.g., for a transposition,

$$\{4+1+1\}=\{3+1+1\}+\{4+0+1\}+\{4+1+0\}=\{3+1+1\}+\{4+1\}.$$

The values of these symbols can be obtained by a further application of the recursive formula, since, for a transposition, all symbols can be reduced finally to $\{2\}$ and $\{1+1\}$ which are $+1$ and -1, respectively. They are, for a transposition, 0 and 2, so that the character corresponding to a transposition in $\{4+1+1\}$ is 2.

[15] The simplest method for this is described in Section 4 of reference 3. (Cf. Table I there.)

interaction must be calculated separately for each case.

It is well known that all potential energy integrals for the p^n configuration can be expressed in terms of the following two,

$$L=\int\cdots\int (x/r)^2R_p(r)^2(x'/r')^2R_p(r')^2 \times J(|r-r'|)d\tau d\tau',$$
$$K=\int\cdots\int (xy/r^2)R_p(r)^2(x'y'/r'^2) \times R_p(r')^2J(|r-r'|)d\tau d\tau' \quad (9)$$

by means of the identity

$$L-2K=\int\cdots\int (x/r)^2R_p(r)^2(y'/r')^2 \times R_p(r')^2J(|r-r'|)d\tau d\tau', \quad (10)$$

where $(x/r)R_p(r)$ denotes the p wave function. If there is any ambiguity we shall use L and K with the index $\nu\pi$ if J signifies the interaction between unlike particles, with an index $\nu\nu$ if it is the interaction between like particles, and with an index c if J is the electrostatic potential.

The matrix elements for the interaction energies between like particles are tabulated in Table III.

Table IV contains the matrix elements

TABLE IV. *Matrix elements of the interaction between unlike particles.*[16]

Li^6

$(^2P^2P)^{22}S$	$L+2K$,
$(^2P^2P)^{22}D$	$L-K$,
$(^2P^2P)^{22}P$	$-L+3K$

Li^7

$(^2P^1D)^{21}F$	$2L-2K$,
$(^2P^1D)^{21}D$	$-L+4K$,
$(^2P^3P)^{23}P$	$L+2K$,
$(^2P^3P)^{23}S$	$-2L+6K$,
$(^2P^3P)^{23}D$	L,

	$(^2P^1S)^{21}P$	$(^2P^1D)^{21}P$
$(^2P^1S)^{21}P$	$2(L+2K)/3$	$(20)^{\frac{1}{2}}(L-K)/3$
$(^2P^1D)^{21}P$	$(20)^{\frac{1}{2}}(L-K)/3$	$(L+14K)/3$

Be^8

	$(^1S^1S)^{11}S_+$	$(^1D^1D)^{11}S_+$
$(^1S^1S)^{11}S_+$	$4(L+2K)/3$	$(80)^{\frac{1}{2}}(L-K)/3$
$(^1D^1D)^{11}S_+$	$(80)^{\frac{1}{2}}(L-K)/3$	$2(L+14K)/3$

	$(^1S^1D)^{11}D_+$	$(^1D^1D)\ D_+$
$(^1S^1D)^{11}D_+$	$4(2L+K)/3$	$(56)^{\frac{1}{2}}\ L-K)/3$
$(^1D^1D)^{11}D_+$	$(56)^{\frac{1}{2}}(L-K)/3$	$(-2L+23K)/3$

$(^1D^1D)^{11}G_+$ $\quad 4L-4K.$

Li^8

	$(^2P^2P)^{22}P$	$(^2P^2D)^{22}P$
$(^2P^2P)^{22}P$	$(L+7K)/2$	$(15)^{\frac{1}{2}}(L-K)/2$
$(^2P^2D)^{22}P$	$(15)^{\frac{1}{2}}(L-K)/2$	$(-L+13K)/2$

	$(^2P^2D)^{22}D$	$(^2P^2P)^{22}D$
$(^2P^2D)^{22}D$	$(L+7K)/2$	$3^{\frac{1}{2}}(L-K)/2$
$(^2P^2P)^{22}D$	$3^{\frac{1}{2}}(L-K)/2$	$(3L+K)/2$

$(^2P^2D)^{22}F$ $\quad 2L-K.$

Be^9

	$(^1S^2P)^{12}P$	$(^1D^2P)^{12}P$	$(^1D^2D)^{12}P$
$(^1S^2P)^{12}P$	$2L+4K$	0	$(20/3)^{\frac{1}{2}}(L-K)$
$(^1D^2P)^{12}P$	0	$(L+17K)/2$	$-(49/12)^{\frac{1}{2}}(L-K)$
$(^1D^2D)^{12}P$	$(20/3)^{\frac{1}{2}}(L-K)$	$-(49/12)^{\frac{1}{2}}(L-K)$	$(-L+23K)/2$

	$(^1S^2D)^{12}D$	$(^1D^2D)^{12}D$	$(^1D^2P)^{12}D$
$(^1S^2D)^{12}D$	$2L+4K$	0	$2(L-K)$
$(^1D^2D)^{12}D$	0	$(L+17K)/2$	$(7/4)^{\frac{1}{2}}(L-K)$
$(^1D^2P)^{12}D$	$2(L-K)$	$(7/4)^{\frac{1}{2}}(L-K)$	$(3L+11K)/2$

	$(^1D^2P)^{12}F$	$(^1D^1D)^{12}F$
$(^1D^2P)^{12}F$	$3L+K$	$-2^{\frac{1}{2}}(L-K)$
$(^1D^2D)^{12}F$	$-2^{\frac{1}{2}}(L-K)$	$2L+4K$

$(^1D^2D)^{12}G$ $\quad 4L-2K.$

Be^{10}

	$(^1S^1S)^{11}S$	$(^1D^1D)^{11}S$
$(^1S^1S)^{11}S$	$8(L+2K)/3$	$-(80)^{\frac{1}{2}}(L-K)/3$
$(^1D^1D)^{11}S$	$-(80)^{\frac{1}{2}}(L-K)/3$	$(-8L+50K)/3$

	$(^1S^1D-{}^1D^1S)^{11}D$	$(^1S^1D+{}^1D^1S)^{11}D$	$(^1D^1D)^{11}D$
$(^1S^1D-{}^1D^1S)^{11}D$	$4L+4K$	0	0
$(^1S^1D+{}^1D^1S)^{11}D$	0	$(4L+20K)/3$	$(56)^{\frac{1}{2}}(L-K)/3$
$(^1D^1D)^{11}D$	0	$(56)^{\frac{1}{2}}(L-K)/3$	$(5L+28K)/3$

$(^1D^1D)^{11}F$ $\quad 4L+4K,$ $\qquad (^1D^1D)^{11}G$ $\quad 4L.$

B^{10}

	$(^2P^2P)^{22}S_+$	$(^2D^2D)^{22}S_+$
$(^2P^2P)^{22}S_+$	$2L+9K$	$(15)^{\frac{1}{2}}(L-K)$
$(^2D^2D)^{22}S_+$	$(15)^{\frac{1}{2}}(L-K)$	$15K$

	$(^2P^2P)^{22}D_+$	$(^2P^2D+{}^2D^2P)^{22}D_+$	$(^2D^2D)^{22}D_+$
$(^2P^2P)^{22}D_+$	$(7L+9K)/2$	0	$(21)^{\frac{1}{2}}(L-K)/2$
$(^2P^2D+{}^2D^2P)^{22}D_+$	0	$5L+5K$	0
$(^2D^2D)^{22}D_+$	$(21)^{\frac{1}{2}}(L-K)/2$	0	$(3L+21K)/2$

$(^2D^2P+{}^2P^2D)^{22}F_+$ $\quad 5L+2K,$ $\qquad (^2D^2D)^{22}G_+$ $\quad 5L.$

The + sign signifies that the wave function remains unchanged if the proton coordinates are interchanged with the neutron coordinates. This quantum number exists only for elements with equal numbers of protons and neutrons and also in this case only if the multiplicity for both is the same. If the multiplicities for protons and neutrons are different, the + term coincides with the − term and the degeneracy is doubled.

[16] The matrix elements for Li^6 are given by Bethe and Bacher, reference 8, §36.

for the proton-neutron interaction. The symbol $(^1D^3P)^{13}F$ denotes the wave function with the azimuthal quantum number 3 which can be constructed out of the ^1D protonic and the ^3P neutronic wave functions.

Table IV contains all matrix elements for Li^6 and Li^7, but for the other nuclei only those which are necessary for the calculation of the "low terms" (as determined by the equal orbital forces approximation). The matrix elements $\bar{V}_{\epsilon\lambda}$ for the nucleus with $6-n_1$ protons and $6-n_2$ neutrons are obtained from the corresponding matrix elements $V_{\epsilon\lambda}$ of the nucleus with n_1 protons and n_2 neutrons by means of the relation

$$\bar{V}_{\epsilon\lambda}=V_{\epsilon\lambda}+(6-n_1-n_2)(2L+4K)\delta_{\epsilon\lambda}, \quad (11)$$

which can be derived from the theory of holes. Thus we have all the matrix elements for the Majorana forces.

The next task is the calculation of the integrals L and K. Because of

$$\int\cdots\int(xy'-x'y)^2/r^2r'^2\cdot R_p(r)^2R_p(r')^2 \times J(|r-r'|)d\tau d\tau'=2L-6K>0 \quad (12)$$

we know that at any rate $3K<L$. The actual calculation of the ratio and absolute values of L and K is given in the appendix. It is clear that these quantities depend principally on the radius r_p of the p shell and on the range r_0 of the nuclear forces. If r_0/r_p is very large, K will vanish. This corresponds to the approximation made in Eqs. (7) and (8). The appendix shows that K, though not zero, is 7 to 11 times smaller than L.

For the calculation of energies of terms which do not appear as solutions of secular equations, the interaction energy of like particles has to be added directly to the matrix element of Table IV. In the other cases, the like particle interaction matrix elements must be added to the diagonal elements of the secular determinant of Table IV. It must be remembered that the L and K in Table III are not identical with the corresponding quantities in Table IV. If, however, we suppose that the two different L's are equal and set $K=0$, the result must be that given by Eq. (8). This shows that in the equal orbital forces model, the differences between the "low terms" are due to the finite value of K. With the other models the numerical results for the spacing of the "low terms" in a multiplet depend essentially on the value of K and hardly at all on the L/K ratio.

The actual solutions of the secular equations are given in Table V in units of mc^2 for the terms which are "low" in the equal orbital forces approximation. Although the term differences are independent of the choice of like particle interaction, we do not believe them to be correct (because of the use of the Hartree method). However, we think that the order of the terms will be right. The situation is the same in the corresponding atomic spectra.[6]

The symbols (*i*) and (*ii*) designate different methods of making the numerical calculations which are fully described in the appendix. Models (2*a*) and (2*b*) (and consequently also model (2*c*)) give the same order and spacing of the "low terms" within a multiplet. The spacing is also practically independent of the method of calculation, because K has nearly the same value in both methods. Fig. 1 gives the calculated total energy (method (*ii*)) of the lowest term and the experimental binding energy. Only the most stable nucleus with a given total mass is shown on the diagram. To obtain the theoretical curve a linear function $c(n_1+n_2)+d$ is added to the computed total energy and the constants c and d determined to fit the experimental points at He^4 and O^{16}. The observed "4 shell" structure is clearly evident in the computed curve, although the wave functions used do not correspond to preformed alpha-particles. In general the agreement is somewhat worse than for the similar calculation in atomic spectra.[17]

For the comparison of the calculated excited levels with experiment there is available only a limited amount of experimental material. P. Savel[18] and W. Bothe[19] have investigated the gamma-radiation associated with some nuclear transmutations. Unfortunately, Savel's results do not allow any conclusions to be drawn as to the character of the excited states. Bothe seems to have found three states in the C^{12} nucleus, the positions of which agree fairly well with our "low" terms. However an interpretation of Bothe's terms on these lines hardly seems

[17] R. Peierls, Zeits. f. Physik **59**, 738 (1929).
[18] P. Savel, Ann. d. Physik **4**, 88 (1935).
[19] W. Bothe, Zeits. f. Physik **100**, 273 (1936).

TABLE V. *Calculated p shell potential energies in units mc².*

TERM	(2a) (i)	(2a) (ii)	(2b) (i)	(2b) (ii)
Li^6				
^{22}S	−18.6	−12.7	−18.6	−12.7
^{22}D	−14.3	−8.4	−14.3	−8.4
^{22}P	11.5	5.5	11.5	5.5
For N^{14} add	−137.1	−105.7	−195.9	−133.6
Li^7				
^{12}P	−44.0	−28.4	−44.0	−28.4
^{12}F	−37.8	−22.1	−37.8	−22.1
For C^{13} or N^{13} add	−102.8	−79.3	−146.9	−100.2
Li^8				
^{22}P	−39.2	−27.4	−46.5	−30.9
^{22}D	−36.2	−23.9	−43.5	−27.4
^{22}F	−32.8	−22.4	−40.1	−25.9
For B^{12} add	−68.5	−52.9	−97.9	−66.8
Be^8				
^{11}S	−88.1	−56.8	−88.1	−56.8
^{11}D	−84.3	−53.0	−84.3	−53.0
^{11}G	−75.6	−44.1	−75.6	−44.1
For C^{12} add	−68.5	−52.9	−97.9	−66.8
Be^9 or B^9				
^{12}P	−83.1	−55.8	−90.5	−59.3
^{12}D	−80.7	−53.3	−88.1	−56.8
^{12}F	−77.0	−49.5	−84.4	−53.0
^{12}G	−72.0	−44.4	−79.4	−47.9
For B^{11} or C^{11} add	−34.3	−26.4	−49.0	−33.4
Be^{10} or C^{10}				
^{11}S	−90.0	−62.6	−104.7	−69.6
^{11}D	−87.6	−60.2	−102.3	−67.2
^{11}D	−86.8	−59.4	−101.5	−66.4
^{11}F	−84.1	−56.7	−98.8	−63.7
^{11}G	−78.4	−50.9	−93.1	−57.9
B^{10}				
^{22}S	−96.9	−67.6	−111.6	−74.6
^{22}D	−92.9	−63.5	−107.6	−70.5
^{22}D	−92.5	−63.0	−107.2	−70.0
^{22}F	−88.7	−59.2	−103.4	−66.2
^{22}G	−84.1	−54.5	−98.8	−61.5
C^{14} or O^{14}				
^{11}S	−148.9	−113.7	−207.7	−141.6
^{11}D	−146.2	−111.0	−205.0	−138.9
N^{15} or O^{15}				
^{12}P	−171.4	−132.2	−244.9	−167.1
O^{16}				
^{11}S	−205.6	−158.6	−293.8	−200.5

feasible, because the transition from ^{11}G to ^{11}S should be so much less probable than the transition to the ^{11}D level that the gamma-ray corresponding to the former transition should be unobservable. Hence, if our results are correct, at least one of his lines must have another interpretation. A possible interpretation is that two of the lines observed by Bothe come from the transitions $^{11}G-^{11}D$, $^{11}D-^{11}S$ and the third from another excited level which happens to be near ^{11}G. Such an excited level might arise from an excited configuration. This interpretation gains in plausibility from the fact that N^{15} has an excited state[20, 21] with an excitation energy of 10.5 mc². Since the normal state configuration of N^{15} has only one term, all the excited states must be ascribed to configurations in which one or more particles are excited. The occurrence of short and long range groups of particles together in transmutations in which C^{12} is produced confirms the existence of an excited level about 10 mc² above the normal state.[20, 21, 22] Cockcroft and Lewis[21] find two excited states in B^{11}, one of which falls between the levels ^{12}G, ^{12}F and the other between the levels ^{12}F, ^{12}D of the theoretical calculation. Bonner and Brubaker[22] observe three excited states in B^{10} with the energy 8.4 mc² available to produce excitation. The theoretical calculation shows three triplet levels and one singlet level in this range.

If we assume in analogy with H^2 that there

[20] E. O. Lawrence, E. McMillan and M. C. Henderson, Phys. Rev. **47**, 273 (1935).

[21] J. D. Cockcroft and W. B. Lewis, Proc. Roy. Soc. **A154**, 261 (1935).

[22] T. W. Bonner and W. M. Brubaker, Phys. Rev. **50**, 308 (1936).

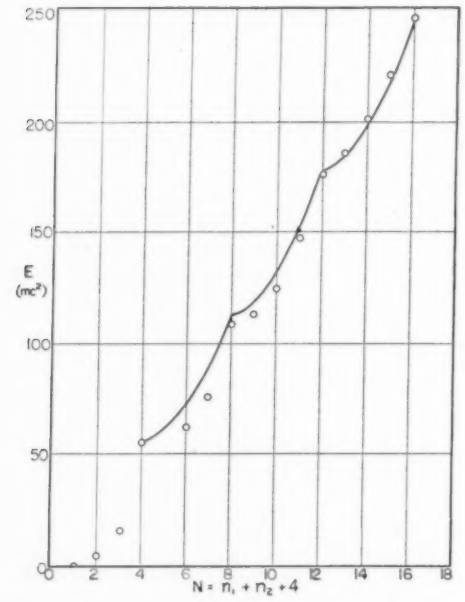

FIG. 1. Binding energy against nuclear mass. The calculated values lie on the solid curve; the circles mark experimental points.

are forces which tend to direct the proton spin parallel to the neutron spin (the Heisenberg forces will be shown to have such an effect), we obtain Table VI for the total angular momenta of the ground states. The ambiguity, in the cases for which several possible values of the angular momentum are given, is caused by the lack of knowledge concerning forces coupling the spin to the orbit. Experimentally the following momenta are known: Li^6-1, $Li^7-3/2$, $C^{12}-0$, $N^{14}-1$, $O^{16}-0$. These agree with the theory.

III. The Heisenberg Force Between Unlike Particles

The comparatively large singlet-triplet separation in H^2 (~ 4 mc²) points to an interaction between protons and neutrons which involves the spin in some way. The simplest assumption for such an interaction—though not the only possible one—is the Heisenberg force (1*b*) which involves the exchange of both Cartesian and spin coordinates of the interacting particles.

It is characteristic of this interaction that it is invariant with respect to the rotation of all spin coordinates—though it is not invariant with respect to the rotation of the proton spin alone any more, as were the Majorana forces. Consequently, it will leave the total spin angular momentum an exact quantum number, not, however, the proton spin and the neutron spin separately.

By Dirac's identity the exchange of the spin coordinates can be written

$$Q_{12}=\tfrac{1}{2}+\tfrac{1}{2}(\sigma_1\cdot\sigma_2). \tag{13}$$

The first part gives matrix elements which are, apart from the factor $g/(1-g)$, just half as great as the matrix elements of the Majorana force, thus effectively increasing this by the factor $(1-\frac{1}{2}g)/(1-g)$. The matrix elements of the second part vanish by the selection rules if both wave functions have a proton spin 0 or a neutron spin 0 or if the proton spins or the neutron spins differ by 2 or more. In these cases the addition of the Heisenberg force amounts only to an increase of the Majorana force by the factor $(1-\frac{1}{2}g)/(1-g)$. For most purposes it is more practical to unite the first part of the Heisenberg force with the Majorana force and consider the rest as an interaction involving P, the interchange of the Cartesian coordinates, and the scalar product of the spin operators. The effect of the first part of the Heisenberg force is numerically much greater than the second in most cases. It has been included in Tables IV and V and in Fig. 1 by calculating with a modified form of (1*a*) in which g is replaced by $\frac{1}{2}g$.

The splitting of a term with proton multiplicity s and neutron multiplicity σ is caused by the second part only. There are new components with the total spin angular momenta $S=|s-\sigma|,\ |s-\sigma|+1,\ \cdots,\ s+\sigma$ the displacement of the term with the total spin S being proportional to

$$s(s+1)+\sigma(\sigma+1)-S(S+1). \tag{14}$$

The matrix elements of the second part of (1*b*) for the ground state when they do not vanish

TABLE VI. *Angular momenta for normal states.*

Li^6	Li^7	Li^8	Be^9	Be^9	B^9	Be^{10}	B^{10}	C^{10}
1	$\frac{1}{2},\frac{3}{2}$	0,1,2	0	$\frac{1}{2},\frac{3}{2}$	$\frac{1}{2},\frac{3}{2}$	0	1	0
B^{11}	C^{11}	B^{12}	C^{12}	C^{13}	N^{13}	N^{14}	N^{15}	O^{16}
$\frac{1}{2},\frac{3}{2}$	$\frac{1}{2},\frac{3}{2}$	0,1,2	0	$\frac{1}{2},\frac{3}{2}$	$\frac{1}{2},\frac{3}{2}$	1	$\frac{1}{2},\frac{3}{2}$	0

(in all these cases $s=\sigma=\frac{1}{2}$) are given in Table VII for the triplet state only, since the elements for the singlet state can be obtained by multiplication with -3. Here L and K are identical with the same symbols in Table IV. These matrix elements must be multiplied by the factor $g/2(1-\frac{1}{2}g)$ and added to the corresponding effective Majorana matrix elements in Table IV.

The numerical calculation (method (*i*)) yields a splitting of 9 mc² for both Li^6 and B^{10} (and thus also for N^{14}), the triplet term being always the lowest. Method (*ii*) gives a splitting of 6.3 mc² for Li^6 and N^{14} and of 6.6 mc² for B^{10}. For Li^8 both methods give very little splitting so that it is impossible, in this case, to tell what should be the normal state.

Since the azimuthal quantum number and the resultant spin angular momentum both remain good quantum numbers, the Heisenberg force does not introduce a splitting of the ^3P or similar terms into the fine structure components $^3P_0$, $^3P_1$, $^3P_2$. It has been suggested by D. R. Inglis (at the summer symposium at Ann Arbor, as yet unpublished) that the spin orbit coupling should have the same sign (giving the larger j the lower energy) for both neutrons and protons in nuclei. A relativistic (Thomas) term results from the acceleration of the particles by the nuclear forces. According to Inglis this is the preponderating spin orbit coupling term in nuclei.

IV. The Coulomb Energy

A further question of interest is that concerning the difference between proton-proton and neutron-neutron interaction. The simplest assumption is that the only difference is the electrostatic interaction between protons.

According to this assumption the binding energy and the whole spectrum of two nuclei should differ only in the Coulomb energy if the number of neutrons in the first element is equal to the number of protons in the second element and *vice versa*. Known pairs of this type are H^3-He^3, Be^9-B^9, $B^{11}-C^{11}$, $C^{13}-N^{13}$, $N^{15}-O^{15}$, $O^{17}-F^{17}$.

For He^3 there already exists a simple calculation of the Coulomb energy[1] and a more accurate calculation giving substantially the same result has been made by S. S. Share.[23] The computed Coulomb energy for He^3 appears to be about 15 percent smaller than the experimental H^3-He^3 energy difference. For the other pairs we have performed the calculation, adding the electrostatic energy to the like particle interaction. The details of the computation are given in the appendix. For all cases in which the positron spectrum has been observed the experimental energy difference is obtained as a sum of three terms: (1) the upper limit of the positron spectrum (in electron mass units, taking the inspection value for the upper limit),[24] (2) the n^1-H^1 mass difference, (3) the mass of two electrons. Table VIII exhibits the electrostatic and experimental differences. The agreement is quite good. Nevertheless the experimental values are always somewhat greater than the theoretical ones. Considering the rather large uncertainty of these calculations, one cannot claim with certainty at present that the neutron-neutron interaction is stronger than the proton-proton interaction.

TABLE VII. *Matrix elements of the second part of the Heisenberg force.*

Li^8	$(^3P^3P)^2S$ $L+2K$	
Li^8	$(^3P^3P)^2P$	$(^3P^3D)^2P$
$(^3P^3P)^2P$ $(^3P^3D)^2P$	$(-L+3K)/2$ $(15)^{\frac{1}{2}}(L-3K)/6$	$(15)^{\frac{1}{2}}(L-3K)/6$ $(-5L+11K)/6$
B^{10}	$(^3P^3P)^3S$	$(^3D^3D)^3S$
$(^3P^3P)^3S$ $(^3D^3D)^3S$	$(2L-K)$ $(15)^{\frac{1}{2}}(-L+3K)/3$	$(15)^{\frac{1}{2}}(-L+3K)/3$ $(8L-5K)/3$

V. Comparison of Isobaric Nuclei

In this section we wish to make a few remarks concerning the spectra of isobars and the possibility of deciding between the alternatives (2*a*), (2*b*) and (2*c*) for the interaction between like particles.

It is clear from Table V that for the same values of the depth and range of the potentials, (2*a*) gives much less binding than (2*b*). Hence using the statistical method one obtains a smaller discrepancy with (2*b*) than with (2*a*). This cannot be considered, however, to be decisive evidence in favor of (2*b*), since it is possible that

[23] S. S. Share, Phys. Rev. **50**, 488 (1936).

[24] W. A. Fowler, L. A. Delsasso and C. C. Lauritsen, Phys. Rev. **49**, 561 (1936); F. N. D. Kurie, J. R. Richardson and H. C. Paxton, Phys. Rev. **48**, 167 (1935); L. Meitner, Nature **22**, 420 (1934).

TABLE VIII. *Electrostatic and measured energy differences.*

	H^3-He^3	Be^9-B^9	$B^{11}-C^{11}$	$C^{13}-N^{13}$	$N^{15}-O^{15}$	$O^{17}-F^{17}$
Electrostat.	1.37	3.11	4.06	4.62	5.54	5.62
Experim.	1.57	3.20	4.90	5.10	6.00	6.80

the correlation energy can account for the greater difference between the observed energies and the results of the statistical calculation with (2*a*). The discrepancy for (2*c*) is even greater than for (2*a*), but (2*c*) also cannot be excluded on this basis.[25]

In all cases only a small fraction of the binding energy is due to the interaction between like particles. This makes it very difficult to draw conclusions concerning these forces from experimental term values. If we consider, however, the Schrödinger equations of two isobars in the equal orbital forces approximation, their characteristic values will be absolutely equal. Nevertheless, the energy values will not necessarily be equal even in this approximation, because a characteristic value which is allowed for one isobar, may be forbidden for the other by Pauli's principle. Thus the low terms of Be^8 arise from the partition 4+4 of the equal orbital force approximation, but this gives no allowed terms for Li^8, the low terms of which come from the 4+3+1 partitions. These are allowed for Be^8 also, but correspond to excited states. For Be^{10} and B^{10}, however, the low states come in both cases from the 4+4+2 partition, in the first case giving singlet-singlet, in the second doublet-doublet terms. These coincide exactly in the equal orbital forces approximation and their similarity can be seen even in Table V. If one now introduces the difference between (2) and (1*a*) as a perturbation, the Be^{10}, B^{10} energy separation will appear as a difference of two small quantities.

Experimentally the binding energy of Be^{10} is greater than that of B^{10} by 0.8 mc^2. From Table VIII we estimate that the difference between the proton-proton and the neutron-neutron interactions (Coulomb energy) has decreased the binding energy by 3.2 mc^2. Thus the binding energy due to nuclear forces alone is greater for B^{10} than for Be^{10} by 2.4 mc^2. The corresponding quantity for the $N^{14}-C^{14}$ pair is $5.1-0.8=4.3$ mc^2. *Such small differences are possible only if the constants in the interactions between like and unlike particles are essentially equal.*

With (2*a*) or (2*b*) the difference between the Majorana energies of the B^{10} and Be^{10} ground states is seen from Table V to be 5.0 mc^2 (method (*ii*)). This must be increased by the amount 1.6 mc^2 by which the normal state of B^{10} is lowered when account is taken of the second part of the Heisenberg force between unlike particles. This gives a total difference of 6.6 mc^2. Using (2*c*) it can be shown that the ground state of Be^{10} coincides with the singlet state arising from ^2S in B and hence the difference between the binding energies of Be^{10} and B^{10} is 6.6 mc^2 for all three models. The agreement between models (2*a*), (2*b*) and (2*c*) in this case is not due to numerical coincidence, but can be shown to be true for all values of L and K simply by comparing the like particle contributions to the secular equations of the two systems for each of the three different models.

We see that the experimental difference between the binding energies of Be^{10} and B^{10} is much smaller than the theoretical difference. For C^{14} and N^{14} the situation is similar. Both sets of low terms belong to the partition 4+4+2 and hence coincide in the equal orbital forces approximation. Here also the energy difference is independent of the model. From Table V (method (*ii*)) the $C^{14}-N^{14}$ energy difference is $4.7+1.6=6.3$ mc^2, while experimentally the difference is only 4.3 mc^2.

In view of these discrepancies it is surprising to find excellent agreement between the computed and experimental Li^6-He^6 energy differences. Bjerge and Broström[26] report the value 7.5 ± 1.0 mc^2 for the maximum kinetic energy of the electrons produced in the transformation of He^6 into Li^6. Since the additional Coulomb energy in Li^6 is almost exactly balanced by the greater mass of the constituents of He^6, we

[25] H. A. Bethe and R. F. Bacher, reference 8, §6, have shown that a symmetrical Hamiltonian gives stable nuclei consisting of protons or of neutrons alone if one does not take into account the Pauli principle. However the Pauli principle causes the effective interaction between like particles to be smaller than that between unlike particles, even though the fundamental Hamiltonian does not distinguish between like and unlike particles. A good example in this connection is Li^3 which is much less stable than Be^3.

[26] T. Bjerge, Nature **138**, 400 (1936), and T. Bjerge and K. J. Broström, Nature **138**, 400 (1936).

obtain 7.5 ± 1.0 mc² for the experimental singlet-triplet splitting in Li^6. The computed value is 6.3 mc² (method (*ii*)) or 9.0 mc² (method (*i*)).

The secular equations for the states of Be^8 corresponding to the 4+3+1 partitions are given in Table IX.

We obtain -1.0 mc² for the $(Li^8)\ ^3P-(Be^8)\ ^1P$ energy difference using model (2*a*) and -3.4 mc² using model (2*b*). These numbers, added to the experimental normal state energy difference, yield the results 21 mc² (2*a*) or 24.4 mc² (2*b*) for the excitation energy of the ^1P term in Be^8. This term could be observed directly since it is stabilized by the spin conservation law.[27] A similar result can be deduced for C^{12} also, by comparison with B^{12}, since the experimental binding energy difference is nearly the same. It should be noted that method (*ii*) gives a Li^8-Be^8 normal state spacing in fair agreement with experiment. Here, as well as in the problems of the "four shell" structure and the singlet-triplet separation, method (*ii*) gives better agreement with the experimental facts than method (*i*).

Appendix

We assume that each particle has a separate wave function (Hartree-Fock model) and, furthermore, that this has the form

$$R_s(r)=ce^{-r^2/r_0^2}=ce^{-\alpha\sigma r^2} \tag{15}$$

for the *s* particles and

$$\begin{aligned}&(x/r)R_p(r),\quad (y/r)R_p(r),\quad (z/r)R_p(r),\\ &R_p(r)=c're^{-r^2/r_0^2}=c'e^{-\tau\alpha r^2}\end{aligned} \tag{16}$$

for the *p* particles, where α is the reciprocal square of the range of the forces and is defined in (1).

It is well known that if a determinantal wave function for the whole system is built up out of these functions and the energy calculated, choosing the parameters σ and τ so as to make the energy a minimum, the absolute value of this minimum will be very small and the corresponding radii greater than the radius of the nucleus. The reason for this discrepancy is that it is impossible to express the finer statistical correlations between the positions of the particles assuming a separate wave function for each particle. In order to take into account at least approximately the correlation energy, a semi-empirical method is used, modifying the Hamiltonian in such a way that it gives the experimental binding energy for O^{16}.

Table IX. *Continuation of Table V. Be^8.*

	$(^1S^3P)\ ^3P$	$(^1D^3P)\ ^3P$
$(^1S^3P)\ ^1P$	$4(L+2K)/3$	$-(20)^{\frac{1}{2}}(L-K)/3$
$(^1D^3P)\ ^1P$	$-(20)^{\frac{1}{2}}(L-K)/3$	$-(4L-25K)/3$
$(^1D^3P)\ ^3D$	$2L+3K$.	$(^1D^3P)\ ^3F$ $2L$

The kinetic energy per particle is $(3/2)\alpha\sigma$ and $(5/2)\alpha\tau$ for the *s* and *p* particles, respectively. For a system with *N* particles the total kinetic energy is taken to be

$$(1-1/N)(6\sigma-10\tau+(5/2)N\tau)\alpha. \tag{17}$$

The factor $(1-1/N)$ serves to eliminate the spurious kinetic energy of the center of gravity which arises from the use of single particle wave functions with coordinates measured from a fixed point.[28] For the Coulomb energy we obtain

$$\begin{aligned}&CE(s)\ =(\alpha\sigma/8)^{\frac{1}{2}},\quad \text{(within the } s \text{ shell)},\\ &CE(sp)=(1/3)(\sigma\tau)^{\frac{1}{2}}(\sigma+\tau)^{-\frac{1}{2}}(3\tau+2\sigma-2\tau^2\sigma(\sigma+\tau)^{-2})\alpha^{\frac{1}{2}},\end{aligned} \tag{18}$$

(between the *s* shell and each proton in the *p* shell),

$$\begin{aligned}L_c&=(49/120)(\alpha\tau/2)^{\frac{1}{2}},\\ K_c&=(1/40)(\alpha\tau/2)^{\frac{1}{2}}.\end{aligned} \tag{19}$$

If we use the relation $A_{sr}\sim(1-2g)A_{rr}$ the total potential energy in the *s* shell is

$$6(1-g)A_{rr}B(\sigma),\quad B(\sigma)=(\sigma/\sigma+1)^{\frac{1}{2}}, \tag{20}$$

for all three forms of the like particle interaction.

The total interaction energy between the *s* shell and a single particle in the *p* shell (including both like and unlike particle forces) has the form

$$\begin{aligned}&3(1-g)A_{rr}D+(1-2g)A_{rr}(D-C),\quad (1a+2a),\\ &3(1-g)A_{rr}D,\qquad\qquad\qquad\quad (1a+2b),\\ &3(1-g)A_{rr}D+(1+g)A_{rr}(D-C),\quad (1a+2c),\end{aligned} \tag{21}$$

with

$$\begin{aligned}D(\sigma,\tau)&=16\sigma^{\frac{3}{2}}(\tau/(\sigma+\tau))^{5/2}(\sigma+\tau+2)^{-5/2},\\ C(\sigma,\tau)&=(2\sigma)^{\frac{3}{2}}\tau^{5/2}(1+2\sigma)(2\sigma\tau+\sigma+\tau)^{-5/2}.\end{aligned} \tag{22}$$

Within the *p* shell

$$\begin{aligned}&L_{rr}=A_{rr}(1-g/2)L^0,\quad L_{sr}=A_{sr}(1-2g)L^0,\\ &\qquad\qquad\qquad\qquad\qquad\text{(for 2}a\text{ and 2}b\text{)},\\ &K_{rr}=A_{rr}(1-g/2)K^0,\quad K_{sr}=A_{sr}(1-2g)K^0,\\ &L^0=(\tau/\tau+1)^{\frac{1}{2}}\{1-(4\tau+1)/4(\tau+1)^2\}\\ &K^0=(\tau/\tau+1)^{\frac{1}{2}}/4(\tau+1)^2.\end{aligned} \tag{23}$$

In computing Eqs. (21) and (22) the Majorana interaction between unlike particles is given the depth $(1-g/2)A_{rr}$ in order to take into account part of the Heisenberg interaction (as discussed in Section III).

It appears to be sensible to try to compensate for the correlation energy by either multiplying the potential

[27] The spin conservation law is practically rigorous for nuclei if the singlet-triplet splitting is produced by a force of the form (1*b*). We should mention at this occasion that it is not sufficient for the validity of such a conservation law that the forces acting on the spin be small. It is necessary, in addition to this, that the separation of states with different spin should not be small also. For atomic spectra, this follows from the fact that the singlet-triplet separation is of electrostatic nature, while the spin forces are magnetic. For nuclei, if (1*b*) is correct, the singlet-triplet separation is due to the Heisenberg force, while the spin forces still are, under this assumption, of magnetic nature. Thus if (1*b*) is correct, the situation is much better for the spin law in nuclei than in the external shells. It is invalidated, however, by any force, coupling the spin to orbit, as e.g. that assumed by Inglis (cf. Section III, end).

[28] S. Flügge, reference 7.

energy by a suitable constant,[7,8] or by allowing the particles to interact at a greater distance than they really do. With (2*b*) we found that multiplying the potentials by 1.36 yields a function for the sum of all energies which has a minimum value of -246 mc^2 at $\sigma=0.80$ (taking $\tau=\sigma$ since very little improvement is obtained from varying both τ and σ independently). The second method (method (*i*)) is believed to be somewhat more reliable. With (2*b*) the radius of action must be increased by the factor 1.3 to make the minimum value of $E(O^{16})$ agree with experiment. The minimum is assumed at $\sigma=1.01$ (again taking $\sigma=\tau$ for the same reason as before). To obtain the numerical results discussed in the text we use the values

$$\begin{aligned} L_{\tau\tau}&=15.74, \quad K_{\tau\tau}=1.41,\\ L_{\tau\tau}&=10.05, \quad K_{\tau\tau}=0.90,\\ L_c&=0.892, \quad K_c=0.055, \quad \text{Method } (i).\\ CE(s)&=1.09, \quad CE(ps)=1.63,\\ 3(1-g)D(\sigma,\sigma)A_{\tau\tau}&=14.95,\\ 6(1-g)B(\sigma)A_{\tau\tau}&=120.00. \end{aligned} \tag{24}$$

In computing the kinetic and Coulomb energies α is replaced by $\alpha/(1.3)^2$.

The straight-forward application of this procedure to the models (2*a*) and (2*c*) is not very satisfactory, because an increase in the strength of the potentials or in the radius of action which serves to fit the experimental O^{16} energy will give far too much energy to the lighter elements.

Finally it was found most satisfactory to make the calculations without modifying either the range or depth of the potentials. With $\sigma=1.01/(1.3)^2$ the kinetic and Coulomb energies are exactly as in method (*i*). The other matrix elements have the values

$$\begin{aligned} L_{\tau\tau}&=9.83, \quad K_{\tau\tau}=1.44,\\ L_{\tau\tau}&=6.19, \quad K_{\tau\tau}=0.90, \quad \text{Method } (ii).\\ 3(1-g)D(\sigma,\sigma)A_{\tau\tau}&=12.13,\\ 6(1-g)B(\sigma)A_{\tau\tau}&=77.37. \end{aligned} \tag{25}$$

The correlation energy is introduced by adding to the total computed energy a linear function of the number of particles. Since the general linear function contains two parameters it is possible in this way to fit exactly the measured binding energies of two different nuclei, i.e., He^4 and O^{16}. Then the energies of all the others are uniquely determined.

JANUARY 15, 1937 PHYSICAL REVIEW VOLUME 51

On the Consequences of the Symmetry of the Nuclear Hamiltonian on the Spectroscopy of Nuclei

E. WIGNER*
Princeton University, Princeton, New Jersey

(Received October 23, 1936)

The structure of the multiplets of nuclear terms is investigated, using as first approximation a Hamiltonian which does not involve the ordinary spin and corresponds to equal forces between all nuclear constituents, protons and neutrons. The multiplets turn out to have a rather complicated structure, instead of the S of atomic spectroscopy, one has three quantum numbers S, T, Y. The second approximation can either introduce spin forces (method 2), or else can discriminate between protons and neutrons (method 3). The last approximation discriminates between protons and neutrons in method 2 and takes the spin forces into account in method 3. The method 2 is worked out schematically and is shown to explain qualitatively the table of stable nuclei to about Mo.

1

RECENT investigations[1] appear to show that the forces between all pairs of constituents of the nucleus are approximately equal. This makes it desirable to treat the protons and neutrons on an equal footing. A scheme for this was devised in his original paper by W. Heisenberg[2] who considered protons and neutrons as different states of the same particle. Heisenberg introduced a variable τ which we shall call the isotopic spin, the value -1 of this variable can be assigned to the proton state of the particle, the value $+1$ to the neutron state. The assumption that the forces between all pairs of particles are equal is equivalent, then, to the assumption that they do not depend on τ or that the Hamiltonian does not involve the isotopic spin.

* A paper delivered at the Tercentenary Conference of Arts and Sciences at Harvard University, September, 1936.

[1] M. A. Tuve, N. P. Heydenburg and L. R. Hafstad, Phys. Rev. **50**, 806 (1936); G. Breit, E. U. Condon and R. D. Present, Phys. Rev. **50**, 825 (1936).

[2] W. Heisenberg, Zeits. f. Physik **77**, 1 (1932).

In addition to this isotopic spin τ, we must keep, of course, the ordinary spin variable s also; s also can assume the two values $+1$ and -1. It has been pointed out lately[3] that the Pauli principle requires that the wave function

$$\Psi(r_1 s_1 \tau_1, r_2 s_2 \tau_2, \cdots, r_n s_n \tau_n) \qquad (1)$$

be antisymmetric with respect to the simultaneous interchange of Cartesian, spin and isotopic spin variables of any pair of heavy particles. This fact is quite analogous to the similar statement for ordinary spin.

Of course, if Eq. (1) is to represent the state of a given nucleus, say with n_P protons and n_N neutrons, it must vanish at every place where the sum of the τ's

$$\tau_1+\tau_2+\cdots+\tau_n \neq n_N-n_P \qquad (2)$$

is not equal to the "isotopic number" of this element. All wave functions which are finite for several sums of the τ's, refer to states which can be different elements with finite probabilities. No such states are known to be of any importance and the mathematical apparatus of the isotopic spin is, hence, somewhat redundant. It will turn out that it is very useful in spite of this.

In addition to the assumption of the approximate equality of forces between all pairs of particles, it appears to be a useful approximation to neglect the forces involving the ordinary spin. The Hamiltonian depends then on the space coordinates alone. By keeping both, one or none of these assumptions, one comes to four possible schemes:

(1) Take into account forces depending on space coordinates alone.

(2) Take into account forces depending on space and ordinary spin coordinates, assuming, however, interactions between all kinds of pairs to be equal.

(3) Neglect ordinary spin forces, take into account forces depending on space coordinates and isotopic spin, i.e., discriminate between proton-proton, proton-neutron and neutron-neutron interactions.

(4) Take all kinds of interaction into account.

The first is the roughest method, the last the most exact and it is probable that (2) is more accurate for light elements, (3) for heavy elements. On the other hand, of course, one can obtain most results from symmetry considerations for 1, fewest for 4. Approximation (1) is identical with the "all orbital forces equal" model.[4]

The statement that an operator involves only one or another set of variables needs further amplification. As used in the ordinary theory of spectra, this expression means that the operator *can be written* in terms of these variables alone. It did not mean that it cannot be written in some other way as well. Thus, e.g., the interchange P of the space coordinates acts only on space coordinates, although it can be written by Dirac's identity,

$$P=-\tfrac{1}{2}-\tfrac{1}{2}(s_1\cdot s_2)$$

entirely in terms of spin operators for antisymmetric functions. We shall keep this definition for the forces depending on Cartesian and ordnary spin coordinates for nuclei also.

The operators which involve τ are, however, somewhat specialized to begin with. Using Heisenberg's notation for isotopic spin operators

$$\tau=\tau_\zeta=\begin{Vmatrix}-1 & 0\\ 0 & 1\end{Vmatrix},\quad \tau_\xi=\begin{Vmatrix}0 & i\\ -i & 0\end{Vmatrix},\quad \tau_\eta=\begin{Vmatrix}0 & 1\\ 1 & 0\end{Vmatrix} \qquad (4)$$

the conservation law for electric charge requires that all operators commute with

$$\tau_{\zeta 1}+\tau_{\zeta 2}+\cdots+\tau_{\zeta n}=n_N-n_P=2T_\zeta. \qquad (3)$$

In addition to this, one hardly would say that

$$\tau_{\xi 1}\tau_{\xi 2}+\tau_{\eta 1}\tau_{\eta 2}+\tau_{\zeta 1}\tau_{\zeta 2}=-1-2PQ. \qquad (5)$$

(P interchange of space, Q interchange of spin coordinates) does not involve the Cartesian or spin coordinates, since Eq. (5) is a rather artificial expression, τ_ξ and τ_η having no immediate physical significance. We shall assume hence for approximation (3) only such operators which are equivalent to operators acting on the Cartesian coordinates alone, but in a different way for protons and neutrons. This is equivalent to using only operators involving the space coordinates and the τ_ζ's. If we do this, the results of method (3) must become equivalent to the usual theory (without τ's) which neglects

[3] J. H. Bartlett, Phys. Rev. **49**, 102 (1936); W. Elsasser, J. de phys. et rad. **7**, 312 (1936), and especially B. Cassen and E. U. Condon, Phys. Rev. **50**, 846 (1936).

[4] E. Feenberg and E. Wigner, Phys. Rev. This issue.

the spin. As a matter of fact, for approximation (3), the introduction of τ is entirely useless and it is taken up here only in order to establish the transition from approximation (1) to (3).

2

The interaction in the electronic shells of atoms is a sum of terms containing two particles only and the momenta is no higher than the second power. The reason for the first is, that the interaction occurs through a field and this gives in first approximation only interaction between two particles. The reason that one can stop with the second power of the momenta is that these always enter in the combination p/mc which is a small quantity.

An advantage of introducing the variable τ is[2, 3] that one can take over these assumptions to nuclei. If one does not use the variable τ the interchange of two particles if expressed as a power series of the momenta is an infinite series[5]

$$\sum_{n_1 n_2 n_3} \frac{(x_2-x_1)^{n_1}(y_2-y_1)^{n_2}(z_2-z_1)^{n_3}}{n_1!\,n_2!\,n_3!} \times\left(\frac{\partial}{\partial x_1}-\frac{\partial}{\partial x_2}\right)^{n_1}\left(\frac{\partial}{\partial y_1}-\frac{\partial}{\partial y_2}\right)^{n_2}\left(\frac{\partial}{\partial z_1}-\frac{\partial}{\partial z_2}\right)^{n_3}.$$

However, it can be expressed by means of Dirac's identity also entirely without the momenta by means of Eq. (5). It must be admitted, however, that the spin cannot be considered to be small as in the atomic theory. We shall determine here all interaction forms between two particles which do not contain higher than first power terms of momenta[6] as far as the dependence on s and τ goes. Nothing can be said, of course, on the dependence on the distance, and this factor will be omitted hence. It seems to be of lesser importance for the present.

The interaction must have spherical symmetry, depending on the differences of coordinates and momenta only, be invariant under inversion, substitution of $-t$ for t and also be symmetric in the particles. The first requirements determine the dependence on s, x and p. From the two triples of spin operators, one can form two invariants

$$(i)\quad 1\,;\text{ and }(i')\quad \tfrac{1}{2}+\tfrac{1}{2}(s_{x1}s_{x2}+s_{y1}s_{y2}+s_{z1}s_{z2})=Q_{12}$$

three axial vectors with Z components

$$(v)\quad s_{z1}+s_{z2}\,;\quad s_{z1}-s_{z2}\,;\quad s_{x1}s_{y2}-s_{y1}s_{x2},$$

respectively, and one axial tensor, with components

$$(t)\quad s_{x1}s_{y2}+s_{y1}s_{x2}\,;\quad s_{y1}s_{z2}+s_{z1}s_{y2}\,;\quad s_{z1}s_{x2}+s_{x1}s_{z2}\,;\quad s_{x1}s_{x2}-s_{y1}s_{y2}\,;\quad s_{x1}s_{x2}+s_{y1}s_{y2}-2s_{z1}s_{z2}.$$

The first two of these, (i) and (i'), can be used as they stand, cannot be combined with first power expressions of p, however, since these change sign under the $t'=-t$ substitution. The last one (t) gives the familiar expression

$$(i'')\qquad (s_1\cdot r_{12})(s_2\cdot r_{12})-3(s_1\cdot s_2)r_{12}^2$$

if combined with the similar tensor of the coordinates.[7] It cannot be combined with the p either. The middle one must be combined with the vector p_1-p_2 which gives a useless axial invariant and tensor and an ordinary vector. This combined with the distance vector gives the familiar

$$(ia)(ib)(ic)\quad \begin{vmatrix} s_x & s_y & s_z \\ x_1-x_2 & y_1-y_2 & z_1-z_2 \\ p_{x1}-p_{x2} & p_{y1}-p_{y2} & p_{z1}-p_{z2} \end{vmatrix}.$$

Here s_x, s_y, s_z can be the components of one of the three vectors (v). On the whole, we have 6 invariants. These invariants can be multiplied with one of the six expressions in τ which commute with $\tau_{\xi 1}+\tau_{\xi 2}$. These are, first of all

$$(\tau_0)\quad 1\qquad\text{and}\qquad(\tau_0')\quad -\tfrac{1}{2}-\tfrac{1}{2}(\tau_1\cdot\tau_2)=P_{12}Q_{12}$$

which give the same interaction between all pairs of particles. In addition to these, we have

$$(\tau_1)\quad \tfrac{1}{2}+\tfrac{1}{2}\tau_{\xi 1}\tau_{\xi 2}\qquad\text{and}\qquad(\tau_2')\quad \tfrac{1}{2}(\tau_{\xi 1}=\tau_{\xi 2}).$$

The first of these gives ordinary interaction but only between like particles; the second gives a negative interaction for proton pairs, a positive

[5] J. A. Wheeler, Phys. Rev. **50**, 643 (1936).

[6] Some of these were given previously by Cassen and Condon, reference 3. The expressions given here are invariant only under Galilei transformations. G. Breit has shown that, in order to ensure relativistic invariance, correction terms must be added to the expressions derived here.

[7] (ii) has the property that it is identical with $Q_{12}(ii)$. It is an interaction which shows saturation.

for neutron pairs, none for unlike particles. These interactions are symmetric in the particles and can be combined with (i), (i'), (i'') and (ia), giving in the whole 16 different forms.

Finally we have

$$(\tau_2) \quad \tau_{\xi 1}-\tau_{\xi 2} \quad \text{and} \quad (\tau_2') \quad \tfrac{1}{2}(\tau_{\xi 1}\tau_{\eta 2}-\tau_{\eta 1}\tau_{\xi 2}),$$

which can be combined with (ib) and (ic) giving 4 more types of interaction.

In approximation (1) we can have only $(i)(\tau_0)$ and $(i')(\tau_0')$, i.e., ordinary and Majorana exchange forces.

In approximation (2), all 8 forms derived from (τ_0), (τ_0') and (i) (i') (i'') and (ia). These are, in addition to the previous ones, spin-spin $(i'')(\tau_0)$, spin-orbit $(ia)(\tau_0)$ ordinary forces, Heisenberg forces $(i)(\tau_0')$. Furthermore spin-spin exchange forces $(i'')(\tau_0')$ and spin-orbit exchange forces $(ia)(\tau_0')$ of the Heisenberg type. The Majorana exchange forces of these types are identical with the ordinary forces. Finally, we have the spin-exchange forces $(i')(\tau_0)$ of Bartlett.[8]

In approximation (3) we must permit according to the preceding section, in addition to those of 1, only $(i)(\tau_1)$ and $(i)(\tau_1')$, allowing for different interactions between different kinds of pairs. The coefficient of $(i)(\tau_1')$ is certainly very small, the proton-proton interaction being very nearly equal to the neutron-neutron interaction.

In approximation (4), all 20 types become possible.

3

We next go over to approximation (1), and try to define the analog of the multiplet system. This can be defined in two ways: either by considering the functional dependence of the wave functions on the spins or else by considering their dependence on the space coordinates. We shall first consider the spin function.[8]

The great difference between the ordinary spin and the spin considered here is that we have, for every particle, two spin coordinates s and τ, giving in the whole four different sets of values $-1, -1; -1, 1; 1, -1; 1, 1$. Instead of two two-valued spins, one can introduce one four-valued spin η, which has the values 1, 2, 3, 4 for the four different doublets of values of s and τ, respectively. This η plays the same role which the two-valued spin plays in the ordnary spin theory. However, because of the four-valuedness of η, instead of the representations of the two-dimensional unitary group (or the equivalent three-dimensional rotation group), the representations of the four-dimensional unitary group will characterize the multiplet systems.

Since the Hamiltonian does not contain the spin coordinates, any transformation which affects only these, will bring a characteristic function into a characteristic function. We can consider first, the permutations of the η_i and second, simultaneous unitary transformations of all the η:

$$R_u\psi(\eta_1, \cdots, \eta_n)=\sum_{\vartheta} u_{\eta_1\vartheta_1}u_{\eta_2\vartheta_2}\cdots u_{\eta_n\vartheta_n} \times\psi(\vartheta_1, \cdots, \vartheta_n). \quad (6)$$

We can first define something analogous to the Z component of the spin momentum by considering the u's of the type

$$u(\varphi_1, \varphi_2, \varphi_3, \varphi_4)=\begin{Vmatrix} e^{i\varphi_1} & 0 & 0 & 0 \\ 0 & e^{i\varphi_2} & 0 & 0 \\ 0 & 0 & e^{i\varphi_3} & 0 \\ 0 & 0 & 0 & e^{i\varphi_4} \end{Vmatrix}. \quad (7)$$

These operations all commute and, hence, a system of functions of the η can be found, the members of which are merely multiplied by constants if an R_u with u of the form (7) is applied to them[9]

$$R^{u(\varphi_1\varphi_2\varphi_3\varphi_4)}F^{\nu}{}_{\mu_1\mu_2\mu_3\mu_4}(\eta_1\cdots\eta_n) = e^{i(\mu_1\varphi_1+\mu_2\varphi_2+\mu_3\varphi_3+\mu_4\varphi_4)}F^{\nu}{}_{\mu_1\mu_2\mu_3\mu_4}. \quad (8)$$

The μ must be integers in this equation, they will be called diagonal quantum numbers. The ν serves only to discriminate between different functions of the η with the same diagonal quantum numbers.

[8] The content of this section is based on the fundamental mathematical works of E. Cartan, Bull. Soc. Math. de France **41**, 43 (1913). J. de Math. **10**, 149 (1914); I. Schur, Berl. Ber., pp. 189, 297, 346 (1924) and particularly, H. Weyl, Math. Zs. **23**, 271 (1925). I attempted to compile in this section—often without giving rigorous proofs—those results which suffice for the discussion of the physical problems in question.

[9] The $F_{\mu_1\mu_2\mu_3\mu_4}(\eta_1\cdots\eta_n)$ are zero for every set $\eta_1\eta_2\cdots\eta_n$ of the η, except for those sets in which μ_1 of them have the value 1, exactly μ_2 of them have the value 2, and μ_3 of them are 3. Then μ_4 of them will be equal to 4. Otherwise they can be arbitrary and will still satisfy Eq. (8).

Since $u(\varphi, \varphi, \varphi, \varphi)$ with four equal φ is only multiplication with $e^{i\varphi}$, because of (6), R_u is multiplication with $e^{in\varphi}$. It is, on the other hand, multiplication with $e^{i(\mu_1\varphi+\mu_2\varphi+\mu_3\varphi+\mu_4\varphi)}$ which shows that all possible systems of diagonal quantum numbers satisfy the equation

$$\mu_1+\mu_2+\mu_3+\mu_4=n, \tag{9}$$

where n is the number of variables η. There is a simple connection between the diagonal quantum numbers and the Z component of the spin momentum S. One obtains it by considering a rotation of the spin coordinates around Z by φ, the matrix of which is of the form (7) with $\varphi_1=\varphi_2=-\varphi_3=-\varphi_4=-\frac{1}{2}\varphi$. Under the influence of the corresponding R_u, the wave function will be multiplied by $e^{iS_z\varphi}$ which gives

$$S_z=\tfrac{1}{2}\sum_k s_{zk}=\tfrac{1}{2}(\mu_4+\mu_3-\mu_2-\mu_1). \tag{10a}$$

The $\frac{1}{2}$ before the s_{zk} enters because the usual definition of the Pauli-matrices is 1/2 of that given in (4).

Similarly, we have

$$T_\xi=\tfrac{1}{2}\sum_k \tau_{\xi k}=\tfrac{1}{2}(\mu_4-\mu_3+\mu_2-\mu_1) \tag{10b}$$

and we define also a

$$Y_\xi=\tfrac{1}{2}\sum_k s_{zk}\tau_{\xi k}=\tfrac{1}{2}(\mu_4-\mu_3-\mu_2+\mu_1). \tag{10c}$$

The quantum numbers S_z, T_ξ, Y_ξ can be called magnetic quantum numbers. They determine, together with n, the μ uniquely. Their importance for spectroscopic considerations is the same as that of the single ordinary magnetic quantum number in atomic spectroscopy; they can be easily found simultaneously for all states of a multiplet.

Several states with different magnetic quantum numbers form sets "multiplets" which always have common energy. These sets contain in atomic spectroscopy *one* state with every magnetic quantum number from a maximum, S, to $-S$. We must find the corresponding sets for four-valued spin.

The multiplet will be denoted by the highest set $\Lambda_4\Lambda_3\Lambda_2\Lambda_1$ of μ which occurs in it. The set $\Lambda_4\Lambda_3\Lambda_2\Lambda_1$ is called higher than the set $\mu_4\mu_3\mu_2\mu_1$ if either $\Lambda_4>\mu_4$, or if $\Lambda_4=\mu_4$ but $\Lambda_3>\mu_3$, or finally, if $\Lambda_4=\mu_4$, $\Lambda_3=\mu_3$ but $\Lambda_2>\mu_2$. The reason for several states with different diagonal quantum numbers being united into the same multiplet, is that they are transformed into each other by R_u, the u of which have not the form (7). Instead of the Λ, we can use for the characterization of a multiplet also

$$S=\tfrac{1}{2}(\Lambda_4+\Lambda_3-\Lambda_2-\Lambda_1), \tag{11a}$$

$$T=\tfrac{1}{2}(\Lambda_4-\Lambda_3+\Lambda_2-\Lambda_1), \tag{11b}$$

$$Y=\tfrac{1}{2}(\Lambda_4-\Lambda_3-\Lambda_2+\Lambda_1), \tag{11c}$$

which together with $\Lambda_4+\Lambda_3+\Lambda_2+\Lambda_1=n$ completely determine the Λ.

The character of the multiplets is for the fourfold spin not as simple as for the twofold spin. While the latter ones can be represented by the points on a line from $-S$ to S, the former ones must be represented at least in a three-dimensional space, giving the possible S_z, T_ξ, Y_ξ values and *their multiplicities*. This is necessary because it is not true any more that every combination of $S_zT_\xi Y_\xi$ occurs only once. The multiplicity of every $S_zT_\xi Y_\xi$ is the same as that of any permutation of these numbers and also that of $-S_z-T_\xi Y_\xi$; $-S_zT_\xi-Y_\xi$; $S_z-T_\xi-Y_\xi$. The figure of the multiplet has, therefore, tetrahedral symmetry in the $S_zT_\xi Y_\xi$ space. Using $S_zT_\xi Y_\xi$ has the advantage over using the Λ that the multiplets for $n=1, 5, 9, 13$, are represented by the same figures. The quantum numbers are all half-integers, the occurring $S_zT_\xi Y_\xi$ combinations form a face centered lattice for which $S_z+T_\xi+Y_\xi$ is of the form $2k-1/2$. These figures, reflected in any of the planes $T_\xi Y_\xi$, $Y_\xi S_z$, S_zT_ξ, give the multiplets existing for $n=3, 7, 11, \cdots$, the face centered lattice being characterized by $S_z+T_\xi+Y_\xi$ having the form $2k+1/2$. The quantum numbers S_z, T_ξ, Y_ξ are integers for even n. Their sum is even or $n=4, 8, 12, \cdots$, odd for $n=2, 6, 10, \cdots$.

In order to find the figures for the multiplets, one must know how many states with a certain $\mu_4\mu_3\mu_2\mu_1$ combination are present in the multiplet $(\Lambda_4\Lambda_3\Lambda_2\Lambda_1)$. We shall denote this number by

$$\binom{\Lambda_4\Lambda_3\Lambda_2\Lambda_1}{\mu_4\mu_3\mu_2\mu_1}. \tag{12}$$

The calculation of the quantities (12) is im-

portant for the following section also. The simplest interpretation of (12) is obtained by considering the subgroup of the unitary group formed by the matrices (7). The symbol (12) denotes how often the (one-dimensional) representation $e^{i(\mu_1\sigma_1+\mu_2\sigma_2+\mu_3\sigma_3+\mu_4\sigma_4)}$ occurs in the representation of the total unitary group which is designated by $(\Lambda_4\Lambda_3\Lambda_2\Lambda_1)$.

The symbols (12) are defined only if $\Lambda_1+\Lambda_2+\Lambda_3+\Lambda_4=\mu_4+\mu_3+\mu_2+\mu_1$, $\Lambda_4\geq\Lambda_3\geq\Lambda_2\geq\Lambda_1\geq 0$ and since a permutation of the μ does not change the value of (12), we can assume also $\mu_4\geq\mu_3\geq\mu_2\geq\mu_1\geq 0$. The value of (12) is 0, unless $\Lambda_4\geq\mu_4$ since Λ_4 was the greatest μ of the multiplet. In addition to this, (12) vanishes unless[10]

$$\begin{aligned}&\Lambda_4\geq\mu_4;\quad \Lambda_4+\Lambda_3\geq\mu_4+\mu_3;\\ &\Lambda_4+\Lambda_3+\Lambda_2\geq\mu_4+\mu_3+\mu_2.\end{aligned}\tag{13}$$

The last of these can be written also as $\Lambda_1\leq\mu_1$. There are several ways of evaluating (12). One of them is to consider the matrices μ which correspond to a three-dimensional unitary transformation of the η values 1, 2, 3 only. The representation $(\Lambda_4\Lambda_3\Lambda_2\Lambda_1)$ contains all those representations $(\Lambda_3'\Lambda_2'\Lambda_1')$ of the three dimensional unitary group exactly once for which

$$\Lambda_4\geq\Lambda_3'\geq\Lambda_3\geq\Lambda_2'\geq\Lambda_2\geq\Lambda_1'\geq\Lambda_1.\tag{14}$$

Thus the quartets of diagonal quantum numbers of $(\Lambda_4\Lambda_3\Lambda_2\Lambda_1)$ are those of all $(\Lambda_3'\Lambda_2'\Lambda_1')$ satisfying (14), together with the last diagonal quantum number $\Lambda_4+\Lambda_3+\Lambda_2+\Lambda_1-\Lambda_3'-\Lambda_2'-\Lambda_1'$. After this, we can reduce the representation of the three-dimensional unitary group to a two-dimensional: in $(\Lambda_3'\Lambda_2'\Lambda_1')$ those $(\Lambda_2''\Lambda_1'')$ will occur for which

$$\Lambda_3'\geq\Lambda_2''\geq\Lambda_2'\geq\Lambda_1''\geq\Lambda_1'.\tag{14a}$$

Finally $(\Lambda_2''\Lambda_1'')$ contains the pairs of diagonal quantum numbers Λ_2'',Λ_1''; $\Lambda_2''-1,\Lambda_1''+1$; $\Lambda_2''-2,\Lambda_1''+2$; $\cdots$; Λ_1'',Λ_2''.

For instance, in order to find the multiplet (3 1 1 0) we can calculate $(3\,1\,1\,0)=(3\,1\,1)0+(2\,1\,1)1+\underline{(1\,1\,1)2}+(3\,1\,0)1+\underline{(2\,1\,0)2}+\underline{(1\,1\,0)3}$. It suffices to obtain those quadruplets of μ which are in a descending order. The others can be obtained then by permutation. We can omit hence the underlined ones. To reduce further

$$\begin{aligned}(3\,1\,1)&=(3\,1)1+\underline{(2\,1)2}+\underline{(1\,1)3}\\ (2\,1\,1)&=(2\,1)1+\underline{(1\,1)2},\\ (3\,1\,0)&=\underline{(3\,1)0}+(2\,1)1+\underline{(1\,1)2}+(3\,0)1\\ &\quad+\underline{(2\,0)2}+\underline{(1\,0)3}.\end{aligned}$$

This gives the μ systems 3 1 1 0, 2 2 1 0, 2 1 1 1, 2 1 1 1, 2 1 1 1 and their permutations. In the language of the magnetic quantum number expressed, the multiplet $(S,T,Y)=(3/2,3/2,1/2)$ contains $S_z=3/2$, $T_\xi=3/2$, $Y_\xi=1/2$ once, $S_z=3/2$, $T_\xi=1/2$, $Y_\xi=-1/2$ once, $S_z=T_\xi=Y_\xi=1/2$ three times. In addition to these, all permutations of these and those triplets in which any two of the $S_zT_\xi Y_\xi$ are replaced by their negative values. The multiplet is shown, along with some other ones, in Fig. 1, it is the third one.

According to the general theory[8] the wave functions of the multiplet $\Lambda_4\Lambda_3\Lambda_2\Lambda_1$ belong with respect to interchange of the η to the representation of the symmetric group which is characterized by the partition $\Lambda_4+\Lambda_3+\Lambda_2+\Lambda_1=n$.

It has been shown by Slater[11] for atomic spectra that the knowledge of the structure of multiplets enables one to determine the numbers and characters of the terms whch arise from any configuration. The same is true in principle for nuclear spectra. The difference is that instead of the two-dimensional plot of occurring L_zS_z values, one should prepare a four-dimensional plot of $L_zS_zT_\xi Y_\xi$ values. Or perhaps for every L_z and S_z a two-dimensional plot of the occurring $T_\xi Y_\xi$ values. For every L_z these plots must be decomposed into $S_zT_\xi Y_\xi$ combinations which form multiplets. After this, the L_z values for every multiplet must be grouped together into sets ranging from $-L$ to L thus obtaining the azimuthal quantum member.

The most practical procedure along these lines which I could find was one using the Λ and the diagonal quantum numbers. A state with μ_1 protons and μ_2 neutrons with spin $-1/2$ and μ_3 protons and μ_4 neutrons with spin $1/2$ is a state with the diagonal quantum numbers $\mu_1\mu_2\mu_3\mu_4$. One first makes a plot of the occurring $\mu_1\mu_2\mu_3$ values for every L_z and μ_4. For this purpose, one draws an equilateral triangle with the altitude

[10] Similar formulas hold also for symbols of the kind (12) with more than four Λ's. They can be proved by an argument similar to that of the next section.

[11] J. C. Slater, Phys. Rev. **34**, 1293 (1929).

FIG. 1.

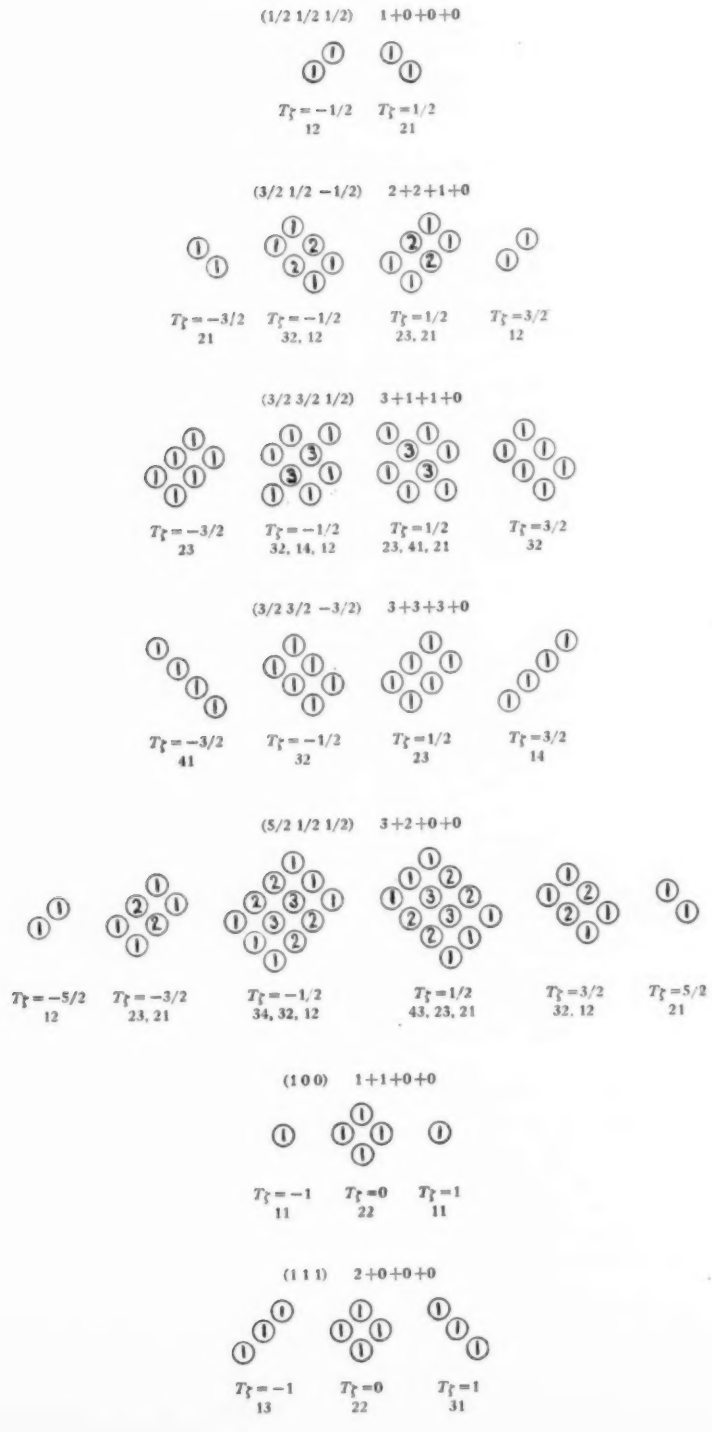
(1/2 1/2 1/2) 1+0+0+0
$T_\zeta = -1/2$ 12
$T_\zeta = 1/2$ 21
(3/2 1/2 −1/2) 2+2+1+0
$T_\zeta = -3/2$ 21
$T_\zeta = -1/2$ 32, 12
$T_\zeta = 1/2$ 23, 21
$T_\zeta = 3/2$ 12
(3/2 3/2 1/2) 3+1+1+0
$T_\zeta = -3/2$ 23
$T_\zeta = -1/2$ 32, 14, 12
$T_\zeta = 1/2$ 23, 41, 21
$T_\zeta = 3/2$ 32
(3/2 3/2 −3/2) 3+3+3+0
$T_\zeta = -3/2$ 41
$T_\zeta = -1/2$ 32
$T_\zeta = 1/2$ 23
$T_\zeta = 3/2$ 14
(5/2 1/2 1/2) 3+2+0+0
$T_\zeta = -5/2$ 12
$T_\zeta = -3/2$ 23, 21
$T_\zeta = -1/2$ 34, 32, 12
$T_\zeta = 1/2$ 43, 23, 21
$T_\zeta = 3/2$ 32, 12
$T_\zeta = 5/2$ 21
(1 0 0) 1+1+0+0
$T_\zeta = -1$ 11
$T_\zeta = 0$ 22
$T_\zeta = 1$ 11
(1 1 1) 2+0+0+0
$T_\zeta = -1$ 13
$T_\zeta = 0$ 22
$T_\zeta = 1$ 31

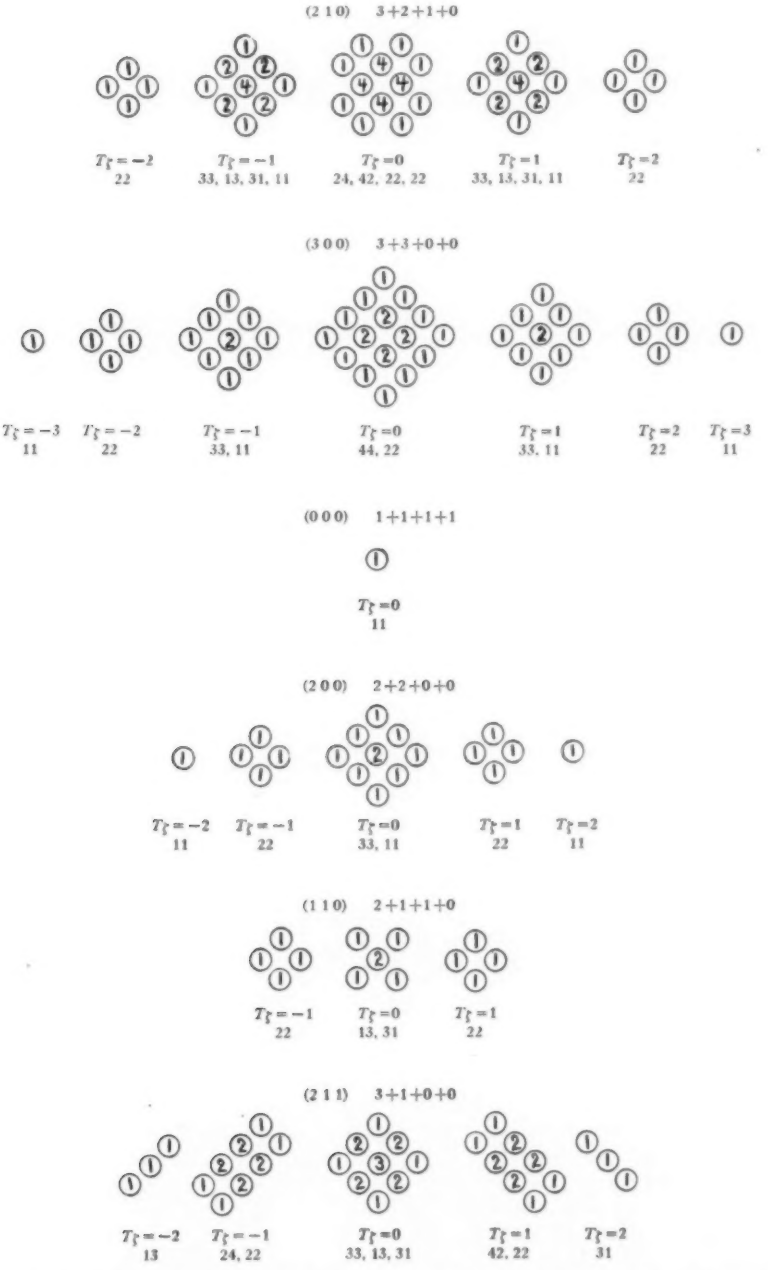

FIG. 1. Every set of figures represents a multiplet, the STY sign of which, together with one corresponding $A_4+A_3+A_2+A_1$, is given on top. Every circle represents a $S_z T_\xi Y_\xi$ state, T_ξ is given below the figure. Y_ξ and S_z are the coordinates of the circle, the origin of the coordinate system being at the center of the figure, the Y_ξ axis runs to the right, the S_z axis downward. The numbers in the circles give the number of states $S_z T_\xi Y_\xi$ in the multiplet. The distance between two adjoining circles on a horizontal or vertical is 2. The multiplets with half integer STY correspond to elements with masses $4n+1$. The multiplets for masses $4n+3$ are obtained from these by reversing the direction of the Y_ξ axis. The sign of Y must be changed also. The 2 at the center of this figure should be replaced by a 3.

$\mu_1+\mu_2+\mu_3=n-\mu_4$. The point which has the distances μ_1, μ_2, μ_3 from the three sides of the triangle, respectively, will correspond to a state with the diagonal quantum numbers μ_1, μ_2, μ_3 and $\mu_4=n-\mu_1-\mu_2-\mu_3$. Every plot forms a representation of the three dimensional unitary group. The irreducible representations of this group are rather simple, their plots are shown in Figs. 2a and 2b: the combination $\mu_1\mu_2\mu_3$ occurs in $\Lambda_1'\Lambda_2'\Lambda_3'$

$$\begin{pmatrix}\Lambda_3'\Lambda_2'\Lambda_1'\\ \mu_3\mu_2\mu_1\end{pmatrix}=1+\text{Min}\,(\Lambda_3'-\mu_3,\ \Lambda_3'+\Lambda_2'-\mu_3-\mu_2,\ \Lambda_3'-\Lambda_2',\ \Lambda_2'-\Lambda_1') \quad (15)$$

times, where Min $(\alpha, \beta, \cdots)$ is the smallest of the numbers $\alpha, \beta, \cdots$ if they are positive and equals -1 if any of them is negative.

One can decompose the $\mu_1\mu_2\mu_3$ plots for every L_z into irreducible plots, characterized by $(\Lambda_3'\Lambda_2'\Lambda_1')$ (the primes on the Λ are omitted in the figure). Having obtained the number of $(\Lambda_3'\Lambda_2'\Lambda_1')$, one unites these for every L_z separately into total multiplets $(\Lambda_4\Lambda_3\Lambda_2\Lambda_1)$ according to

$$(\Lambda_4\Lambda_3\Lambda_2\Lambda_1)=\sum(\Lambda_3'\Lambda_2'\Lambda_1'). \quad (16)$$

The limits of summation are given in (14). Finally the L_z values for every $(\Lambda_4\Lambda_3\Lambda_2\Lambda_1)$ are united separately to total azimuthal quantum numbers L. On the whole, the procedure is much more cumbersome than the analogous one for atomic spectra. It has the disadvantage also, that one first obtains the highest multiplicities, which have the highest energies.

4

An alternative method which leads much more rapidly to the goal is to consider, for the time being, only the dependence of the wave function on space coordinates. This method was worked out for atomic spectra by the present author and Delbrück[12] before the spin theory of Pauli was known. One considers first again the possible configurations i.e. the distributions of the particles into the different states, without, however, taking into consideration the spin. For every such state one determines the L_z (or m_L as it is often called) as the sum of the l_z of all the particles. Next one determines how many terms with a certain partition $\lambda_\rho+\lambda_{\rho-1}+\cdots+\lambda_1$ this configuration gives. Finally, one considers the states corresponding to every partition separately and unites states with L_z from $-L$ to L into a total multiplet with azimuthal quantum number L.

These steps performed, one has all one is interested in for approximation (1): the multiplicities and azimuthal quantum numbers of every term. For later work, it is still necessary to know how to complete the wave functions depending on coordinates alone, by functions depending on the spins, to total wave functions. Since the total wave function must be antisymmetric, the space-coordinate wave function and the spin function used for the completion must have adjoint characters, i.e., belong to two such representations the matrices of which are equal for even, oppositely equal for odd permutations. The adjoint partition to the partition $4+4+\cdots+1$ with n_4 fours, n_3 threes, n_2 twos and n_1 ones is the partition $\Lambda_4+\Lambda_3+\Lambda_2+\Lambda_1$ where

$$\begin{aligned}&\Lambda_4=n_4+n_3+n_2+n_1, \quad &&\Lambda_3=n_4+n_3+n_2,\\ &\Lambda_2=n_4+n_3, &&\Lambda_1=n_4.\end{aligned} \quad (17)$$

Thus, e.g., the partition $4+3+2+2+2+1$ for the spacial wave function is equivalent to the partition $6+5+2+1$ for the Λ, or to the STY set (4 1 0).

The step which involves the difficulty for this procedure is to determine how many terms with a certain partition $\lambda_\rho+\lambda_{\rho-1}+\cdots+\lambda_1$ a configuration gives in which there are μ_1 particles in the first, μ_2 in the second, etc., μ_ν in the ν-th state. We consider the wave function

$$\psi_1(x_1)\psi_1(x_2)\cdots\psi_1(x_{\mu_1})\psi_2(x_{\mu_1+1})\cdots\psi_2(x_{\mu_1+\mu_2})\cdot\psi_3(x_{\mu_1+\mu_2+1})\cdots\psi_\nu(x_n) \quad (18)$$

together with those arising from (18) by a permutation of the x. There are $n!/\mu_1!\mu_2!\cdots\mu_\nu!$ of these. Under a permutation of the x they naturally transform among themselves, the corresponding (reducible) representation of the sym-

[12] E. Wigner, Zeits. f. Physik **43**, 627 (1927); M. Delbrück, Zeits. f. Physik **51**, 181 (1928). Eq. (19) of the former and (14) of the latter give an explicit expression for (20) in the case all λ and μ are 1 or 2. Only this case occurs in ordinary spectroscopy. A similar expression would be too complicated if the λ and μ can be 3 and 4 also.

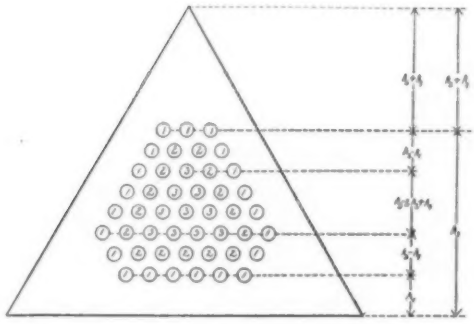

a

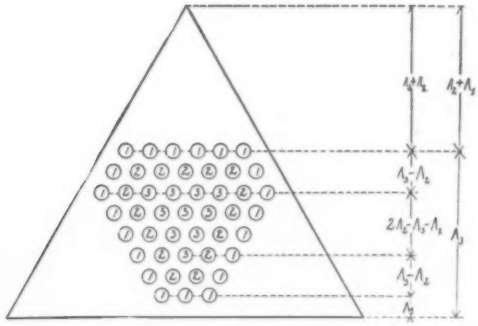

b

FIG. 2. Every circle corresponds to a triple $\mu_1\mu_2\mu_3$, these numbers being the distances of the circle from the three sides of the equilateral triangle, surrounding the figure. The number in the circle tells how often the corresponding set of μ's occurs in the representation characterized by $(\Lambda_3\Lambda_2\Lambda_1)$. Fig. 2a holds for $\Lambda_3-\Lambda_2 \geq \Lambda_2-\Lambda_1$, Fig. 2b for $\Lambda_3-\Lambda_2 \leq \Lambda_2-\Lambda_1$ (the first is actually the multiplet (9 4 2) the second one (8 6 1)). In both cases the boundary hexagon contains one's, the next two's and so on until the hexagon reduces to a triangle. The μ sets within the triangle occur all equally often in the representation: $\Lambda_2-\Lambda_1+1$ times in the first, $\Lambda_3-\Lambda_2+1$ times in the second case.

metric group will be denoted by $[\mu_\nu\mu_{\nu-1}\cdots\mu_1]$. Upon decomposing this into irreducible representations

$$[\mu_\nu\mu_{\nu-1}\cdots\mu_1]=\sum_\lambda \begin{pmatrix}\lambda_\rho\lambda_{\rho-1}\cdots\lambda_1\\ \mu_\nu\mu_{\nu-1}\cdots\mu_1\end{pmatrix}(\lambda_\rho\lambda_{\rho-1}\cdots\lambda_1), \tag{19}$$

the coefficients (some of which occurred previously in (12)) tell us how many terms with the partition $\lambda_\rho+\lambda_{\rho-1}+\cdots+\lambda_1$ the configuration gives. We shall arrange the μ again in a descending order $\mu_\nu \geq \mu_{\nu-1} \geq \cdots \geq \mu_1 \geq 0$.

Only those partitions $\lambda_\rho+\lambda_{\rho-1}+\cdots+\lambda_1$ will correspond to real terms in which none of the λ is greater than 4. This must hold then, because of (13), for the μ as well: no orbit can be more than four times occupied. One can even omit for the calculation of the coefficients all the fourfold occupied states, i.e., drop all the $\mu=4$, since because of (13), the λ above a 4 must be a 4 also.

In the p shell, there are only three states $l_z=-1, 0, 1$ and the coefficients of interest are therefore of the form (15) (if the partition contains only two addends, a 0 can be affixed for λ_1) and they are explicitly given in (15). One must only arrange the μ in descending order.

In this case the calculation is especially simple. For instance, for 3 particles we have the ten configurations of Table I. The figures below the l_z values give the number of particles (μ) in this state, the figure below L_z is the total L_z, the last columns give the number of terms with the partitions 3 or (3+0+0) and 2+1 (i.e., (2+1+0)) which this configuration gives. This gives F and P terms with the partition (3) and D and P terms with the partition (2+1). Table II, reference 4, was prepared in this way. The adjoint partitions to (3) and (2+1) are (1+1+1) and (2+1), respectively, the STY characterization is $(\frac{1}{2}\ \frac{1}{2}\ -\frac{1}{2})$ for the former, $(\frac{3}{2}\ \frac{1}{2}\ \frac{1}{2})$ for the latter. There is in addition to these, one S term of the multiplicity $(\frac{3}{2}\ \frac{3}{2}\ \frac{3}{2})$.

In the general case the explicit formulas for the

$$\begin{pmatrix}\lambda_\rho & \lambda_{\rho-1} & \lambda_{\rho-2} & \cdots & \lambda_1\\ \mu_\nu & \mu_{\nu-1} & \mu_{\nu-2} & \cdots & \mu_1\end{pmatrix} \tag{20}$$

are too complicated. A useful way of evaluating (20) starts from another interpretation of (20) than given in (19). For Frobenius' reciprocity theorem[13] one considers the subgroup which contains the permutations of the first μ_1 elements

TABLE I. *The ten configurations for 3 particles.*

$l_z=-1$ 0 1	L_z	(3)	(2+1)	$l_z=-1$ 0 1	L_z	(3)	(2+1)
3 0 0	−3	1		1 0 2	1	1	1
2 1 0	−2	1	1	0 3 0	0	1	—
2 0 1	−1	1	1	0 2 1	1	1	1
1 2 0	−1	1	1	0 1 2	2	1	1
1 1 1	0	1	2	0 0 3	3	1	—

[13] G. Frobenius, Berl. Ber. 501 (1898). The reader will find a straight forward proof in H. Weyl's *Gruppentheorie und Quantenmechanik* (Leipzig 1928), first edition, p. 254. The proof in the English translation by H. P. Robertson (London, 1931), pp. 332–338, is more abstract.

among themselves, the next μ_2 elements among themselves, etc. and all the products of these permutations. Then (20) gives the number, how often the unit representation in which every element of the subgroup is represented by the "matrix" (1), occurs in $(\lambda_\rho+\lambda_{\rho-1}+\cdots+\lambda_1)$, if this is considered as a representation of the subgroup. This is, however, also the number of times the adjoint representation $(\Lambda_4\Lambda_3\Lambda_2\Lambda_1)$, again considered as a representation of the subgroup, contains the "antisymmetric" representation, in which every even permutation is represented by (1), every odd by (-1). If we denote this by

$$\begin{bmatrix} \Lambda_4\Lambda_3\Lambda_2\Lambda_1 \\ \mu_\nu\mu_{\nu-1}\cdots\quad \mu_1 \end{bmatrix}=\begin{pmatrix} \lambda_\rho\lambda_{\rho-1}\cdots\quad \lambda_1 \\ \mu_\nu\mu_{\nu-1}\cdots\quad \mu_1 \end{pmatrix} \tag{21}$$

(21) expresses Frobenius' theorem. The Λ are defined in (17).

The expressions (21) can be calculated by recursion formulas. If $\mu_\nu=4$, we have

$$\begin{bmatrix} \Lambda_4\Lambda_3\Lambda_2\Lambda_1 \\ 4\quad \mu_{\nu-1}\cdots\quad \mu_1 \end{bmatrix}=\begin{bmatrix} \Lambda_4-1 & \Lambda_3-1 & \Lambda_2-1 & \Lambda_1-1 \\ \mu_{\nu-1} & \mu_{\nu-2}\cdots & & \cdots\mu_1 \end{bmatrix} \tag{22a}$$

By means of this formula, one can get rid of all 4 among the μ. If $\mu_\nu=3$

$$\begin{bmatrix} \Lambda_4\Lambda_3\Lambda_2\Lambda_1 \\ 3\quad \mu_{\nu-1}\cdots\quad \mu_1 \end{bmatrix}=\begin{bmatrix} \Lambda_4-1 & \Lambda_3-1 & \Lambda_2-1 & \Lambda_1 \\ \mu_{\nu-1} & \mu_{\nu-2}\cdots & & \mu_1 \end{bmatrix}+\begin{bmatrix} \Lambda_4-1 & \Lambda_3-1 & \Lambda_2 & \Lambda_1-1 \\ \mu_{\nu-1} & \mu_{\nu-2}\cdots & & \mu_1 \end{bmatrix}$$
$$+\begin{bmatrix} \Lambda_4-1 & \Lambda_3 & \Lambda_2-1 & \Lambda_1-1 \\ \mu_{\nu-1} & \mu_{\nu-2}\cdots & & \mu_1 \end{bmatrix}+\begin{bmatrix} \Lambda_4 & \Lambda_3-1 & \Lambda_2-1 & \Lambda_1-1 \\ \mu_{\nu-1} & \mu_{\nu-2}\cdots & & \mu_1 \end{bmatrix}. \tag{22b}$$

After a sufficient number of reductions of this type, there will be only 2's and 1's among the μ. If one of the [ ], occurring in the right side of (22b) contains a negative number in the upper row, or a number which is greater than the preceding one, the whole [ ] is zero. To get rid of the 2's

$$\begin{bmatrix} \Lambda_4\Lambda_3\Lambda_2\Lambda_1 \\ 2\quad \mu_{\nu-1}\cdots\quad \mu_1 \end{bmatrix}=\begin{bmatrix} \Lambda_4 & \Lambda_3 & \Lambda_2-1 & \Lambda_1-1 \\ \mu_{\nu-1} & \mu_{\nu-2}\cdots & & \mu_1 \end{bmatrix}+\begin{bmatrix} \Lambda_4 & \Lambda_3-1 & \Lambda_2 & \Lambda_1-1 \\ \mu_{\nu-1} & \mu_{\nu-2}\cdots & & \mu_1 \end{bmatrix}+\begin{bmatrix} \Lambda_4-1 & \Lambda_3 & \Lambda_2 & \Lambda_1-1 \\ \mu_{\nu-1} & \mu_{\nu-2}\cdots & & \mu_1 \end{bmatrix}$$
$$+\begin{bmatrix} \Lambda_4 & \Lambda_3-1 & \Lambda_2-1 & \Lambda_1 \\ \mu_{\nu-1} & \mu_{\nu-2}\cdots & & \mu_1 \end{bmatrix}+\begin{bmatrix} \Lambda_4-1 & \Lambda_3 & \Lambda_2-1 & \Lambda_1 \\ \mu_{\nu-1} & \mu_{\nu-2}\cdots & & \mu_1 \end{bmatrix}+\begin{bmatrix} \Lambda_4-1 & \Lambda_3-1 & \Lambda_2 & \Lambda_1 \\ \mu_{\nu-1} & \mu_{\nu-2}\cdots & & \mu_1 \end{bmatrix}. \tag{22c}$$

If all the $\mu=1$, which will be true after some reductions of this type, one can use a formula analogous to the previous ones. It is quicker to notice that (23) is the dimension of $(\Lambda_4\Lambda_3\Lambda_2\Lambda_1)$ and hence

$$\begin{bmatrix} \Lambda_4\Lambda_3\Lambda_2\Lambda_1 \\ 11\cdots\quad 1 \end{bmatrix}=\frac{(\Lambda_4+\Lambda_3+\Lambda_2+\Lambda_1)!(\Lambda_4+3-\Lambda_1)(\Lambda_4+2-\Lambda_2)(\Lambda_4+1-\Lambda_3)}{(\Lambda_4+3)!(\Lambda_3+2)!(\Lambda_2+1)!\Lambda_1!}$$
$$\cdot(\Lambda_3+2-\Lambda_1)(\Lambda_3+1-\Lambda_2)(\Lambda_2+1-\Lambda_1). \tag{23}$$

One will use the formulas (22), (23) very rarely. In most practical cases, the calculation of the coefficients (21) is greatly facilitated by special conditions.

5

We can go over, now, to approximation (2). In this approximation the Hamiltonian will be invariant with respect to all operations involving τ only. Since τ has, mathematically, the same properties as the ordinary spin variable, we shall have the analogs of the quantum numbers L and S of ordinary spectroscopy. Instead of the azimuthal quantum number of the common spectroscopy, we have the total quantum number J, since the spin forces are taken into account in

approximation 2; instead of the total spin, we have an isotopic spin T. Of course, the interaction of J and T in the higher approximation 4 will be entirely different from the interaction between azimuthal and spin quantum numbers of ordinary spectroscopy. Above all, the resulting angular momentum J will be a good quantum number in all approximations.

The existence of a total isotopic spin means that terms with different ζ components of the isotopic spin have the same energy in approximation 2. These are, of course, terms of different isobaric nuclei, and a total isotopic spin T will be a term with the same binding energy for all nuclei with isotopic numbers from $-T$ to T. This shows that to every term of an element with a certain isotopic number T_ζ, terms of all elements with smaller isotopic numbers will correspond. The element with the smallest isotopic number ($n_P=n_N$ for even masses, $n_P=n_N\pm1$ for odd masses) has the greatest number of terms. In approximation 4, the equality of these term values will cease to hold and the Coulomb energy, already, will introduce a splitting.

If one is interested in the number of terms of approximation (2), arising from a certain configuration, one can use the ordinary Hund-Russell-Saunders method to determine these. The only difference is that the "orbits" contain the ordinary spin quantum number already and one has, therefore, for instance, six p states, with Z components of the angular momentum $3/2$, $1/2$, $1/2$, $-1/2$, $-1/2$, $-3/2$. Everyone of these six states can be doubly occupied, with a particle $\tau=1$ and $\tau=-1$ (neutron or proton). The half sum of the τ is denoted by T_ζ and the different T_ζ from $-T$ to T united into a multiplet. The number of terms, arising even from a simple configuration, is very great, however.

It is more important, perhaps, to consider the terms into which a term of approximation (1) splits if we introduce the spin forces and thus go over to (2). The transition from approximation (1) to (2) can be performed in two steps: first disregarding Y_ζ, every multiplet goes over into several multiplets which still have an S and T. One obtains these by simply projecting every point of Fig. 1 into the S_zT_ζ plane. This is done in Fig. 3 for the multiplet $(3/2, 3/2, 1/2)$ as an example. We see that it gives one term with $S=3/2$, $T=3/2$, one with $S=3/2$, $T=1/2$, one with $S=1/2$, $T=3/2$, and one with $S=1/2$, $T=1/2$. The second step, then, is to combine the S's with the azimuthal quantum number L to J's, according to the vector addition model.

It would be very important to know experimentally the relative separation of the terms which arise from the same approximation 1 term, since this would allow us to tell which of the 6 possible interactions, given in Section 2, describes the spin forces.

Fig. 4 shows what can be expected in approximation (2). Every figure corresponds to a set of isobars. The abscissa is the isotopic number, the ordinate the total energy. Every line corresponds to a term of approximation (2) all lines arising from the same term of approximation (1) are grouped close together. The STY symbol of this term is given on the right, it is, of course, the same for all the group. The T of the term is represented by the length of its line, so that the term exists for elements with those isotopic numbers T_ζ, over which the line extends. The number on the left of the line is the S, characterizing its spin after the first step in the transition from approximation (1) to (2) is performed. This S will be the total angular momentum J of the nucleus, if the azimuthal quantum number was zero, which will be very frequently the case. The energy of the approximation (1) term is estimated on the basis of Eq. (8), reference 4. This estimate gives the same value for all terms of the same configuration with the same multiplicity STY which is, of course, only approximately true. We are interested, of course, only in the lowest term of every multiplicity. The distances between the lines of the same group have no significance.

We see that in several cases the approximation (2) terms extend over several isobars and the question of the most stable isobar will be decided, hence, only in the next approximation. We may assume that the most important term in the next approximation is the Coulomb energy.[14] This will

[14] The most stable isobar has the smallest mass, not the greatest binding energy. For the consideration of the stability, therefore, T_ζ times the mass difference between neutron and H^1 should be added to the total energy. This will cause the lines of Fig. 3 to slope upward to the right. This slope is soon overcompensated, however, by the opposite effect of the Coulomb energy.

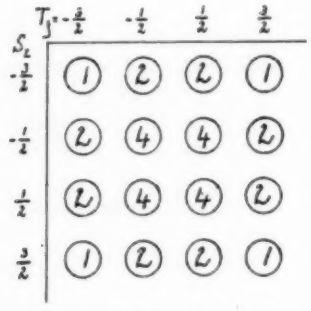

FIG. 3. Determination of the spin angular momentum S and isotopic spin T of the terms arising from the multiplet (3/2, 3/2, 1/2) if the spin forces are introduced. The spin angular momenta S must be added, subsequently, to the orbital angular momentum L, according to the vector addition principle, in order to obtain the total angular momentum J.

decrease the binding energy of the nuclei with negative T_z, compared with the binding energy of nuclei with positive T_z and cause the horizontal lines of Fig. 4 to slope downward to the right. The slope will be very roughly proportional to the 2/3 power of the charge.

This slope will have the most noticeable effect for isobars with masses $4n+2$. While for small charge, the point a is most stable, beginning at O^{18}, the point b will become stable.

We can proceed even to higher elements, by successively increasing the slope of the lines more and more. For elements $4n$, if the slope becomes 3/2, in the arbitrary units of the figure, the point b will become most stable. This happens to be at A^{40}. The point c never will become most stable, since b reaches a before c does. This seems to be the explanation why no nuclei of mass $4n$ with odd number of protons and neutrons exist. There are, however, radioactive nuclei of this type.

The situation is very similar for nuclei with masses $4n+2$. Here the critical slope is 2, when the point c reaches a. Again, point d is not the most stable for any slope, and there are (apart from a) no stable nuclei with odd neutron and proton number, for elements $4n+2$ either. The slope 2 seems to be reached at Ti^{50}, later, of course, than slope 3/2.

It should be mentioned that the whole Fig. 4 will be compressed in energy scale as we proceed to higher elements, because the exchange integrals decrease. It has been shown by Bethe and

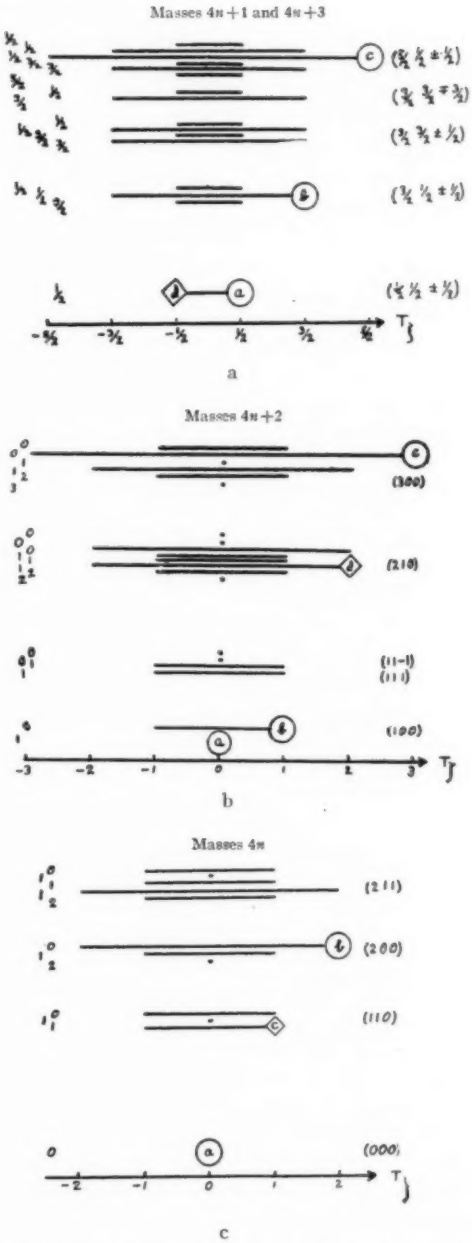

FIG. 4. The different kinds of multiplets are shown for elements with mass numbers of the form $4n$, $4n\pm1$, $4n+2$. The ordinate is the energy in arbitrary units. Only one term for every multiplet system is given, with a position on the energy scale corresponding to long range forces. The abscissa is the difference between the number of neutrons and protons, divided by 2. The circles correspond to stable nuclei, the squares to unstable nuclei.

Bacher[15] that this happens in discontinuous steps, corresponding to the completion of shells. There is, therefore, an increased probability for the slope to pass a certain amount in the regions where shells are completed.

In case of elements with mass numbers $4n+1$ and $4n+3$ we obtain the same picture. First, the point a is most stable, at a slope $3/2$ the point b reaches a. This seems to happen at Cl^{37} and Ca^{43}, respectively, quite in the neighborhood of A^{40}. For the slope 2, the point c passes b and Ti^{49} and V^{51} become the stable isobars. These are near indeed to Ti^{50}. This explanation of the places where the isotopic number of stable isobars shifts to higher values works rather better than could be expected and the agreement is beyond doubt, partly accidental.

6

As a last point, I should like to establish the connection between approximations 1 and 3, i.e., determine the terms into which an STY term of approximation (1) splits if one introduces, as a perturbation, the difference between proton-proton, proton-neutron, neutron-neutron interactions, neglecting, however, spin forces.

The operator

$$\tfrac{1}{4}(s_{z1}(1+\tau_{\xi 1})+s_{z2}(1+\tau_{\xi 2})+\cdots +s_{zn}(1+\tau_{\xi n}))=\tfrac{1}{2}(S_z+Y_\xi)=S_{zN} \quad (24)$$

gives the Z component of the neutron spin angular momentum, since $1+\tau_\xi$ gives 0, if applied to a proton state. Similarly

$$\tfrac{1}{4}(s_{z1}(1-\tau_{\xi 1})+s_{z2}(1-\tau_{\xi 2})+\cdots +s_{zn}(1-\tau_{\xi n}))=\tfrac{1}{2}(S_z-Y_\xi)=S_{zP} \quad (24a)$$

gives the Z component of the proton spin angular momentum. If we go through all the points of Fig. 1 for a certain T_ξ and insert their S_{zN} and S_{zP} values into a table, one can unite the points of the table in the normal way to a S_NS_P multiplet.[16] The azimuthal quantum number is, of course, unchanged by the transition from approximation (1) to (3).

If the proton-proton forces are assumed to be equal to the neutron-neutron forces, the S_NS_P term will coincide in case of equal number of protons and neutrons with the S_PS_N term, if $S_N \neq S_P$. In the work of reference 4, these terms were given as one term. The values of the multiplicities $2S_N+1$, $2S_P+1$ are given in Fig. 1 below every T_ξ.

We may consider, as an example, the (3/2 3/2 1/2) multiplet, given in Fig. 1. Below $T_\xi=1/2$ we have the three pairs 23, 41, 21. This means that for an element of the mass $4n+1$ with $T_\xi=1/2$ (e.g., C^{13}), certain states in which the neutrons are in the doublet, the protons in the triplet state, exactly coincides in approximation (1) with a state in which the neutrons are in the quartet, the protons in the singlet state, and with another state in which the neutrons are in doublet, the protons in the singlet state. It may be added that the binding energy of these states is equal in approximation (1), to the binding energy of a hypothetical B^{13} nucleus ($T_\xi=3/2$) in which the neutrons are in the triplet, the protons in the doublet state. In reality, all these states will be unstable for isobars with the mass 13, because of the comparatively high position of the (3/2 3/2 1/2) multiplet in Fig. 4a. The example is thus, perhaps, not a very fortunate one but it illustrates the kind of regularities to be expected more clearly than a simpler case.

[15] H. A. Bethe and R. F. Bacher, Rev. Mod. Phys. 8, 82 (1936), Section VI.

[16] Instead of this, one can simply turn the corresponding level in the diagrams of Fig. 1 by 45°.

The Absolute Photoelectric Yields of Mg, Be and Na

MARVIN M. MANN, JR.* AND LEE A. DUBRIDGE
Department of Physics, University of Rochester, Rochester, N. Y.
(Received October 19, 1936)

Measurements of the absolute photoelectric yields for distilled surfaces of Mg, Be and Na were made and values of α in Fowler's photoelectric equation determined. For Mg, Be and Na the values of the work function are, respectively, 3.68, 3.92 and 2.29 volts and of α, 3.2, 25 and 180×10^{-34} cm² sec./quant. These values of α range from 10^{-2} to 10^{-3} of the maximum theoretical values. The ratios are interpreted as the fraction of light absorbed by the electrons in the surface potential barrier.

INTRODUCTION

FOWLER'S theory of the surface photoelectric effect in metals leads to the following equation[1] for the saturation current I excited by unit intensity of incident light of frequency ν,

$$I=\alpha A T^2\varphi(x), \tag{1}$$

where $\varphi(x)$ is a universal function of the quantity $x=h(\nu-\nu_0)/kT$, A is the thermionic constant having the value 120 amp./cm² deg.² and α is a proportionality constant involving the probability of light absorption by electrons at the surface. Repeated experimental tests have shown this equation to hold quite accurately for reasonably wide frequency ranges in the vicinity of ν_0. It is evident, therefore, that within the frequency range for which the equation is valid, the photoelectric emission from any surface may be fully specified by giving the values of the two constants ν_0 and α, which are quite analogous to the constants b and A in the Richardson thermionic equation. Fowler's method has now become standard for the determination of photoelectric thresholds but very little attention has been given to the absolute values of α. It was the purpose of this investigation to determine values of α for various surfaces and for a single surface under various conditions.

As has been pointed out by one of us,[1] simple considerations allow one to set an upper limit to the value of α for any surface and these considerations also suggest that unless additional factors enter, the values of α for different surfaces should not be widely different. Thus if it is assumed that all incident quanta are absorbed by electrons bound within the surface potential barrier the value of α should be

$$\alpha=(2m/\pi h)(8\pi/3n)^{4/3}=15.1n^{-4/3}, \tag{2}$$

where n is the number of free electrons per unit volume, and the unit of light intensity is taken to be 1 quantum/cm² sec. Since, however, the electrons bound in the surface field occupy a layer of only atomic dimensions and since the light penetrates into the metal a distance of the order of its wave-length one would expect that the fraction of the light absorbed by the surface electrons would be from 10^{-2} to 10^{-3} of the incident light. The ratio of the observed value of α to the value calculated from Eq. (2) might then be taken as a measure of this fraction.

It should be stated, of course, that as more exact theories of the photoelectric effect are developed the exact interpretation of the quantities entering Eq. (1), which is certainly a good first approximation, may be changed. Nevertheless, these qualitative ideas aid greatly in interpreting results and from the experimental point of view a study of the values of α is of great importance.

A further remark should be made in regard to the units in which the I of Eq. (1) is to be expressed. In the present paper I has been expressed in electrons/quantum rather than in amp./watt or other intensity units used in previous work. This is because in these units the value of α has a clearer interpretation and also because the whole theory is based on the quantum picture. Actually, however, we can detect no systematic differences in the fit of the data to

* Now at Washington University, St. Louis, Mo.
[1] See L. A. DuBridge. *Actualités Scientifiques et Industrielles*, No. 268 (Hermann and Cie, Paris, 1935).

the theoretical curve whichever units are used, except for slight differences in the threshold ν_0 and, of course, in α. Cashman and Jamison[2] have recently come to the same conclusion though in their experiments the frequency range was such that the value of x ran up to only about 18, while our experiments extended up to $x=50$. Fig. 4 shows the fitting of data reduced both to amp./watt and to electrons/quantum. In this case the values of ν_0 for the two curves differ by 0.03 volt or by about 0.8 percent.

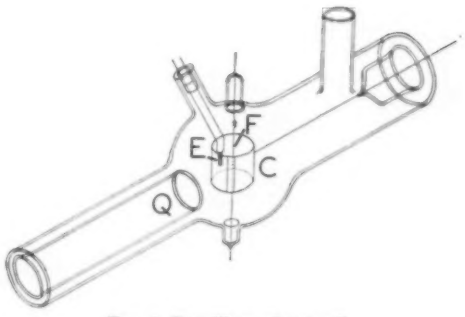

FIG. 1. Beryllium photo-cell.

PROCEDURE

The metals used in this investigation were beryllium, magnesium and sodium, chosen mostly for their interest in connection with other work in progress here and elsewhere, and also because the work functions were sufficiently low to allow a fairly wide range of frequencies to be used. The very careful vacuum technique found necessary in previous photoelectric work was followed throughout to secure surfaces as free from contamination as possible. All of the metals were distilled in vacuum onto a glass or metal surface in the form of an opaque layer. When distillation of successive layers caused no change in photoelectric emission this was taken to mean that the surface was clean, or at least in a stable condition.

The beryllium cell is shown in Fig. 1. The beryllium was held in a small spiral filament E which was coated with an insulating clay. It was evaporated, by heating of the filament, on to the inner surface of the metal cylinder C. The central tungsten filament F served as the anode. The opening of the cylinder and the quartz window Q were oriented in such a manner that the incident light suffered at least two or three reflections, thereby insuring the absorption of a large fraction.

For magnesium a cell of the double distillation type was used and is shown in Fig. 2. The magnesium was enclosed in a small molybdenum box M, open at the front. Immediately behind it was a filament F of 10 mil tungsten which was used to heat the magnesium. From this point the magnesium was evaporated on to the nickel disk N which was then turned around by an external magnet and the magnesium was driven on to the spherical surface G by heating the disk by electron bombardment.

The sodium cell is shown in Fig. 3. The sodium, which had been initially distilled in vacuum and sealed off in small Pyrex pellets, was placed in the side arm A. The tungsten filament F, in the form of a loop, served as the anode. The sodium was evaporated into the main bulb by heating the two parts of the side arm with furnaces. Continued distillation of the sodium for three or four days produced surfaces which gave reasonably reproducible results which are believed to be typical of rather clean sodium.

Each photoelectric cell was baked for several days at high temperatures. The metal parts were then thoroughly bombarded, and a second baking given the tube. The metal to be distilled was then heated to a temperature just below the

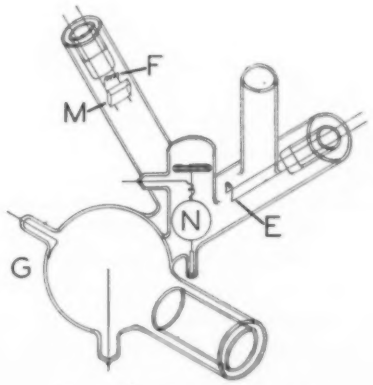

FIG. 2. Magnesium photo-cell.

[2] R. J. Cashman and N. C. Jamison, Phys. Rev. **50**, 568 (1936).

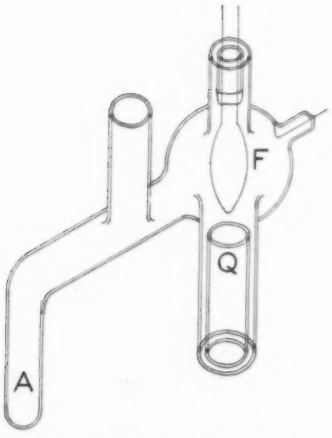

FIG. 3. Sodium photo-cell.

vaporization point for one to three days or until appreciable gas evolution had ceased. The temperature was then very slowly raised to the point where an opaque layer was deposited in about 10 hours. Further layers were laid down on the first after each series of measurements and additional check runs were made by cleaning out the cell and depositing new layers.

Energy measurements of the radiation emerging from the slit of the Bausch and Lomb quartz monochromator were made with a Bi-Te vacuum thermopile constructed by Mr. J. P. Foerst of the University of Wisconsin after the design developed by the late Professor Mendenhall. By subtracting both from the thermopile and the photoelectric measurements the average background radiation between spectral lines of the mercury arc, the effects of scattered light of other wave-lengths was effectively eliminated. In the measurements on sodium the continuous radiation from a projection lamp was used in addition to the mercury arc. In this case the slit widths were reduced to values so small that scattered light was unimportant, as was evidenced by the agreement between the arc and lamp data. The thermopile was calibrated in absolute units by a National Bureau of Standards standard lamp. In all cases the photoelectric cells approached the "black body" conditions so that practically all of the light incident was absorbed by the surface and no correction for reflection coefficients need be introduced.

RESULTS AND DISCUSSION

Typical Fowler plots for Mg, Be and Na are shown in Figs. 4, 5 and 6. The best values of the work functions and of α for clean surfaces of these metals are given in Table I:

The value of 3350A for the threshold of Mg is in reasonably good agreement with the value 3430 reported by Cashman and Huxford[3] for carefully prepared surfaces.

In the case of Be no previous measurements have come to our attention. Inasmuch as Dr. Zworykin, of the RCA Victor Company, informed us that Be sensitized with O_2 showed a rather high secondary emission we attempted to see whether such surfaces showed a high photoelectric yield. Short glow discharges in O_2 at low pressures, however, produced changes in threshold of only about 0.1 volt and a longer discharge at higher pressure desensitized the surface completely shifting the threshold to below 2200A. There was no evidence of a condition of low work function, though the possibilities were by no means exhaused.

The values found for the work function of Na by various workers are notoriously inconsistent.[4] The value found in this work for a distilled layer on glass was quite reproducible under the conditions of the experiment. It is in fairly good agreement with the theoretical value 2.35 volts, predicted by Bardeen,[5] and the value of 2.4 volts reported by Brady and Jacobsmeyer[6] for a thin film on Al. It will be noted, however, that the sodium data do not fit the Fowler plots over as wide a frequency range as for the other metals, a point which is being further investigated. This is shown also in Fig. 7 where yields are plotted against λ. For the other metals the data fit the theory for a range of x values of about 50, a much wider range than used in most previous experiments.

The relation between the observed values of α and the values calculated from Eq. (2) can be seen from Table II, in which are listed also values reported by other workers.

---

[3] R. J. Cashman and W. S. Huxford, Phys. Rev. **48**, 734 (1935).

[4] See Hughes and DuBridge, *Photoelectric Phenomena*, p. 75.

[5] J. Bardeen, Phys. Rev. **49**, 653 (1936).

[6] J. J. Brady and V. P. Jacobsmeyer, Phys. Rev. **49**, 620 (1936).

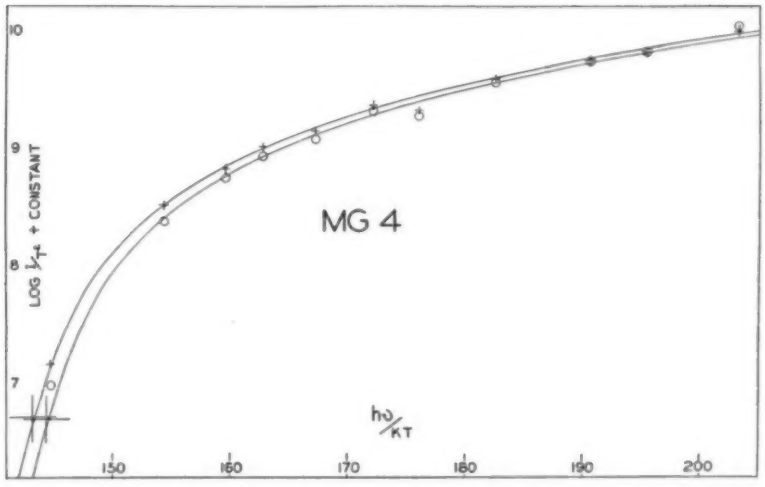

FIG. 4. Fowler plot for Mg. Upper curve, amp./watt, const. = 20, $\varphi = 3.65$ V. Lower curve, electrons/quant., const. = 19.3, $\varphi = 3.68$ V.

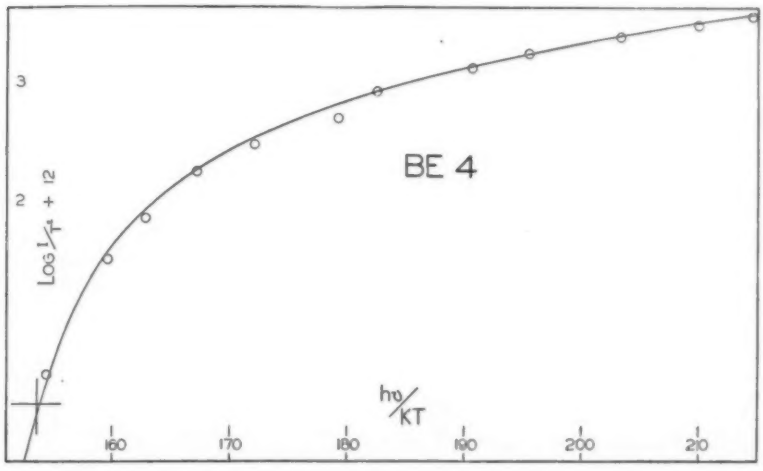

FIG. 5. Fowler plot for Be. elec./quant., $\varphi = 3.92$ V.

Table III shows the variation of α with contamination of the surface for Na and Be. In the

TABLE I. *Work functions and values of α, the probability of light absorption by electrons.*

Metal	φ Volts	λ_0 A.U.	$\alpha \times 10^{24}$ sec. cm^2 quant.$^{-1}$
Mg	3.68	3350	3.2
Be	3.92	3150	25.
Na	2.29	5390	180.

TABLE II. *Observed and calculated values of α.*

Metal	α(obs.) $\times 10^{22}$ sec. cm^2 quant.$^{-1}$	$\alpha \times 10^{22}$ calc.	Ratio calc./obs.	Ref.
Be	0.25	12.5	50	1
Mg	.032	48.8	1520	1
Na	2.29	198.	86.5	1
W	.026	29.4	1140	2
Ba	.43	140.	325	3

1. Present work.
2. A. King, unpublished.
3. Cashman and Jamison, reference 2.

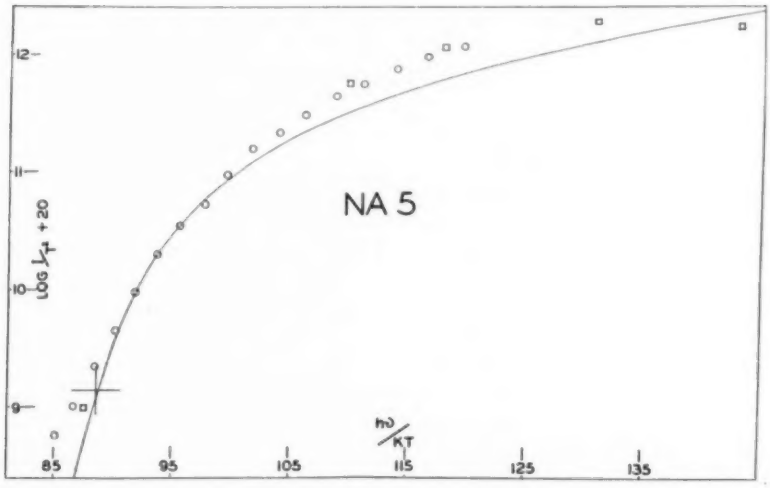

FIG. 6. Fowler plot for Na. $\varphi = 2.29$ V.

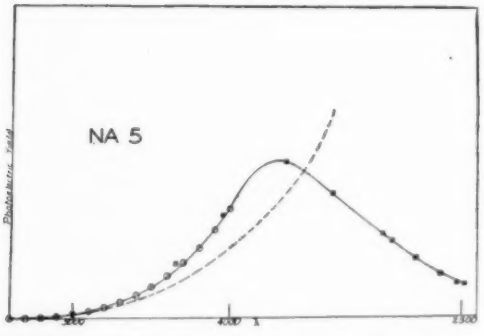

FIG. 7. Spectral distribution curve for Na. Dashed curve, Fowler's theory. ○ tungsten lamp, □ Hg arc.

case of Be the values represent the effects of successive glow discharge in O_2 and for Na the values are for successive layers laid down, the last being most free of gas contamination. These variations in α are relatively small and show no systematic trend.

TABLE III. *Showing variation of α with contamination.*

Metal	φ	α	α calc./α obs.
Be	3.92	17.9×10^{-34}	70
	3.89	7.0	178
	3.81	5.8	215
	3.81	4.6	262
	3.82	4.0	312
	3.92	5.7	219
Na	2.24	1.8×10^{-32}	110
	2.27	2.0	98
	2.29	2.0	98
	2.29	1.5	131

It is evident that the values of $\alpha_{obs.}$ lie in general between 10^{-32} and 10^{-34}. If we interpret the ratio obs./calc. as the fraction of light absorbed in the surface layer it is evident that this varies rather widely but lies in general in the range 10^{-2} to 10^{-3}. It is hoped that further developments of the quantum theory of photoelectric emission now being carried out in this laboratory will provide a theoretical basis for predicting the absolute values of photoelectric yields.

To compute the actual photoelectric emission in electrons/quantum at any wave-length for a surface for which ν_0 and α are known it is only necessary to use Eq. (1). Since this involves only the difference $(\nu-\nu_0)$ it is often convenient to compare the yields of surfaces for a given value of this quantity, or of x. Thus for $x=40$, $\varphi(x)=800$. Hence at 300°K we have

$$I_{40}=\alpha\times5.35\times10^{28}\ \text{elec./quant.}$$

For values of α of the order of 10^{-33} then $I_{40}\leqq5\times10^{-5}$ elec./quant.

In conclusion the authors wish to express their appreciation to Mr. R. J. Maurer who assisted in analyzing the data.

A Symmetry Theorem in the Positron Theory

W. H. FURRY
Physics Research Laboratory, Harvard University, Cambridge, Massachusetts
(Received October 26, 1936)

In the positron theory considerable interest attaches to the consideration of processes in which the occurrence of electrons and positrons is transitory only, such as the scattering of light by a Coulomb field (Delbrück), and the scattering of light by light (Euler and Kockel). Calculations of such effects can frequently be simplified on account of cancellations brought about by the distribution's symmetry between electrons and positrons. An abstract proof is here presented for the theorem which predicts the appearance of such cancellations in the general case. Certain modifications are found to be required when interactions other than the usual electric forces are introduced.

I. INTRODUCTION

AN interesting feature of the Dirac theory of the positron is the possibility of processes in which electrons and positrons, though they are not actually created so as to be experimentally observable, are able to play the part of catalytic agents producing effects which otherwise could not appear. Examples of such effects are the scattering of light from a Coulomb field, suggested by Delbrück,[1] and the scattering of light by light, suggested by Halpern[2] and by Debye and calculated by Euler and Kockel.[3] The linear field equations on which the present electrodynamics is based do not provide any direct interactions between different components of the field such as would produce such scatterings; but the transitory or virtual presence of charged particles provides a means of mediating indirect interactions. Thus for instance the possibility of the Delbrück scattering may be seen by supposing that the incident light quantum produces a (virtual) pair, that these particles are scattered in the Coulomb field, and that in being destroyed they emit the scattered light quantum. The transitory presence of the pair is possible even when there is not enough energy available to produce an actual observable pair.

It is to be expected that the symmetry between the two kinds of particles can be used to simplify calculations of such effects; in particular, since electrons and positrons are induced in equal numbers and are oppositely affected by electric fields, it would seem likely that cancellations should occur. Immediately after the Delbrück effect was suggested, it was remarked by Oppenheimer that, on account of such a cancellation, the transition probability for such scattering is of order $(Z\alpha)^4$ instead of $(Z\alpha)^2$. Such reasoning has been applied in some other cases. Neither a statement nor a proof of the general theorem involved has been published, however, and it evidently is by no means universally known. The writer has recently been interested in obtaining a proof so formulated that one can readily see how the result has to be modified in the case of hypothetical particles which obey the Dirac equations and are subject to other sorts of forces than the usual electric ones.[4] In this note such a proof is presented.

II. STATEMENT OF THEOREM AND OUTLINE OF PROOF

Theorem: In calculations using plane wave functions as a basis ("Born approximation") for processes in which the appearance of electrons and positrons is transitory only, the odd order contributions vanish identically.

This statement applies to calculations actually possible with the existing theory. The way in which it would have to be modified if nonelectric forces were introduced will be made clear in the discussion of Section IV.

It is evident that to any set of transitions through intermediate states by means of which a given process can be brought about, there corre-

[1] M. Delbrück, Zeits. f. Physik **84**, 144 (1933).
[2] O. Halpern, Phys. Rev. **44**, 885 (1934).
[3] H. Euler and B. Kockel, Naturwiss. **23**, 246 (1935); H. Euler, Ann. d. Physik **26**, 398 (1936).
[4] W. H. Furry, Phys. Rev. **50**, 784 (1936); Abstract No. 28, American Physical Society, New York, October, 1936.

sponds another possible set in which the roles of electrons and positrons are reversed. The proof of the theorem consists in showing that the corresponding contributions to the probability amplitude are equal and opposite if the order of the transition-scheme is odd.

A typical nth order term in the probability amplitude is N/D, with

$$N=\sum_{\text{spins}}\cdots(u^{+}(\mathbf{k},\sigma,\tau)\mathbf{O}u(\mathbf{k}',\sigma',\tau'))\cdots \quad (n \text{ factors}), \tag{1}$$

$$D=(\Delta E)_1\cdots(n-1 \text{ factors}). \tag{2}$$

Here $u(\mathbf{k}',\sigma',\tau')$ is the four-component amplitude of the Dirac plane wave function of an electron of momentum $\mathbf{k}mc$, spin σ, and energy $\tau\epsilon mc^2(\epsilon=(1+k^2)^{\frac{1}{2}},\ \tau=\pm1)$; $\mathbf{O}$ is a four-rowed matrix characteristic of the type of interaction regarded as producing the transition from $(\mathbf{k}',\sigma',\tau')$ to $(\mathbf{k},\sigma,\tau)$; and the (ΔE)'s are the energy differences between the initial state of the total system and the various intermediate states. If (1) were written out in full, the various $\mathbf{k}$'s, σ's, τ's and $\mathbf{O}$'s would have to be distinguished by subscripts. Since only a typical factor has to be discussed, a simpler notation is used to save writing.

Turning now to the analogous term in which the roles of electrons and positrons are interchanged, we find that its relation to our original term is described as follows:

(*a*) All energy differences (ΔE) are unchanged, because the dependence of energy on momentum is the same for both kinds of particles.

(*b*) Our new term is perhaps to be prefixed with the opposite sign to that given the old, on account of the different exchange characteristics of the two sets of transitions.

(*c*) Apart from such a possible intrinsic change of sign, the change in numerator is given by replacing N as given by (1) by:

$$N'=\sum_{\text{spins}}\cdots(u^{+}(-\mathbf{k}',\sigma',-\tau')\times\mathbf{O}u(-\mathbf{k},\sigma,-\tau))\cdots(n \text{ factors}). \tag{1'}$$

We have to reverse the direction of all transitions, change the signs of all energies (in the *electron* wave functions as used), and reverse all momenta. This corresponds to the fact that a positron of momentum $\mathbf{k}mc$ is equivalent to the absence of a negative energy electron of momentum $-\mathbf{k}mc$.

The theorem will be established by proving the following two lemmas concerning the changes noted under (*b*) and (*c*), respectively:

Lemma I: An intrinsic difference of sign on account of different exchange characteristics appears if and only if the number n of transitions is odd.

Lemma II: Apart from such an intrinsic difference of sign, the two numerators are equal $(N'=N)$, *and indeed the separate factors are equal respectively in pairs.*

It obviously follows from these lemmas that the contributions cancel for odd n in such a way as to make the theorem correct. However, before we go on to the formal proofs we should mention a certain difficulty which arises in connection with these cancellations. The actual probability amplitudes for these effects are sums of integrals of such terms as we have written, the integrals being taken over one or more momentum spaces.[5] Although two convergent integrals must cancel if their integrands are identically equal and opposite, this is not in any absolute sense true of divergent integrals: by choosing different origins or different coordinate systems for the comparison of the two, one can obtain indeterminate, and frequently infinite, discrepancies. The integrals met with in calculating the sort of transition probabilities under consideration will quite commonly be divergent. The resulting situation is one which is usual in calculations in positron theory: to obtain the result, one has to find a reasonable method of excluding the infinite and indeterminate contributions, and use what is left.[6] In the present case the reasonable procedure is to match the coordinate systems according to the physically sensible idea of interchanging the roles of the two kinds of particles. When this is done, the result is zero as stated in the theorem.

III. Proofs of the Lemmas

Lemma I: This is readily seen by inspection in some of the simpler cases. It may be proved in general by using quantized amplitudes. The

[5] Conservation of momentum holds for the intermediate states, but it fixes only the *total* momentum of the pair field. Since this field contains more than one particle, there remain undetermined one or more momentum *differences*, over which one must integrate.

[6] Cf. R. Serber, Phys. Rev. **49**, 545 (1936).

transition scheme (1) can be regarded as characterized by a product of amplitudes

$$A = \cdots a^+(\mathbf{k}, \sigma, \tau)a(\mathbf{k}', \sigma', \tau')\cdots. \quad (3)$$

Here

$$a_i^+a_j^+ + a_j^+a_i^+ = a_ia_j + a_ja_i = 0, \quad (4)$$

$$a_i^+a_j + a_ja_i^+ = 0, \quad i \neq j,$$

$$a_i^+a_i + a_ia_i^+ = 1. \quad (5)$$

When such a product is applied to the situation postulated in the "hole" theory, in which all levels $\tau = +1$ are empty and all levels $\tau = -1$ are full,[7] we can replace (5) by

$$\begin{aligned} &a^+(\mathbf{k}, \sigma, +1)a(\mathbf{k}, \sigma, +1) = 0, \\ &a(\mathbf{k}, \sigma, +1)a^+(\mathbf{k}, \sigma, +1) = 1, \\ &a^+(\mathbf{k}, \sigma, -1)a(\mathbf{k}, \sigma, -1) = 1, \\ &a(\mathbf{k}, \sigma, -1)a^+(\mathbf{k}, \sigma, -1) = 0. \end{aligned} \quad (6)$$

The fact that the appearance of particles is transitory only assures us that if $a(\mathbf{k}, \sigma, \tau)$ appears in (3), $a^+(\mathbf{k}, \sigma, \tau)$ also appears, and *vice versa;* and the fact that the transition scheme chosen is a possible one means that when interchanges of adjacent factors are made so that each factor finds its partner, a nonvanishing product will be obtained. This product will be $+1$ if the number of interchanges required is even, -1 if it is odd.

Exactly the same situation obtains for the product

$$A' = \cdots a^+(-\mathbf{k}', \sigma', -\tau')a(-\mathbf{k}, \sigma, -\tau)\cdots, \quad (3')$$

which corresponds to (1′) as (3) does to (1). Apart from irrelevant changes in the designations of the factors, the only significant difference between (3′) and (3) consists in n interchanges of adjacent factors. Thus

$$\begin{aligned} A' &= A, \quad && n \text{ even}, \\ A' &= -A, && n \text{ odd}. \end{aligned} \qquad Q.E.D.$$

Lemma II. Given

$$M = (u^+(\mathbf{k}, \sigma, \tau)\mathbf{O}u(\mathbf{k}', \sigma', \tau')) \quad (7)$$

we want to show that to every $u^+(\mathbf{k}, \sigma, \tau)$ we can correlate a $u(-\mathbf{k}, \bar{\sigma}, -\tau)$[8] and to every $u(\mathbf{k}, \sigma, \tau)$ a $u^+(-\mathbf{k}, \bar{\sigma}, -\tau)$, in such a way that if the original functions form a complete normalized orthogonal set the correlated ones do too, and that if

$$M' = (u^+(-\mathbf{k}', \bar{\sigma}', -\tau')\mathbf{O}u(-\mathbf{k}, \bar{\sigma}, -\tau)) \quad (7')$$

we shall have $M' = M$. Let us try to do this by finding a matrix A such that

$$\begin{aligned} u(-\mathbf{k}, \bar{\sigma}, -\tau) &= \{\overline{u^+(\mathbf{k}, \sigma, \tau)A^+}\}, \\ u^+(-\mathbf{k}, \bar{\sigma}, -\tau) &= \{\overline{Au(\mathbf{k}, \sigma, \tau)}\}. \end{aligned} \quad (8)$$

(The bar indicates transposition.)

The requirements as to completeness, orthogonality, and normalization are satisfied provided

$$\begin{aligned} &(u^+(-\mathbf{k}', \bar{\sigma}', -\tau')u(-\mathbf{k}, \bar{\sigma}, -\tau)) \\ &\qquad = (u^+(\mathbf{k}, \sigma, \tau)u(\mathbf{k}', \sigma', \tau')). \end{aligned} \quad (9)$$

Substituting from (8) in the left member of (9) we get

$$(\{\overline{Au(\mathbf{k}', \sigma', \tau')}\}\ \{\overline{u^+(\mathbf{k}, \sigma, \tau)A^+}\}).$$

Since this is a mere number, we do not change its value by transposition, which gives

$$(u^+(\mathbf{k}, \sigma, \tau)A^+Au(\mathbf{k}', \sigma', \tau')).$$

Thus (9) is equivalent to the requirement

$$A^+A = 1; \quad (10)$$

i.e. A must be unitary.

The requirement that the new functions so formed be solutions of the Dirac equations means that

$$\begin{aligned} (\tau\epsilon + \boldsymbol{\alpha}\cdot\mathbf{k} + \beta)u(\mathbf{k}, \sigma, \tau) &= 0, \\ u^+(\mathbf{k}, \sigma, \tau)(\tau\epsilon + \boldsymbol{\alpha}\cdot\mathbf{k} + \beta) &= 0 \end{aligned} \quad (11a, b)$$

must imply

$$\begin{aligned} \{\overline{Au(\mathbf{k}, \sigma, \tau)}\}(-\tau\epsilon - \boldsymbol{\alpha}\cdot\mathbf{k} + \beta) &= 0, \\ (-\tau\epsilon - \boldsymbol{\alpha}\cdot\mathbf{k} + \beta)\{\overline{u^+(\mathbf{k}, \sigma, \tau)A^+}\} &= 0. \end{aligned} \quad (12a, b)$$

[7] The changes in notation which might be made to cover up the baldness of this statement and replace (6) by a pair of symmetrical rules would have no effect here except to make the proof slightly more cumbersome.

[8] By $\bar{\sigma}$ we mean not necessarily an index different in *numerical value* from σ but an index whose *significance* may be different, i.e. $u(\mathbf{k}, \bar{\sigma}, \tau)$ may not be the same function of $\bar{\sigma}$ that $u(\mathbf{k}, \sigma, \tau)$ is of σ. There is no need to trace the correlation between the two types of spin quantization, because the spin-sums (1) and (1′) are independent of the type used, as long as we are careful always to use complete normalized orthogonal function sets.

Transposing (12, a, b) we get

$$(-\tau\epsilon-\bar{\alpha}\cdot\mathbf{k}+\bar{\beta})Au(\mathbf{k},\sigma,\tau)=0,$$
$$u^+(\mathbf{k},\sigma,\tau)A^+(-\tau\epsilon-\bar{\alpha}\cdot\mathbf{k}+\bar{\beta})=0. \qquad (13a, b)$$

(13a) is implied by (11a) provided

$$\bar{\alpha}_i A=A\alpha_i,\quad \bar{\beta}A=-A\beta. \qquad (14)$$

Since $\bar{\alpha}_i$, $\bar{\beta}$ are Hermitian as well as α_i, β, by taking the adjoint of (14) we see that it is also a sufficient condition for (13b) to be implied by (11b).

On account of the use of transposition in fixing the conditions on A, it does not seem to be possible to prove that an A exists satisfying (10) and (14) without referring to an explicit form of the Dirac matrices. If we suppose that they have the form originally given by Dirac, we see that α_x, α_z, β are real symmetric, while α_y is imaginary antisymmetric. Thus for this representation (14) means that A must commute with α_x and α_z, and anticommute with α_y and β; and $i\alpha_y\beta$ is obviously a unitary matrix which does this. Having found a suitable A for this one representation, we can readily determine one for any other. This other representation must be connected with the one discussed by a unitary transformation,

$$\alpha_i'=S^{-1}\alpha_i S=S^+\alpha_i S,\quad \beta'=S^+\beta S, \qquad (15)$$

and one finds that a suitable unitary matrix A' is now given by

$$A'=\bar{S}AS. \qquad (16)$$

A does not transform according to the unitary transformation applied to $\boldsymbol{\alpha}$, β, and hence does not have the same expression in terms of $\boldsymbol{\alpha}$, β in different representations. This is due to the fact that the conditions (14) placed on A are not invariant under unitary transformation.

We now have only to substitute (8) into (7′) and apply (14) to evaluate M':

$$M'=\overline{M'}=(\overline{\{Au(\mathbf{k}',\sigma',\tau')\}}\mathbf{O}\overline{\{u^+(\mathbf{k},\sigma,\tau)A^+\}})$$
$$=(u^+(\mathbf{k},\sigma,\tau)A^+\bar{\mathbf{O}}Au(\mathbf{k}',\sigma',\tau')). \qquad (17)$$

From (10) and (14), $A^+\bar{\mathbf{O}}A=\pm\mathbf{O}$ whenever $\mathbf{O}$ is a product of Dirac matrices. Thus for such $\mathbf{O}$'s, $M'=\pm M$. In detail,

$$\mathbf{O}_1=\beta: \qquad M'=-M, \qquad (18a)$$
$$\mathbf{O}_2=1;\ \alpha_i: \qquad M'=M, \qquad (18b)$$
$$\mathbf{O}_3=i\beta\alpha_i;\ i\beta\alpha_i\alpha_j: \qquad M'=M, \qquad (18c)$$
$$\mathbf{O}_4=i\alpha_1\alpha_2\alpha_3;\ i\alpha_i\alpha_j: \qquad M'=-M, \qquad (18d)$$
$$\mathbf{O}_5=\beta\alpha_1\alpha_2\alpha_3: \qquad M'=-M. \qquad (18e)$$

The various operators have been listed according to the relativistic transformation properties of $u^+\mathbf{O}_p u$.[9] The five types of $\mathbf{O}_p$ listed give respectively a scalar, a four-vector, an antisymmetric tensor, an axial four-vector (antisymmetric tensor of the third rank), and a pseudo-scalar. As will be explained at the beginning of the next section, (18b) establishes Lemma II for the case contemplated in the original statement of the theorem.

IV. Discussion of the Various Operators

The interactions involved in all effects so far discussed are those with the radiation field and with Coulomb fields. These interactions are given by the product of the potential four-vector with the four-vector $\mathbf{O}_2$ of (18b). Thus Lemma II is established for all these effects, and with it the theorem as stated.

Another possible form of interaction with the electromagnetic field is that obtained by multiplying the tensor $\mathbf{O}_3$ of (18c) by the field tensor. For such interactions the theorem also holds. This form of interaction corresponds to the particle's possessing a magnetic moment differing from that given by its charge and spin. It was first invented by Pauli as a possible interaction between a neutral particle (precursor of the neutrino) and the field; also it has been suggested that the proton may possibly obey a Dirac equation in which such a term is inserted to give agreement with the observed magnetic moment. For the electron this interaction must be supposed to vanish.

The only other one of the operators (18) which can be supposed to describe an interaction of the particle with a field of force is the scalar $\mathbf{O}_1$ of (18a). The writer has recently pointed out, in connection with the question of the spin-orbit

[9] Cf. W. Pauli, *Handbuch der Physik* 24/1, 221. The rather unsymmetrical appearance of the operators listed in (18) is due to our use of the original Dirac notation α, β instead of the γ^μ notation which is better adapted for clear display of the transformation properties.

interaction of a particle moving under the action of a nonelectric force,[4] that this scalar may be associated with a scalar potential such as occurs in Nordström's special-relativistic gravitational theory. One sees from (18a) that in applying our theorem to any process in which such an interaction might play a part we must *omit* the matrix elements of this **O** in counting the number of factors in the numerator (1) to get n. This is just what is to be expected, since the reason for the alternation of relative signs from order to order in the electric case is to be found in the opposite action of the field on the two signs of charge. The result is of some interest academically, though at present there seems not to be much utility in the concept of a particle which is susceptible both to the action of nonelectric forces and to creation and destruction in pairs.

The operators $\mathbf{O}_4$ and $\mathbf{O}_5$ of (18d) and (18e) cannot be associated with any sort of interaction which has a classical analogue, on account of their unsuitable transformation properties as regards reflection. If, however, an interaction between *two matter-fields* is described by a *biquadratic* form in the Dirac amplitudes, the antisymmetry under reflection can be eliminated by squaring. In fact Wigner, and also Bethe and Bacher,[10] have remarked that these operators, quite as well as the others, can reasonably be used in neutrino theory. It is possible that the symmetry property here described may find applications in this connection.

[10] H. A. Bethe and R. F. Bacher, Rev. Mod. Phys. **8**, 190 (1926).

JANUARY 15, 1937 PHYSICAL REVIEW VOLUME 51

Energy Bands for the Face-Centered Lattice

WILLIAM SHOCKLEY
Massachusetts Institute of Technology, Cambridge, Massachusetts

(Received October 2, 1936)

The Slater method of obtaining wave functions for metallic lattices is applied to the face-centered lattice. The solutions previously obtained by Krutter for this lattice were mainly for certain simple lines in momentum space. Methods are developed for obtaining more general solutions from these special ones. On this basis the entire 110 plane is worked out. For certain new lines in this plane especially simple solutions are given. An approximate method suitable for calculating energy contours in momentum space for small values of momentum is developed.

INTRODUCTION

SLATER[1] has proposed an extenison of the method of Wigner and Seitz[2] for the calculation of wave functions in the periodic field of metallic lattices. He applied his method to the body-centered lattice with metallic sodium particularly in mind. The method has been applied to lithium[3] (body-centered), to copper[4] (face-centered), and with modifications to diamond[5] and the sodium chloride lattice.[6]

Briefly, the method consists of dividing the lattice into polyhedral cells centered about each atom and containing those points of space nearer that atom than any other atom. The wave function ψ in one of these cells is expanded in terms of surface harmonics times radial functions which are numerical solutions of wave equation. For an atom at a center of symmetry this function is most conveniently handled in the form $\psi = u_g + iu_u$ where u_g is a real even function of the coordinates having the atom as a center (i.e., is expanded in harmonics of even l) and u_u is an odd real function. The functions in other cells are obtained by translating ψ and multiplying it by $e^{i\mathbf{k}\cdot\mathbf{R}}$ where $\mathbf{R}$ is the translation vector. The wave function and its normal derivative are required to be continuous from cell to cell at the midpoints of the cell boundaries.

[1] J. C. Slater, Phys. Rev. **45**, 794 (1934).
[2] Wigner and Seitz, Phys. Rev. **43**, 804 (1933) and **46**, 509 (1934).
[3] J. Millman, Phys. Rev. **47**, 286 (1935); F. Seitz, Phys. Rev. **47**, 400 (1935).
[4] H. M. Krutter, Phys. Rev. **48**, 664 (1935).
[5] George E. Kimball, J. Chem. Phys. **3**, 560 (1935); F. Hund, Physik Zeits. **36**, 888 (1935).
[6] Ewing and Seitz, Phys. Rev. **50**, 760 (1935); W. Shockley, Phys. Rev. **50**, 754 (1935).

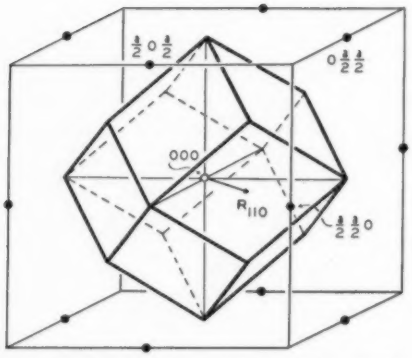

FIG. 1. Cell for the face-centered lattice showing the vector positions of various lattice points and the midpoints of the faces.

For the face-centered lattice, the translations are of the form $a(0\pm\frac{1}{2}\pm\frac{1}{2})$, etc. The polyhedral cell (Fig. 1) is a rhombic dodecahedron whose surfaces are planes bisecting the lines from the origin to the points $a(0\pm\frac{1}{2}\pm\frac{1}{2})$, the midpoints of the faces being $\mathbf{R}_{0\pm1\pm1}=a(0\pm\frac{1}{4}\pm\frac{1}{4})$, etc. Each pair of diametrically opposite midpoints gives rise to two equations of continuity for ψ and the normal derivative ψ' of the form

$$T_{011}u_g-u_u=0, \tag{1}$$

$$u_g'+T_{011}u_u'=0, \tag{2}$$

where $T_{011}=\tan \mathbf{k}\cdot\mathbf{R}_{011}=\tan(k_y+k_z)a/4$. u_g and u_u and their derivatives in respect to increasing r are evaluated at $\mathbf{R}_{011}$. It is convenient to let $\mathbf{k}=(2\pi/a)\boldsymbol{\kappa}$. If $\boldsymbol{\kappa}$ is increased by 111, the $e^{i\mathbf{k}\cdot\mathbf{R}}$ and $\tan \mathbf{k}\cdot\mathbf{R}$ terms are unaltered in value. Hence, our solutions are periodic in $\boldsymbol{\kappa}$-space with the periodicity of a body-centered lattice having $\pm1\pm1\pm1$, ±200, etc., as lattice points. The tangent factors take the simple forms: $T_{011}=\tan\pi(\kappa_y+\kappa_z)/2$, etc.

The six independent directions give twelve conditions and, in order to satisfy them, ψ is expanded in terms of twelve linearly independent functions with arbitrary coefficients. The homogeneous system of equations for these coefficients is then soluble if, and only if, its determinant vanishes. This establishes a functional dependence between $\boldsymbol{\kappa}$ and the energy parameter, which enter through the tangent factors and the values and derivatives of the radial functions, respectively. It is with the nature of this functional relationship that we are concerned.

Krutter has already made a satisfactory choice of the 12 expansion functions. With a modification[7] of notation, these may be listed as in Table I in accordance with their representations in the octahedral group[8] which is the point group for the cell center.

I. Special Directions

No means have been developed for dealing with the determinant for general values of $\boldsymbol{\kappa}$. However, for special directions of $\boldsymbol{\kappa}$ it is possible to get relatively simple expressions. This is a consequence of symmetry of the directions. For the 100 direction, $\boldsymbol{\kappa}=u00$, for example, the functions can be separated into their various symmetry types about the x axis. When this is done, it is found that each type must satisfy the boundary conditions separately and that the satisfying of the conditions on the 110 face, for example, satisfies simultaneously the conditions on the 1–10, 101, 10–1 faces. This reduces the order of the determinantal equations from the 12th to at most the 3rd order for these directions. The corresponding solutions for this line and for 011 and 111 have been published by Krutter and are listed in Table II, along with new solutions developed in this paper.

II. The 001 Plane

For values of $\boldsymbol{\kappa}$ lying in certain planes, sufficient symmetry is still preserved to be of considerable help. For $\boldsymbol{\kappa}$ in the 001 plane, that is $\boldsymbol{\kappa}$

TABLE I. *Expansion functions of Krutter.*

	u_g FUNCTIONS
Γ_1	s
Γ_2	$(x^2-y^2)d$, $(y^2-z^2)d$
Γ_5	yzd, zxd, xyd
	u_u FUNCTIONS
Γ_4	xp, yp, zp
Γ_5	$x(y^2-z^2)f$, $y(z^2-x^2)f$, $z(x^2-y^2)f$

[7] Since all the surface harmonics are evaluated for directions such as $0\pm1\pm1$ the factors r^{-l} may conveniently be omitted. x, y, z are then understood to be on the sphere of radius $=\sqrt{2}$. The radial functions s, p, d and f have the customary significance. The ratios s'/s, p'/p, d'/d and f'/f are denoted by σ, π, δ and φ.

[8] For a discussion of the representations of the octahedral group see H. Bethe, Ann. d. Physik **3**, 133 (1929).

of the form $uv0$, it is possible to separate functions into sets which are even and odd with respect to $z \rightarrow -z$. There are only four functions of the odd type, leading to a fourth-order determinant which has been expanded by Krutter and is listed in Table II. The even set appears too complicated to handle in general; however, in addition to the lines 100 and 110 which lie in this plane it is possible to get reduction along the line $\kappa = u10$.

Line I, $\kappa = u10$ [9]

The simplicity of this line is due to its lying in a 001 plane and a 010 plane simultaneously (Fig. 4a). Hence, it is possible to utilize odd and even classifications for $y \rightarrow -y$ and $z \rightarrow -z$. The results of this classification are shown in Table II.

It is to be noted that Eq. (Ia) is reasonably simple for numerical work, since by virtue of the relation $CT = 1$ it is a quadratic in T^2. Thus, for given values of σ, π, δ, and φ, it is possible to solve directly for T and thus find u.

III. The $01\bar{1}$ Plane

For this plane, $\kappa = uvv$, the symmetry in the interchange of y and z is preserved. Hence, the functions can be separated into two sets: odd for interchange of y and z and even. The tangent factors for the dodecahedron are shown in Fig. 2. Only four need be considered, since the two others, $10\bar{1}$ and 110, are related to $1\bar{1}0$ and 101 by interchange of y and z.

Odd set[9]

There are five functions odd in this plane. By the same method as given by Krutter for the odds of 001, we obtain the solution given in Table II.

We shall establish this equation by a different method which we shall use later with the even set. Since the odd functions vanish on 011, the expression cannot involve $K = T_{011}$. Hence, the determinantal equation will be a polynomial in L and M of no higher degree than the second in each term, since each tangent factor occurs in only two of the continuity Eqs. (1) and (2).

[9] This solution was developed independently by the writer and Dr. Krutter. The writer is indebted to Dr. Krutter for a check of his work.

TABLE II. *Classification of the solutions for the face-centered lattice.*[7]

100 direction	$\kappa = u00$	$T_{110} = \tan \pi u/2 = M$
100_a	s, $(2x^3-y^3-z^3)d$, xp	$M^2+3\sigma\delta/\pi(\sigma+2\delta)=0$
100_b	$(y^3-z^3)d$, $x(y^3-z^3)f$	$M^2+\delta/\varphi=0$
100_c	yzd	M arbitrary for $\delta=0$
100_d	xyd, yp, $y(x^3-z^3)f$	$M^2+2\delta/(\pi+\varphi)=0$
100_e	xzd, zp, $z(x^3-z^3)f$	$M^2+2\delta/(\pi+\varphi)=0$
111 direction	$\kappa = uuu$	$T_{111} = \tan \pi u = K$
111_a	s, $(xy+yz+zx)d$, $(x+y+z)p$	$K^2+2\sigma\delta/\pi(\sigma+\delta)=0$
111_b	$[2x^3-y^3-z^3 +x(y+z)-2yz]d$, $(2x-y-z)p$, $[y(x^3-z^3)+z(x^3-y^3)]f$	$K^2+4\delta/(\pi+3\varphi)=0$
111_c	$[y^3-z^3+x(y-z)]d$, $(y-z)p$, $[y(x^3-z^3)-z(x^3-y^3)]f$	$K^2+4\delta/(\pi+3\varphi)=0$
111_d	$[2x^3-y^3-z^3 -x(y+z)+2yz]d$	K arbitrary for $\delta=0$
111_e	$[y^3-z^3-x(y-z)]d$	K arbitrary for $\delta=0$
111_f	$[x(y^3-z^3)+y(z^3-x^3) +z(x^3-y^3)]f$	K arbitrary for $\varphi=\infty$
011 direction	$\kappa = 0uu$	$T_{011} = K = \tan \pi u$, $T_{101} = L = \tan \pi u/2$
011_a	s, yzd, $(2x^3-y^3-z^3)d$, $(y+z)p$, $[y(x^3-z^3)+z(x^3-y^3)]f$	$2K^2L^2\pi\varphi(5\delta+\sigma)+K^2\delta(\pi+\varphi)(5\sigma+\delta)$ $+4KL\delta(\varphi-\pi)(\sigma-\delta)+2L^2\delta(\pi+\varphi)(\sigma+2\delta)+12\delta^2\sigma=0$
011_b	$x(y+z)d$, xp	$L^2+\delta/\pi=0$
011_c	$(y^3-z^3)d$, $(y-z)p$, $[y(x^3-z^3)-z(x^3-y^3)]f$	$L^2+2\delta/(\pi+\varphi)=0$
011_d	$x(y-z)d$, $x(y^3-z^3)f$	$L^2+\delta/\varphi=0$
001 plane	$\kappa = uv0$	$T_{101} = \tan \pi u/2$ $T_{011} = \tan \pi v/2$
xzd, yzd, zp, $z(x^3-y^3)f$	$\left[T^2_{101}+\frac{\delta(\pi+\varphi)}{2\pi\varphi}\right]\left[T^2_{011}+\frac{\delta(\pi+\varphi)}{2\pi\varphi}\right]=\left[\frac{\delta(\pi-\varphi)}{2\pi\varphi}\right]^2$	
$01\bar{1}$ plane	$\kappa = uvv$	$T_{101} = \tan \pi(u+v)/2$ $T_{110} = \tan \pi(u-v)/2$
$(y^3-z^3)d$, $x(y-z)d$, $(y-z)p$, $x(y^3-z^3)f$, $[y(x^3-z^3)-z(x^3-y^3)]f$	$\left[T^2_{110}+\frac{\delta(\pi+3\varphi)}{2\varphi(\pi+\varphi)}\right]\left[T^2_{101}+\frac{\delta(\pi+3\varphi)}{2\varphi(\pi+\varphi)}\right]=\left[\frac{\delta(\pi-\varphi)}{2\varphi(\pi+\varphi)}\right]^2$	
Line 1	$\kappa = u10$	$T_{110} = \tan \pi(u-1)/2$ $= -\cot \pi u/2 = -C$ $T_{101} = \tan \pi u/2 = T$
I_a	s, $(2x^3-y^3-z^3)d$, $(y^3-z^3)d$, xp, $x(y^3-z^3)f$	$(T^2+C^2)(2\delta+\sigma)(\pi+\varphi)+2(\delta-\sigma)(\varphi-\pi)$ $+2\delta(\delta+2\sigma)+6\pi\varphi=0$
I_b	xyd, yp, $y(x^3-z^3)f$	$C^2+\delta(\pi+\varphi)/2\pi\varphi=0$
I_c	xzd, zp, $z(x^3-y^3)f$	$T^2+\delta(\pi+\varphi)/2\pi\varphi=0$
I_d	yzd	u arbitrary for $\delta=\infty$

For the even set of the $01\bar{1}$ plane, 311 direction, and Lines II, III, and IV see text.

Furthermore, the symmetry of the problem assures us that if $\kappa_0 = uvv$ is a solution, $-\kappa_0$ must be an equally good solution. Hence, our ex-

pression must not be altered by replacing κ_0 by $-\kappa_0$. Similarly, replacing κ_0 by $\kappa=-uvv$ and $\kappa=u-v-v$ must leave its value unchanged. This means that the determinant must be invariant under the four (including, of course, identity) symmetry operations in the $01\bar{1}$ plane. If we denote the four operations above by I, R, S, T, we see that determinant D regarded as a function of κ must satisfy the relationship $D=ID=RD=SD=TD$. The transformation scheme of the individual factors is readily found. For example,

$$T_{1\bar{1}0}=\tan\pi(u-v)/2=M,$$
$$RM=\tan\pi(-u+v)/2=-M,$$
$$SM=\tan\pi(-u-v)/2=-L,$$
$$TM=\tan\pi(u+v)/2=L.$$

This is expressed in tabular form in Table III. From this it is possible to list the allowable terms which may occur in D. For example, if L^bM^c occurs, it must be present in a combination with L^cM^b that is unaltered by the operations R, S and T. From the group property of I, R, S, T, it may easily be verified that the only such form is $(I+R+S+T)L^bM^c=[1+(-1)^{b+c}][L^bM^c+L^cM^b]$. Hence, the most general form of D will be, except for a factor independent of L and M, $D=A+BLM+C(L^2+M^2)+L^2M^2$. It is now possible to evaluate the constants, A, B and C, from the solutions in special directions.

100 direction

For this $M=L$ and $D=0$ reduces to $D=A+(B+2C)M^2+M^4=0$. This must factor into $100b$ and $100d$ ($100d-100e$ is odd in the $01\bar{1}$ plane and has the same equation as $100d$ and $100e$); the two known solutions for the odd functions. Hence, D must contain $M^2+\delta/\varphi$ and $M^2+2\delta/(\pi+\varphi)$ as factors. Therefore,

$$A=2\delta^2/\varphi(\pi+\varphi),$$
$$B+2C=\delta(\pi+3\varphi)/\varphi(\pi+\varphi).$$

011 direction

For this $M=-L$ and $D=0$ becomes $D=A+(-B+2C)L^2+L^4=0$. The known solutions $110c$ and $110d$ are the same as $100b$ and $100d$. Hence, $B=0$, and

$$D=2\delta^2/\varphi(\pi+\varphi)+[\delta(\pi+3\varphi)/2\varphi(\pi+\varphi)][L^2+M^2]+L^2M^2=0.$$

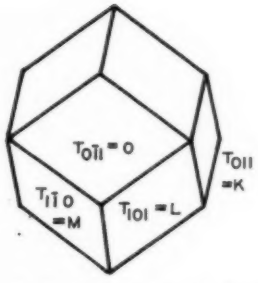

FIG. 2. Cell for the face-centered lattice showing the values of the tangent factors for $\kappa=uvv$ (the $01\bar{1}$ plane).

This is equivalent to the solution in Table II.

Even set

The procedure of the odd set can be carried out for the even set also. For this set we expect to get terms in K as well as L and M. The allowed form is given below. Since only the ratios of the coefficients can be found by this method, the coefficient of the zeroth order term has been made unity.

$$D=1+[BK(L-M)+CLM+DK^2+E(L^2+M^2)]+[FK^2LM+GK^2(L^2+M^2)+HKLM(L-M)+JL^2M^2]+PK^2L^2M^2.$$

100 direction

For this line $K=0$, $L=M$, and

$$D=1+[C+2E]M^2+JM^4=0.$$

From Table II we see that this must have the factors $M^2+3\sigma\delta/\pi(2\delta+\sigma)$ and $M^2+2\delta/(\pi+\varphi)$. Equating the ratios of coefficients, we get

$$C+2E=\frac{(5\sigma\pi+4\delta\pi+3\sigma\varphi)}{6\sigma\delta},$$

$$J=\frac{\pi(\pi+\varphi)(2\delta+\sigma)}{6\sigma\delta^2}.$$

011 direction

For this $M=-L$ and $|M|\neq|K|\neq0$ and

$$D=1+2BKL+(-C+2E)L^2+DK^2+(-F+2G)K^2L^2-2HKL^3+JL^4+PK^2L^4=0.$$

Proceeding as above, we find that the factors are $011a$ and $011b$ and that the coefficients are

$$B=\frac{(\varphi-\pi)(\sigma-\delta)}{6\sigma\delta},$$

$$-C+2E=\frac{(\pi+\varphi)(2\delta+\sigma)+6\sigma\pi}{6\sigma\delta},$$

$$D=\frac{(\pi+\varphi)(\delta+5\sigma)}{12\sigma\delta},$$

$$-F+2G=\frac{\pi[2\varphi(5\delta+\sigma)+(\pi+\varphi)(\delta+5\sigma)]}{12\sigma\delta^2},$$

$$H=\frac{\pi(\pi-\varphi)(\sigma-\delta)}{6\sigma\delta^2},$$

$$J=\frac{\pi(\pi+\varphi)(2\delta+\sigma)}{6\sigma\delta^2},$$

$$P=\frac{\pi^2\varphi(5\delta+\sigma)}{6\sigma\delta^3}.$$

111 direction. $M=0$, $K=L$

$$D=1+(B+D+E)K^2+GK^4=0.$$

The known solutions are 111*a* and 111*b* and the results are

$$B+D+E=\frac{3\sigma\pi+3\sigma\varphi+2\delta\pi}{4\sigma\delta},$$

$$G=\frac{\pi(\pi+3\varphi)(\sigma+\delta)}{8\sigma\delta^2}.$$

TABLE III. *Transformation scheme for the tangent factors of the 011 plane.*

I	R	S	T
uvv	$-u-v-v$	$-uvv$	$u-v-v$
K	$-K$	K	$-K$
L	$-L$	$-M$	M
M	$-M$	$-L$	L

TABLE IV.

COEFFICIENT	TERM
$B=(\varphi-\pi)(\sigma-\delta)/6\sigma\delta$	$K(L-M)$
$C=(\varphi-\pi)(\sigma-\delta)/6\sigma\delta$	LM
$D=(\pi+\varphi)(\delta+5\sigma)/12\sigma\delta$	K^2
$E=(3\pi+\varphi)(2\sigma+\delta)/12\sigma\delta$	L^2+M^2
$F=\pi(\pi-\varphi)(\delta-\sigma)/6\sigma\delta^2$	K^2LM
$G=\pi(\pi+3\varphi)(\sigma+\delta)/8\sigma\delta^2$	$K^2(L^2+M^2)$
$H=\pi(\pi-\varphi)(\sigma-\delta)/6\sigma\delta^2$	$KLM(L-M)$
$J=\pi(\pi+\varphi)(2\delta+\sigma)/6\sigma\delta^2$	L^2M^2
$P=\pi^2\varphi(5\delta+\sigma)/6\sigma\delta^3$	$K^2L^2M^2$

From these three lines we thus get 11 equations for the 9 coefficients of D. From them we can determine all the coefficients and have two extra equations as a check. The results are given in Table IV.

IV. SPECIAL LINES IN THE 01$\bar{1}$ PLANE

For certain lines in the 01$\bar{1}$ plane, D takes a specially simple form.

311 direction

For the 311 direction, $\kappa=3v, v, v$ and $K=M=\tan(\pi v)$ and $L=\tan(2\pi v)$. Hence, there are only two distinct tangent factors in D. Such expressions as this result and 011*a* can best be used in calculation by making a table of the values of the terms such as K^2, K^2L^2, etc., which occur in them. Then for a fixed value of the energy, D is evaluated as a function of v and the zeros are found.

Line II. $\kappa=u\frac{1}{2}\frac{1}{2}$

$K=\infty$, $L=\tan\pi(u+\frac{1}{2})/2=-\cot\pi(u-\frac{1}{2})/2=-C$, $M=\tan\pi(u-\frac{1}{2})/2=T$. For this we must equate the coefficients of K^2 to zero, obtaining

$$(C^2+T^2)G+(D-F+P)=0.$$

which, as a consequence of $CT=1$, is a quadratic in C^2 as is solution Ia.

Line III. $\kappa=(1-v), v, v$

$K=\tan\pi v=T$, $L=\infty$, $M=-\cot\pi v=-C$. For this we must equate the coefficient of L^2 to zero, obtaining

$$GT^2+JC^2+(E+H+P)=0.$$

This is again a quadratic in C^2.

V. THE CASE OF $\kappa\ll1$

From an inspection of D it can be seen that when $\kappa\to0$ either σ or $\delta\to0$ or π or $\varphi\to\infty$.[10] It can also be seen that for a given small value of κ, the equation becomes linear in σ for $\sigma\to0$; cubic in δ; quadratic in π; and linear in φ. This is a consequence of the fact that one s function, three d functions, two p functions and one f function compose the even set of the 01$\bar{1}$ plane.

[10] The pathological case of several of these requirements being met at once will not be considered.

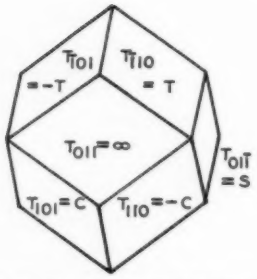

FIG. 3. Cell for the face-centered lattice showing the values of the tangent factors for $\kappa = u(01\bar{1}) + \frac{1}{2}(111)$, line IV. $T = \tan \pi u/2$, $C = \cot \pi u/2$, $S = \tan \pi u$.

If κ is small enough, it is possible to expand K, L and M in powers of u and v. It is more convenient to use symmetry arguments, however, in order to establish the form of the result and then evaluate the unknown coefficients from special directions. For example, the result for $\sigma \to 0$ must be

$$\sigma + au^2 + bv^2 = 0.$$

From the 100 condition, we see that

$$-\sigma = 2p'M^2/3p \doteq (p'\pi^2/6p)u^2 \doteq au^2$$

(here π has its conventional meaning and does not denote p'/p) and from 111,

$$-\sigma = 2p'K^2/p \doteq (p'\pi^2/2p)u^2 \doteq (a+b)u^2.$$

Hence, $2a = b = \pi^2 p'/3p$, and the σ contour is a circle.[11]

For the p functions, the form must be

$$(p/p')^2 + (p/p')(au^2 + bv^2) + (cu^4 + du^2v^2 + ev^4) = 0.$$

The coefficients of this form can be evaluated from the 100, 011 and 111 directions.

A similar process or else direct expansion of D can be used for the d functions; and the same methods are applicable to the 001 plane or to general space directions.

For all the cases we shall find that for a given direction of κ the values of σ and the values of $1/\pi$ will be linear functions of $|\kappa|^2$. For $|\sigma|$ and $|1/\pi| \ll 1$, these quantities will be approximately linear functions of the energy. Hence the energy *versus* κ curves will be single (for s), double (for p), etc., parabolas in κ.

[11] This can also be seen from the more general statement that for the three-dimensional case of $|\kappa| \ll 1$ the cubic symmetry requires $\sigma + a(\kappa_x^2 + \kappa_y^2 + \kappa_z^2) = 0$, the equation of a sphere.

VI. LINE IV. $\kappa = u(01\bar{1}) + \frac{1}{2}(111)$

For functions of the form $\psi = u_g + iu_u$ for which $\kappa = u(01\bar{1}) + \frac{1}{2}(111)$, it is possible to split the set of 12 functions into smaller sets of 5 and 7. Consider the function $A\psi$ obtained from ψ by interchanging y and z; it will satisfy the same continuity requirements as ψ save that its κ will be $A\kappa = u(0\bar{1}1) + \frac{1}{2}(111) = -\kappa + 111$. Due to the periodicity of κ-space, $-\kappa + 111$ is equivalent to $-\kappa$. Now the complex conjugate ψ^* of ψ will clearly correspond to $-\kappa$. We can now introduce an operator $P = (A)^*$ which operating on ψ leaves its κ value invariant and also its energy value (since both A and * do). Since P is its own reciprocal, we can conclude from the representation theory of groups (or from considerations of $(\psi + P\psi)$ and $(\psi - P\psi)$) that we can classify the functions into two sets according to whether $P\psi = \psi$ or $-\psi$.

Set 1

For $P\psi = \psi$ we find that $Au_g = u_g$ and $Au_u = -u_u$ so that we should use even harmonics which are even in yz interchange and odd harmonics which are odd. This gives the set of functions:

$$s, \quad x(y+z)d, \quad yzd, \quad (2x^2 - y^2 - z^2)d, \quad (y-z)p,$$
$$x(y^2 - z^2)f, \quad [y(x^2 - z^2) - z(x^2 - y^2)]f.$$

Set 2

From $P\psi = -\psi$ we find $Au_g = -u_g$ and $Au_u = u_u$ so that even harmonics should be odd for yz interchange; odd harmonics, even. The functions of this set are:

$$x(y-z)d, \quad (y^2 - z^2)d, \quad xp, \quad (y+z)p,$$
$$[y(x^2 - z^2) + z(x^2 - y^2)]f.$$

The scheme of the tangent factors is shown in the Fig. 3. $\bar{1}01$ and 110 are equivalent to $\bar{1}10$ and 101, respectively, by the P symmetry. The 011 face gives only one condition on each set, since for set 1 the u_u functions automatically vanish there as do the u_g of set 2. Due to its complexity, set 1 has not been worked out. The seventh-order determinant to which it leads can be easily set up, but the expansion is tedious.

Expansion of set 2

Set 2 is simpler, since all of its functions vanish on $01\bar{1}$, thus leading to only five conditions for the coefficients. The resultant determinantal

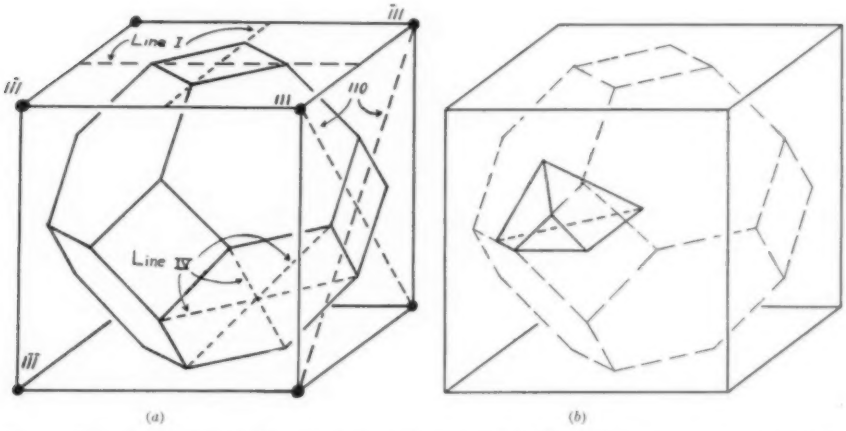

FIG. 4. Views of body-centered κ-space. *a*. κ lattice and first Brillouin zone showing the various solutions. *b*. Fundamental segment of the first zone.

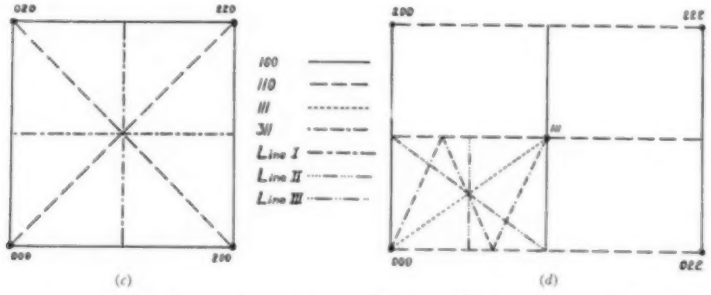

FIG. 4. *c*. 001 plane, showing the solutions. *d*. $01\bar{1}$ plane, showing the solutions. Only one-quarter of the diagram is completed; the remainder follows from symmetry.

equation may be reduced to

$$(C^2+T^2)\delta\pi(3+\pi/\varphi)+2[\delta^2(1+\pi/\varphi)+2\pi^2]=0.$$

This can be treated by the same method as was used for line Ia.

SUMMARY AND FINAL REMARKS

Fig. 4*a* shows the first Brillouin zone in body-centered κ-space. Fig. 4*b* shows the fundamental segment of the zone which contains all representative points. Any point outside the segment is equivalent to some point of the segment by the symmetry of the lattice. The solutions for the 001 and $01\bar{1}$ planes are indicated in 4*c* and 4*d*. Four of the five faces of the fundamental segment are of 001 or 011 type, and the fifth contains line IV which is a line of symmetry for this face. Hence the energy contours may be considered as well known on the surface of the segment. When this information is combined with that obtained for $|\kappa|\ll 1$ and the symmetry conditions required by reflection planes in the κ lattice, it should be possible to draw fairly accurate space contours in κ-space.[12]

An attempt to apply the methods used for the even functions of the $01\bar{1}$ plane to the even functions of the 001 plane has been made. It is found that there are more coefficients to be determined than can be evaluated from the known solutions of 100, 110, and line I. The remaining coefficients could be evaluated by partial expansion of the eighth-order determinant for the plane.

[12] Some space contours drawn according to this scheme have been published by the writer. Phys. Rev. **50**, 754 (1936).

Ferromagnetic Anisotropy in Nickel-Cobalt-Iron Crystals at Various Temperatures

L. W. McKeehan
Sloane Physics Laboratory, Yale University, New Haven, Connecticut

(Received November 19, 1936)

Single crystals of ternary alloys of nickel, cobalt and iron with forty percent nickel or more have been examined, with a pendulum magnetometer, for ferromagnetic anisotropy. All alloys in this region have face-centered cubic structures, like that of nickel. A region of low anisotropy, for nearly equal cobalt and iron contents, appears to be connected with the points where binary alloys of nickel and cobalt on one side and of nickel and iron on the other side change their anisotropy types. Measurements were made in all cases at room temperature, at about 200°C, and at about 400°C. At the higher temperatures anisotropy of either type generally diminishes and, in the region of low anisotropy, the principal anisotropy constant may change sign. The previously reported data for the binary alloys and single components in this system are recomputed and presented so as better to show the boundaries of the ternary field.

THE experimental work here reported may be considered as an extension of studies on binary alloys of nickel and cobalt[1] and of nickel and iron,[2] and is confined to the nickel-rich corner of the nickel-cobalt-iron triangular diagram. In this entire region there is only one solid-solution phase with the face-centered cubic structure characteristic of nickel at room temperature and of cobalt and iron at much higher temperatures. Whether or not there are any super-structures in this region has not yet been decided, and the results here presented do not seem to furnish evidence for or against their existence.

G. W. Elmen and G. A. Kelsall, of the Bell Telephone Laboratories, were kind enough to let me select eight ternary alloys from their extensive series.[3] The compositions, given in Table I, are also shown by the dots inside the boundary in Fig. 1. All were obtained as polycrystalline rods 0.32 cm in diameter. They were remelted under a low pressure of hydrogen and progressively frozen to give castings about 0.6 cm in diameter from which single crystals of suitable

TABLE I. *Description of specimens.*

Ni-Co-Fe, NOMINAL	80–10–10	70–20–10	65–15–20	60–30–10	60–25–15	50–40–10	50–25–25	40–10–50
CASTING NUMBER	950	1092	898	979	899	926	1006	941
WEIGHT PERCENT Ni	79.29	69.38	64.56	61.19	60.05	50.79	50.26	40.19
Co	10.21	20.20	14.84	28.38	24.79	38.66	25.04	10.21
Fe	10.27	9.85	20.52	10.43	15.12	10.41	24.63	49.51
Mn	0.46	0.42	0.33	0.19	0.32	0.31	0.27	0.32
DENSITY, G.CM^{-3}	8.796	8.793	8.633	8.748	8.703	8.741	8.574	8.309
SPHEROIDS ($01\bar{1}$)								
DIAMETER, 10^{-4} CM	3140	3103	3021	3013	2920	2810	3044	3168
THICKNESS, 10^{-4} CM	312	262	249	247	244	229	250	265
MASS, 10^{-3} G	14.4	11.6	10.4	10.5	9.68	8.58	10.5	11.45
VOLUME, 10^{-6} CM^{-3}	1637	1319	1205	1200	1112	982	1225	1378
DEMAGNETIZING FACTOR	0.860	0.740	0.720	0.738	0.739	0.720	0.739	0.730
ORIENTATION FACTORS								
[100] f_1 (0)*	0.0009	0.0077	0.0019	0.0116	0.0076	0.0191	0.0200	0.0016
f_2 (0)*	0	0	0	0	0	1	0	0
[011] d_1 (0.25)*	2496	2433	2509	2500	2500	2546	2573	2479
d_2 (0)*	1	18	5	5	0	45	42	2
[111] t_1 (0.3)*	3331	3247	3320	3277	3316	3196	3210	3308
t_2 (0.037)*	370	341	366	353	365	323	335	361

* Ideal values, for explanation see text.

[1] J. W. Shih, Phys. Rev. **50**, 376–379 (1936).
[2] J. D. Kleis, Phys. Rev. **50**, 1178 (1936).
[3] G. W. Elmen, Bell Sys. Tech. J. **15**, 113–135 (1936) gives references to earlier papers.

size were chosen for the preparation of oblate spheroids. The technique of this process, and the use of the pendulum magnetometer to find magnetization curves for important crystallographic directions lying in the equatorial plane of a spheroid, have been described in previous papers.[4] Table I gives the necessary information concerning the eight specimens used in measurements. Most of the entries are self-explanatory but the part of the table headed "Orientation Factors" requires some further remark.

Although efforts were made to cut each spheroid so that its equatorial plane should be the crystallographic plane $(01\bar{1})$, and to mark a diameter parallel to the crystallographic direction [100], neither operation was precisely accomplished. Careful x-ray inspection, after all magnetic measurements had been made, gave the actual indices of the directions, nominally [100], [011] and [111], in which measurements had been made. The work per unit volume necessary to magnetize a crystal to saturation in a direction with direction cosines α_1, α_2, α_3 referred to the three cubic axes of the crystal can be approximated by the equation[5]

$$W_a = K_0 + K_1(\alpha_2^2\alpha_3^2 + \alpha_3^2\alpha_1^2 + \alpha_1^2\alpha_2^2) + K_2(\alpha_1^2\alpha_2^2\alpha_3^2), \quad (1)$$

in which K_0, K_1 and K_2 are energy-density coefficients independent of direction. For small angles of departure from a fourfold (cubic) axis we may write this

$$W_{100} = K_0 + f_1K_1 + f_2K_2, \quad (2)$$

where f_1 and f_2 are the appropriate functions of the direction cosines. For ideal cutting $f_1 = 0$ and $f_2 = 0$. Similarly for a direction near a digonal axis,

$$W_{011} = K_0 + d_1K_1 + d_2K_2, \quad (3)$$

where the ideal values are $d_1 = 1/4$, $d_2 = 0$. Finally, near a trigonal axis,

$$W_{111} = K_0 = t_1K_1 + t_2K_2, \quad (4)$$

where the ideal values are $t_1 = 1/3$, $t_2 = 1/27$. The experimentally determined values of the six coefficients thus defined are given in Table I for each spheroid. It will be noticed that the deviations from the ideal values are not large in any case. Once the coefficients are determined the values of K_0, K_1 and K_2 can easily be found from the experimental values of W_{100}, W_{011} and W_{111} at any temperature.

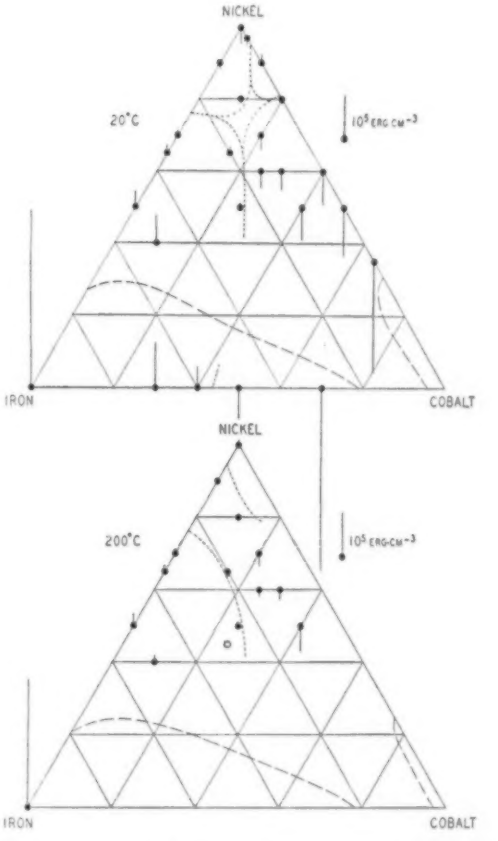

FIG. 1. The principal anisotropy constant (K_1) as a function of composition in nickel-cobalt-iron alloys at 20°C (upper figure) and at 200°C (lower figure). Lines up or down from a dot indicate positive or negative K_1 according to the scale at the right. Dashed lines show phase boundaries, dotted lines show changes in sign of K_1.

The procedure just described has been used in less extended form by Lichtenberger[6] and by Shih,[1] who thus obtained the values of K_1 (or rather of $K_1/2$) on the assumption that $K_2(\alpha_1^2\alpha_2^2\alpha_3^2)$ is negligible.

Magnetization curves were taken twice at

[4] L. W. McKeehan, Rev. Sci. Inst. **5**, 265–268 (1934); L. W. McKeehan, R. G. Piety, J. D. Kleis, Rev. Sci. Inst. **7**, 494 (1936); R. G. Piety, Phys. Rev. **50**, 1173 (1936).

[5] R. Gans, Physik. Zeits. **33**, 924–928 (1932); R. M. Bozorth, Phys. Rev. **50**, 1077 (1936).

[6] F. Lichtenberger, Ann. d. Physik [5] **15**, 45–71 (1932).

each of three different temperatures in all cases, and in two cases single runs were taken at a still higher temperature. About sixteen points were obtained for each separate curve. Most of the curves are so nearly similar in appearance that graphical presentation on any reasonable scale would not be especially interesting. Instead of this the areas between the curves and the magnetization axis (up to $I=I_{sat}$) have been carefully computed from faired curves drawn separately on a large scale (5 cm = 100 in I and in H) and these results are collected in Table II. Saturation was easily attained in all cases and the applied field was generally carried about 300 oersted higher than necessary for saturation. The differences $(W_{011}-W_{100})$ and $(W_{111}-W_{100})$ which are used in computing K_1 and K_2 are believed to be correct to about $\pm 0.02\times(10)^4$ erg·cm^{-3}. Inspection of the formulae used then shows that the corresponding uncertainty in K_1 is about $\pm 0.1\times(10)^4$, the uncertainty in K_2 not less than $\pm 1\times(10)^4$. The irregular variations of K_2 with rise in temperature suggests that these limits are actually exceeded in some cases. Tabular values are carried to one more decimal place than their precision warrants.

As regards K_0 the usual difficulty arises in estimating the demagnetizing factor, N, with the desired precision. It is encouraging to observe, however, that the same value of N, within a total range of about two percent, was obtained for each spheroid regardless of the direction chosen. A troublesome, though slight, variation of N with temperature, already noted by Kleis,[2] again appeared in these experiments, but there were now enough data to permit a decision as to its origin. There is little doubt that the apparent decrease in N as the temperature rises is due to a real decrease in the coercive force. Instead, therefore, of choosing N so that the whole magnetization curve up to $I=I_{sat}/2$ nearly coincides with the line $H=0$, we must choose N so that the part of the magnetization curve just below $I=I_{sat}/2$ is parallel to the line $H=0$. We then find this vertical part moving in toward the magnetization axis as the temperature rises, practically coinciding with it at temperatures just below the Curie point. The precision in measurement necessary to disclose this phenomenon in the present instance was rather high, for the maximum coercive force thus disclosed was always less than 10 and the applied magnetizing field at half saturation was 300 or more. There is, accordingly, some variation in the apparent coercive force for different directions. Part of this may be systematic rather than accidental, but the precision of the data is hardly high enough to permit a decision. It may be mentioned that Sixtus[7] has reported higher coercive forces for directions of easier magnetization in silicon-iron crystals. No such correlation could be established in the present work.

TABLE II. *Results on ternary alloys.*

Ni-Co-Fe	Temp. °C	I_{sat}	Energy Densities, erg. cm$^{-3}\times(10)^4$					
			W_{100}	W_{011}	W_{111}	K_0	K_1	K_2
80–10–10	22	768	1.03	0.98	0.82	1.03	−0.20	−3.9
	200	710	0.65	0.60	0.51	0.65	−0.20	−2.0
	400	560	0.16	0.12	0.13	0.16	−0.16	0.6
	516	359	0.14	0.06	0.11	0.14	−0.32	2.1
70–20–10	22	872	2.32	1.64	1.46	2.34	−2.90	1.7
	200	822	1.69	1.11	1.13	1.71	−2.52	7.0
	398	701	0.74	0.42	0.40	0.75	−1.38	2.9
	598	407	0.12	0.12	0.10	0.12	0.00	−0.6
65–15–20	22	1005	1.29	1.51	1.18	1.29	0.91	−11.2
	201	936	1.01	0.99	0.92	1.01	−0.08	−1.8
	398	808	0.30	0.22	0.20	0.30	−0.32	0.2
60–30–10	22	974	3.29	2.38	1.80	3.33	−3.80	−8.2
	203	926	2.03	1.61	1.30	2.05	−1.75	−5.0
	397	834	1.23	0.95	0.73	1.24	−1.17	−3.7
60–25–15	22	1027	2.25	1.61	1.52	2.27	−2.64	3.4
	201	971	1.55	1.30	1.05	1.56	−1.03	−4.5
	398	857	0.85	0.77	0.69	0.85	−0.33	−1.5
50–40–10	22	1044	3.72	2.02	1.54	3.86	−7.21	−0.4
	205	993	2.94	1.68	1.44	3.04	−5.43	4.1
	398	902	1.51	1.26	0.92	1.53	−0.87	−10.2
50–25–25	22	1152	0.91	1.00	1.07	0.90	0.35	1.6
	205	1083	0.60	0.69	0.72	0.59	0.38	0.2
	398	973	0.34	0.29	0.34	0.34	−0.25	2.2
40–10–50	22	1325	1.30	2.80	2.72	1.29	6.10	−16.4
	200	1143	0.78	1.24	1.41	0.78	1.87	0.4
	398	682	0.36	0.54	0.39	0.36	0.74	−5.9

Fig. 1 shows how the principal anisotropy constant, K_1, measured at room temperature, 20°C, varies over the range of compositions now available for comparison. This includes the ternary alloys here studied as well as the binary alloys of the same crystal structure dealt with by Shih[1] and Kleis.[2] The values for iron[4] and for iron-cobalt alloys[8] have been added for the sake of completeness. The crystal structure in this corner of the diagram is body-centered cubic. The cobalt corner has hexagonal structure. The boundaries of these regions, which are not well established, have been sketched in to agree with a diagram given by Kühlewein.[9] All points have

[7] K. J. Sixtuś, Phys. Rev. **50**, 395 (1936).
[8] J. W. Shih, Phys. Rev. **46**, 139–142 (1934).
[9] H. Kühlewein, Wiss. Veröffentl. a.d. Siemens-Konzern **11** [1], 124–140 (1932).

TABLE III. *Components and binary alloys. Computations from previous data.*

Ni-Co-Fe, nominal	20°C		200°C		
	K_1	K_2	K_1	K_2	NOTE
100–00–00	− 3.44	5.3	0.50	2.0	(a)
97–03–00	− 1.00	0.9			(b)
90–10–00	1.57	− 3.8			(b)
90–00–10	− 0.70	− 2.3	−0.20	−1.0	(c)
80–20–00	− 0.35	0.8			(b)
70–00–30	0.68	− 1.7	0.15	−0.4	(c)
65–00–35	1.47	− 7.0	1.22	−4.2	(c)
60–40–00	− 7.39	3.7			(b)
50–50–00	−10.80	− 4.0			(b)
50–00–50	3.33	−18.1	2.52	−8.3	(c)
35–65–00	−25.83	15.5			(b)
00–70–30	−43.30	5.3			(d)
00–50–50	− 6.80	−38.7			(d)
00–40–60	4.54	−11.1			(d)
00–30–70	10.21	16.2			(d)
00–00–100	42.1	15	30.0	22	(e)

Notes. (*a*) Honda, Masumoto and Shirakawa.[10] From original curves. Variations of K_1 and K_2 over a wide range in temperature have been considered. (*b*) Shih.[1] From original curves and tabulated values of $W_{111}-W_{100}$. (*c*) Kleis.[2] Values at 200°C interpolated between values given for 150°C and 300°C. (*d*) Shih.[8] From tables of $W_{111}-W_{100}$ and $W_{011}-W_{100}$. (*e*) Piety.[4] Values at 200°C interpolated between values given for 18°C and 296°C.

been plotted at their intended compositions. The sign and magnitude of K_1 are indicated by the direction and length of the vertical line drawn from each dot. The data for nickel have been recomputed from the curves given by Honda, Masumoto and Shirakawa.[10] The plotted values for boundary points are given in Table III and have all been corrected for errors in cutting where these are known. The extension of the lines for $K_1=0$ into the ternary field are made in a manner consistent with the measured values, but there are too few points to make the location of these transitions very precise. In particular it cannot be decided whether the region of positive K_1 is separated into two parts by an isthmus of negative K_1, or *vice versa*. The evidence is regarded as favoring the first of these alternatives. It should be noticed that the ternary alloys contained an appreciable amount of manganese, the binary alloys did not.

Fig. 1 also shows the values of K_1 at or near 200°C. It will be noticed that the lines $K_1=0$ pass over only one of the selected compositions as the temperature rises from 20° to 200°C. At 400°C the left-hand transition line has moved still more toward the left but the absolute magnitude of K_1 has fallen at all points. It is probably significant that the best perminvars lie in the region in which the anisotropy becomes very small at or above 400°C. (An open circle in the figure shows a preferred composition.) Elmen[3] has shown that the best of these alloys are greatly altered by baking at 450°C. The crystalline anisotropy must be so low at this temperature that magnetostrictive strains should largely control the directions in which domains can remain saturated.[11] Local short-circuiting of magnetic flux should be especially easy in these alloys at such temperatures.

It is suggestive that the sign of K_1 seems to depend more upon proximity to pure iron or pure cobalt than upon the particular cubic structure of a ternary or binary alloy. One is tempted to connect the lines $K_1=0$ across the phase boundary in Fig. 1.

The values of K_2 given in Tables II and III show no such regularity as the values of K_1 and in view of the low precision with which K_2 has generally been measured it seems premature to discuss its variations. It should however be noted that the maximum possible values of (l_1-f_1) and (l_2-f_2) are, respectively, 1/3 and 1/27 so that the absolute values of K_2 may be much larger than those of K_1 without having nearly as much effect upon magnetic anisotropy.

In conclusion I wish to express my particular indebtedness to J. D. Kleis who postponed his own affairs to complete the necessary measurements, which he had undertaken as my research assistant. I am also obliged to J. W. Shih who sent me his paper on nickel-cobalt alloys[1] prior to its publication and thus led me to undertake this special study of the nickel-rich alloys of the ternary system.

[10] K. Honda, H. Masumoto, Y. Shirakawa, Sci. Rep. Tohoku Imp. Univ. [1] **24**, 391–410 (1935).

[11] R. M. Bozorth, J. F. Dillinger, Physics **6**, 285–291 (1935).

LETTERS TO THE EDITOR

Prompt publication of brief reports of important discoveries in physics may be secured by addressing them to this department. Closing dates for this department are, for the first issue of the month, the eighteenth of the preceding month; for the second issue, the third of the month. The Board of Editors does not hold itself responsible for the opinions expressed by the correspondents.

Communications should not in general exceed 600 words in length

Emission of Neutrons from Chlorine and Argon Under Alpha-Particle Bombardment

In some recent experiments in this laboratory[1] it was established that A^{40} does not emit protons when bombarded by Th C′ alpha-particles. It seemed likely that if the emission of protons is energetically not favored, the emission of neutrons might, for the same reasons, be favorable. Accordingly we set up an ionization chamber filled with boron trifluoride,[2] surrounded by paraffin and connected to a linear amplifier as a neutron detector. We placed a Th C′ source (average strength 1.5 mc) at the center of a flask which could be evacuated or filled with argon and found that on admitting argon the counts rose from 2 per minute to 20 per minute, corresponding to 18 per minute due to argon. This is to be compared with roughly 6 per minute from nitrogen under the same circumstances, so that the yield of neutrons is considerable.

A rough excitation curve showed that the neutrons were emitted for alpha-particle ranges greater than 5.6 ± 0.5 cm, the yield becoming proportional to the thickness of argon traversed at 6.9 ± 0.5 cm. These figures mean that Ra C′ alpha-particles should have sufficient energy to cause the reaction to take place. We therefore mixed 50 mc radon with argon and attempted to observe hydrogen recoils in a hydrogen-filled proportional counter. We found that the number of counts rose from 20 per hour to 60 per hour when the argon plus radon was brought near. Only deflections well above the gamma-ray background were recorded. No recoils were observed from a paraffin layer when 6.5 cm absorption had to be traversed although a very small yield could not have been detected. The great majority of the neutrons, however, must have energies between 0 and 1.5 Mev.

A similar experiment with chlorine gave an increase of five per minute per millicurie with the BF_3 detector. The kicks began when the alpha-particle range exceeded 5.3 ± 0.5 cm, the yield becoming proportional to thickness at 7.2 ± 0.5 cm.

We suggest that the following reactions take place.

$$A^{40}+He^4\rightarrow Ca^{43}+n^1,$$
$$Cl^{37}+He^4\rightarrow K^{40}+n^1.$$

The excitation curves suggest that unless a series of closely spaced resonance levels are present the nuclear radii of Cl^{37} and A^{40} are 6.1×10^{-13} cm and 7.3×10^{-13} cm. Both values should be regarded as provisional, but it is interesting to note that the value for A^{40} agrees with Bethe's revised radius for the radioactive elements[3] while that for Cl^{37} is rather low. It is also possible to deduce from the excitation curves that the mass of Ca^{43} and K^{40} (the radioactive isotope of potassium) cannot exceed 42.9768 and 39.9788, with Aston's value for the mass of A^{40} and Bainbridge's value for Cl^{37}.

We wish to express our thanks to Professor A. F. Kovarik for his interest and encouragement.

ERNEST POLLARD
H. L. SCHULTZ
GORDON BRUBAKER

Sloane Physics Laboratory,
Yale University,
New Haven, Connecticut,
December 30, 1936.

[1] E. Pollard and C. J. Brasefield, Phys. Rev. **51**, 8 (1937).
[2] Obtainable in tanks from the Harshaw Chemical Company, New York City.
[3] H. Bethe, Phys. Rev. **50**, 977 (1936).

The Scattering of Electrons by Atomic Nuclei

The failure of a recent experiment[1] to confirm the prediction made by Mott[2] from the Dirac equations of an asymmetry in the intensity of an electron beam twice scattered by atomic nuclei increases the interest in the experimental tests of the equation for single scattering derived by Mott in the same calculation. In most such experiments little attempt has been made to exclude from the scattered beam as measured those electrons (ignored in the theory) which lose energy in being scattered.

We describe an experiment in which scattered electrons were counted only if they retained nearly all their initial energy. Electrons from a filament at about 1600 volts below ground potential were accelerated into a steel chamber where they were scattered by a thin gold foil. The chamber was at high potential throughout except for the region inside a smaller movable chamber, which received scattered electrons through a double diaphragm. The movable chamber contained the collecting electrode behind a grid at ground potential. Between the double diaphragm and this grid the scattered beam was thus strongly retarded and no electron which lost as much as 1600 ev is being scattered could reach the collecting electrode. As observation proved, the retarding field gave an additional advantage by eliminating electrons scattered by other parts than the foil, and all kinds of secondary electrons. This freedom from background made it possible to measure the intensity of scattering over the small angular aperture of 0.00194 rad^2 even at large angles of scattering.

The potential employed in the following observations was 80 kv. The thickness of the gold foil was 5.94×10^{-6} cm, as reckoned from its transparency to sodium light and confirmed by weighing. Scattering was observed only at oblique incidence, the electrons passing through the foil. The angle of scattering was 90°. Under these conditions

Wentzel's criterion for single scattering was roughly approximated.

The ratio of scattered to incident intensity, for the effective thickness of the foil at 45° incidence, *viz.*, 8.40 $\times 10^{-6}$ cm, was 8.92×10^{-6}. Our probable error is believed to be 15 percent.

Our observed scattering is 0.97 of that predicted by Mott, thus differing from that of other observers who, without such rigorous exclusion of retarded electrons, have observed a considerably greater ratio.

We are grateful to Dr. F. E. Myers and Dr. J. F. Byrne for the accelerating equipment and for other assistance, to Dr. O. Halpern for helpful discussion, and to Mr. A. C. Weid for assistance in taking observations.

R. T. Cox
C. T. Chase

New York University,
University Heights,
New York, New York,
December 30, 1936.

[1] E. G. Dymond, Proc. Roy. Soc. **A145**, 657 (1934).
[2] N. F. Mott, Proc. Roy. Soc. **A135**, 429 (1932).

An Explanation of the Relative Stabilities of Isotopes of the Lighter Elements

As is well known[1] the mass and charge of any isotope of the lighter elements may be expressed, in the case of atoms of even atomic number, as n alpha-particles plus zero, one, two or three neutrons; and for atoms of odd atomic number, as n alpha-particles plus H_1^1, H_1^2, H_1^3 or H_1^4. For any given element the existence or nonexistence of all four of these possible isotopes has always been a puzzling problem. The following approximate calculations will show that the solution is surprisingly simple and that it is possible to state with certainty which isotopes are stable.

To make these calculations the experimental energy relations, in terms of atomic weights,[2] between the neutron and the hydrogen isotopes will be used. The assumption will be made that the energies of H_1^1, H_1^2 and H_1^3 remain approximately constant when these groups exist in combination with alpha-particles in heavier nuclei and the problem will be to determine the effect of the nuclear charge upon the transition of hydrogen into neutrons or helium by the emission of positrons or electrons. As an approximation for the coulombic field energy, or field mass, of each nucleus, the classical expression[3] $M_F = \frac{3}{5}Z^2/R$ will be used, where Z is the atomic number and R the nuclear radius. For the latter the best experimental determinations agree well with the equation of Dunning[4] $R = 1.315 \times 10^{-13} \sqrt[3]{\text{at. wt.}}$ If we know Z and R the value of M_F may be calculated for each nucleus and ΔM_F for nuclear reactions. The emission of e^+ reduces M_F and thus ΔM_F is negative for such a process while the emission of e^- increases M_F and ΔM_F is correspondingly positive. The following calculations may now be made:

Type $n\alpha + n_0^1$ *and* $n\alpha + H_1^1$. For the reaction $H_1^1 = n_0^1 + e^+$, the total change in mass, ΔM, is 0.002 mass unit. For the reaction $Li_3^5 = He_2^5 + e^+$, $\Delta M_F = -0.002$ but for $B_5^9 = Be_4^9 + e^+$, $\Delta M_F = -0.003$ and ΔM_F becomes more negative for higher atomic numbers. The decrease in coulombic energy is then sufficient to cause positron emission from all nuclei of the $n\alpha + H_1^1$ type, with the possible exception of Li_3^5. Hence B^9, $N^{13} \cdots K^{37}$ should not exist but all isotopes of the type Be^9, C^{13}, O^{17} should be stable.

Type $n\alpha + 2n_0^1$ *and* $n\alpha + H_1^2$. For the reaction $H_1^2 = 2n_0^1 + e^+$, ΔM is 0.0045. For the reaction $N_7^{14} = C_6^{14} + e^+$, $\Delta M_F = -0.004$ and for the reaction $F_9^{18} = O_8^{18} + e^+$, $\Delta M_F = -0.005$. Hence N^{14} and similar nuclei of lower odd atomic numbers should be stable, i.e., Li^6 and B^{10} but He^6 and Be^{10} should be unstable. Likewise $F^{18} Na^{22} \cdots K^{38}$ are unstable and $O^{18} Ne^{22} \cdots A^{38}$ are stable.

Type $n\alpha + 3n_0^1$ *and* $n\alpha + H_1^3$. For the reaction $H_1^3 = 3n_0^1 + e^+$, ΔM is 0.010. For the reaction $K_{19}^{39} = A_{18}^{39} + e^+$, ΔM_F is -0.008. Hence the coulombic energy is not sufficient to cause e^+ emission and K^{39} and all lighter isotopes of this type, i.e., Li^7, $B^{11} \cdots K^{39}$ are stable and Be^{11}, $C^{15} \cdots A^{39}$ unstable. Also, for the reaction $H_1^3 = He_2^3 + e^-$, $\Delta M = 0.000$ and since the ΔM_F for e^- emission is always positive, isotopes of the type $n\alpha + He_2^3$ should not exist, i.e., Be^7, C^{11}, $O^{15} \cdots$ are unstable.

Type $n\alpha + 4n_0^1$ *and* $n\alpha + H_1^4$. For the reaction, $4n_0^1 = He_2^4 + 2e^-$, $\Delta M = -0.032$. This energy is so large that the coulombic energy is not sufficient for the lighter elements to prevent electron emission from the $n\alpha + 4n_0^1$ type, and no isotopes differing by 4 mass units should exist. For the reaction $H_1^4 = He_2^4 + e^-$, the energy is not known, but it is obviously very highly negative, probably about -0.015 and all elements of the $n\alpha + H_1^4$ type, i.e., Li^8, B^{12}, N^{16}, etc. will undergo β decomposition.

A summary of the predictions for these various types gives a complete picture of the isotopes of the elements of low atomic numbers. Fortunately the energies are large enough so that the approximate calculations of the coulombic terms give the correct qualitative answer. For heavier elements the composition cannot be simply expressed in terms of α-particles. The first exception is Cl^{37}, which might be represented at eight alphas plus a hydrogen five or as nine alphas plus a negative proton and for heavier elements the structures become increasingly complex. In the author's theory this may be interpreted as the conversion of a zinc sulfide type of α-particle lattice to a diamond lattice of neutrons with the positive charge on the surface particles, and even approximate calculations of the energies can only be made for a few very simple structures.

Wendell M. Latimer

Department of Chemistry,
University of California,
Berkeley, California,
December 18, 1936.

[1] Harkins, Chem. Rev. **5**, 371 (1928).
[2] Oliphant, Nature **137**, 396 (1936).
[3] See also Latimer and Libby, J. Chem. Phys. **1**, 133 (1933), and Latimer, J. Am. Chem. Soc. **58**, 1061 (1936).
[4] Dunning, Phys. Rev. **45**, 587 (1934).

Erratum: Investigations of the Deuteron-Deuteron Reaction

R. Ladenburg and R. B. Roberts,
Palmer Physical Laboratory, Princeton, N. J.
(Phys. Rev. **50**, 1190, 1936)

The last lines of Section 4 should read: "Oliphant, Harteck and Rutherford estimate the yield to be of the order of magnitude of 1 in 10^6 at 100 kv."

Proceedings of the American Physical Society

Minutes of the Pasadena Meeting, December 18 and 19, 1936

THE 210th regular meeting of the American Physical Society was held in room 201 of the Norman Bridge Laboratory of the California Institute of Technology, Pasadena, California, December 18 and 19, 1936. The meeting consisted of four sessions, each from two to three hours in length. Three sessions were devoted to the presentation of the thirty-four papers abstracted below, while the morning session of December 19 was utilized for a symposium on the 200-inch telescope with the following invited papers:

1. **The Evaporation Process and its Application to Optical Surfaces.** John Strong, *California Institute of Technology.*

2. **Some Problems Connected with the 200-inch Telescope.** John A. Anderson, *California Institute of Technology.*

Attendance at these sessions ranged from 50 to 75 persons.

On December 18 a luncheon was tendered to visiting members of the American Physical Society by the Institute. At a business meeting held during the morning session of December 18 it was voted to approve the holding of a regular meeting of the American Physical Society in June, 1937, at Denver, Colorado, in affiliation with the meeting of the American Association for the Advancement of Science.

Paul Kirkpatrick,
Local Secretary for the Pacific Coast

Abstracts

1. A Method for Sealing β-Magnesia Windows Into Steel Spectroscopic Absorption Furnaces and a Needle Valve for Controlling the Evacuation of Such Furnaces. R. T. Brice, *California Institute of Technology.*—The resistance of β-magnesia to etching by hot metallic vapors has been utilized to construct a spectroscopic absorption furnace in which the absorption chamber is in thermal equilibrium. A seal is made by grinding and polishing the edge of a $\frac{1}{2}''$ diameter by $\frac{1}{4}''$ thick β-magnesia window to a 1° taper and forcing it into a similar taper in a soft aluminum or copper rod. The soft metal rod is then turned down to 0.020″ wall thickness, using the same taper, leaving a window tightly fitted into a protective collar. A smooth inside-taper is cut in a thick-walled, hollow steel bolt and the encased window forced into this taper. The result is a β-magnesia window tightly sealed in a heavy steel casing which can be easily sealed into an absorption furnace with aluminum, copper or nickel gaskets. Windows mounted with aluminum were tested at 435°C without leaking and a window mounted with copper was tested at 587°C. To control evacuation of the furnace, a stainless-steel valve has been built which seals an opening in the wall of the furnace, does not produce a cold spot, and can be manipulated from outside the furnace. It has worked satisfactorily over a period of eight months. The upper limit of temperature for use of the β-magnesia seals and stainless-steel valve has not been determined.

2. Recording Apparatus for the Measurement of Integrated Intensities of X-Ray Reflections. O. B. Jackson and A. Goetz, *California Institute of Technology.*—The apparatus is used as an integral part of a Bragg-spectrometer with stationary ionization chamber. It is designed especially for simultaneous measurements of $\int J d\vartheta$ and $J_{\max}$ at low temperatures. In principle the device consists of a mechanical coordination of the movement of a narrow slit in front of the ionization chamber with the movement of a photographic plate upon which the deflections of a galvanometer are recorded. The galvanometer indicates by means of a d.c. amplifier the current in the ionization chamber. The difference between this method and the usual method of determining the integrated intensity consists in keeping crystal and x-ray tube stationary and moving the slit of the ionization chamber. The resolving power is thus increased considerably whereas the records obtained for different orders are not directly commensurable due to the mosaicness of the crystal. By means of an empirically determined factor the comparison can be made possible. The integration is performed by weighing cut-out prints of the records on photographic paper.

3. Further Studies of the C. T. R. Wilson Condensation on Charged Carriers Using Various Liquids. Leonard B. Loeb, A. F. Kip, A. W. Einarsson, *University of California.*—Previous investigations reported at the Washington meeting June 19, 1936, have been extended to the substances detailed below. Aside from the addition of three new substances showing preference for the negative ion, the studies of mixtures brought out the following facts. While pure acetic acid has positive preference and water has negative preference the mixtures of any large proportion of either showed no sign preference as might be expected. The limit for condensation on ions was lowered below the value for either constituent as had been observed elsewhere in the case of alcohol and water. This should follow from vapor pressure laws. HCl and

water mixtures show no deviation from pure water at all concentrations. This shows that uncharged molecules of HCl vapor do not form nuclei of condensation. These experiments revealed the formation of the stable uncharged nuclei so often found, to be due to droplets of HCl and water vapor that had condensed about ions or uncharged particles by a previous expansion, and that had not evaporated completely, but had lost their charge.

No sign preference

	Condensation Ratio Charged $E_{\pm}$	Uncharged E_0
Acetone $(CH_3)_2CO$	1.88	2.06
Acetic Acid $+H_2O$	1.24	1.33

Negative Ion Preference

	E_-	E_+	E_0
Aniline $C_6H_5NH_2$	1.44	1.48	—
Chlorobenzene C_6H_5Cl	1.53	1.60	1.80
Toluene $C_6H_5CH_3$	1.60	1.69	1.73
H_2O+HCl	1.27	>1.3	1.37

4. Electron and Negative Ion Mobilities in Oxygen, Air, Nitrous Oxide, and Ammonia. Russell A. Nielsen and Norris E. Bradbury, *Stanford University*.—The electrical shutter method for measuring electron mobilities in gases has been extended to include experiments in oxygen, air, nitrous oxide, and ammonia. The experimental data support the hypothesis that collisions of low energy electrons with molecules of these gases may be inelastic. Such collisions cause excitation of vibrational levels, electronic levels, or dissociation of the molecule. The results are compared with experiments reported elsewhere on negative ion formation in these gases. In general the onset of negative ion formation is accompanied by inelastic collisions which result in a marked increase in the electron drift velocity.

Negative ion mobilities in these gases have been measured in the same apparatus by an adaptation of the Rutherford alternating current method. The ions were formed by electron attachment in an auxiliary field and their mobility determined at various ages. The probable character of the ions is discussed after comparing the experimental results with those predicted by the Langevin theory.

5. A New Radioactive Isotope of Fluorine. Arthur H. Snell, *Radiation Laboratory, University of California (Introduced by Ernest O. Lawrence)*.—When neon gas is bombarded with 5 MV deuterons, an active product is formed which emits positive electrons and decays with a period of 112±4 minutes. This active substance behaves chemically like fluorine, and since it is neither of the two known radiofluorines, F^{17} and F^{20}, it must be F^{18}. The reaction describing its formation is then

$$_{10}Ne^{20}+{}_1H^2 \qquad {}_9F^{18}+{}_2He^4$$

and in decaying it goes to stable O^{18}. Absorption measurements of the positrons indicate that they have a maximum energy of about 500 kv.

6. The Energy and Absorption of the Gamma-Radiation from Lithium Bombarded by Protons. L. A. Delsasso, W. A. Fowler, C. C. Lauritsen, *California Institute of Technology*.—Further cloud chamber studies of pairs and single particles ejected from a thin Pb scatterer by the gamma-radiation from Li^7+H^1 have confirmed the existence of a strong line at approximately 17 Mev. There is some indication of a line at approximately 14 Mev, the intensity of which is not more than 25 percent of the total radiation.

Collimation of the beam has reduced markedly the number of single positrons and low energy electrons apparently originating in the scatterer, without materially changing the number of pairs. The distribution in energy of the Compton electrons is in fair agreement with the predictions of the Klein-Nishina theory.

In order to measure the absorption coefficient of the radiation, the cloud chamber photographs were taken with a 1.0 cm Pb absorber placed alternately in and out of the beam incident upon the scatterer. The total number of pairs observed decreased from 328 with no absorber to 194 with the absorber in the beam, whereas the number of pairs above 15 Mev decreased from 233 to 122. The total absorption coefficient in Pb of the unmodified radiation producing pairs above 15 Mev is thus $\mu=0.66\pm0.09$ cm^{-1}. The theoretical Klein-Nishina absorption coefficient for 17.5 Mev radiation is $\sigma=0.09$ cm^{-1} while the Oppenheimer-Bethe-Heitler absorption coefficient is $\pi=0.64$ cm^{-1}, the total absorption thus being $\mu=0.73$ cm^{-1}, a value with which the observed coefficient is in agreement.

7. The Radioactivity Induced in Calcium under Deuteron Bombardment. Harold Walke,* *Radiation Laboratory, University of California (Introduced by Ernest O. Lawrence)*.—Calcite crystals have been bombarded in the Berkeley cyclotron with 5.5 million volt deuterons and have been rendered strongly radioactive. Several decay periods have been observed, chemical analyses indicating that most of the activity is due to scandium isotopes. The decay of the weak calcium activity shows evidence of only a single period with a half life of 2.3±0.3 hours, whereas the scandium shows periods of 53±3 minutes 4.0±0.1 hours and 52±2 hours. The results of Zyw[1] and of Hevesy[2] suggest that the half lives of Sc^{42} and Sc^{46} are 3 hours and greater than a year, respectively. It is thus possible that the isotopes observed are Sc^{41}, Sc^{43} and Sc^{44} produced by reactions of the type:

$$Ca^N+H^2 \qquad Sc^{N+1}+n^1.$$

The 4-hour period is probably due to Sc^{43} for this half life agrees with the value given by Frisch,[3] namely "4.4 hours with a possible error of 10 percent."

Using the strong source available, an attempt has been made to induce radioactivity in calcium by neutron bombardment. Weak activities, probably due to impurities, have been detected, though the results are not consistent. No evidence of the 4-hour period observed by Hevesy and Levi[4] has yet been obtained.

* Commonwealth Fund Fellow.
[1] Zyw, Nature **134**, 64 (1934).
[2] Hevesy, Nature **135**, 1051 (1935).
[3] Frisch, Nature **136**, 220 (1935).
[4] Hevesy and Levi, Nature **135**, 580 (1935).

8. Are There Metastable Molecules in the Lewis-Rayleigh Glow? Joseph Kaplan, *University of California at Los Angeles*.—During the preparation of nitrogen tubes for the emission of the auroral afterglow, observations

were made which give an answer to the above question. When the nitrogen is being purified by repeated flashing of the tube, a stage is reached, at which the tube shows the Lewis-Rayleigh glow, which is the one characterized by members of the first-positive group only. On further purification, this glow is replaced by the auroral afterglow, the spectrum of which contains the first-positive, second-positive, Vegard-Kaplan and first-negative systems. When pure oxygen is added to this tube, the afterglow is increased in intensity, but the spectrum retains its auroral characteristics, although changes occur in the relative intensities of the bands. It appears that once a tube shows the auroral glow, the addition of pure oxygen does not produce the L–R glow. These, and other results, indicate that no relation exists between these two glows. The absence of the Vegard-Kaplan and the Goldstein-Kaplan bands from the L–R glow is further indication that there are no metastable molecules in this glow. This contradicts the hypothesis presented sometime ago by Cario and the present author.

9. The Thirty Kilowatt Continuous-Rating X-Ray Outfit of the Watters Memorial Research Laboratory at the California Institute of Technology. J. PAUL YOUTZ AND JESSE W. M. DUMOND, *California Institute of Technology.*—Reporting steady operation of DuMond gyrating target x-ray tube at 105 m.a., 287,000 volts continuous current. Output $\frac{3}{4}$ kw of x-rays. Water-cooled gyrating target facilitates focal spot cooling. Tantalum cathode filament (40 mil diam. 30 amp. 5 v) provides stiffness and long life. Gold covered copper targets used. $\frac{1}{4}''$ target-filament gap shielded against field distortion and stray or secondary electrons. Filament current supplied by storage batteries kept charged by two d.c. (automobile) generators, the latter insulated from ground for 500 kv and driven by 72" rubber V-belts. Adequate lead shielding built into the x-ray tube throughout so that the usual lead house is unnecessary. Filament current control remote regulated by horizontal, fixed length, variable section, mercury rheostat. Water circulating in rubber hose used as part of all principal circuit connections to stabilize against surges. Indicating equipment for operation includes DuMond-Knudsen vacuum gauge. Neon lamp by-pass protects against surges through milliammeter. Obstruction charcoal traps directly heated for baking-out, by imbedded heater, assist in clearing system of vapors slow to pump by oil diffusion pumps. Standard voltage doubling power circuit using four banks 150 kv, 1/12 mfd, condensers and two 300 kv kenotrons with 80 mil, 100 amp., 1 kw filaments, baked out before operation by 5000 v a.c. direct to plate. 125-cycle synchronous motor driven alternator supply. Operation comparable with 10 m.a., 50,000 v sets. Steady and quiet, reliable, very compact, occupies 6 m×6 m ×3.2 m.

10. The Coefficient of Recombination of Pure Oxygen as a Function of Pressure and Temperature. M. E. GARDNER, *University of California (Introduced by Leonard B. Loeb).*—A re-determination of the coefficient of recombination, α, for the electron free gas oxygen was made by using a glass chamber which was thoroughly outgassed prior to the introduction of carefully purified oxygen. The value of α was found to be a constant independent of age from 10^{-2} seconds on to 1 second for pure oxygen at constant pressure and temperature. The value of α obtained at atmospheric pressure and room temperature was $(2.0\pm0.1)10^{-6}$. The value of α as a function of the pressure of the gas was found to be in fairly good agreement with the theoretical values of J. J. Thomson for pressures of 10 cm to one atmosphere. The variation of α with temperature was not in such good agreement with the theoretical values as the pressure variations. The deviations from the theoretical values can be partially explained in terms of the experimental difficulties involved.

11. Relations Between the Self-Consistent Field and Bohr's Nuclear Model. W. M. ELSASSER, *California Institute of Technology.*—In Bohr's semiclassical model the nucleus is equivalent to a degenerate gas and it is shown that any excitation energy will in the most probable case be divided among a large number of particles. Starting from a self-consistent Hartree-Fock model as used for instance by Bethe in computing the term density, we can express the quantum equivalent of this picture as follows. The spectral density of terms being very great, their energetic spacing will be much smaller than their mutual interaction under a perturbation which corresponds to the difference between the selfconsistent and the true Hamiltonian. Treating a great number of terms as degenerate together, the new wave functions will be linear combinations of a large number of Hartree-Fock functions. For the lowest terms however the spacing is quite considerable and therefore the original features of a self-consistent field, in particular the formation of "closed shells," will not get entirely lost under the perturbation. This agrees with the well-known empirical behavior of nuclear binding energies. The author has previously shown that these variations are empirically stronger for even than for odd nuclei. This is in full agreement with the above considerations, if allowance is made for forces between like particles.

12. The Refractive Index of Air in the Infrared. DAVID BENDER, *California Institute of Technology.*—There is some disagreement among the experiments on the refractive index of air in the infrared. The results of Perard (1924) are about 0.2 percent higher than those of the Bureau of Standards (1918). More recent results have agreed more closely with Perard than with the Bureau, and have tended to be even higher. The present measurements, though unfinished, also lie above Perard's values, being on the average 0.4 percent higher than those of the Bureau. The measurements are being made on dry CO_2-free air with a Fabry-Perot interferometer having a separation of 14 or 21 millimeters. Neon lines have been used exclusively and wave-lengths out to 8853A have been observed up to the present time. The total fringe shift ranges from 8 to 15 fringes and the error in the order of interference is about 0.005 fringe. Thus the error in the index from this source

is about 0.05 percent. The pressure and temperature measurements are accurate to within 0.08 percent. Although the spread in the individual index measurements covers nearly 0.3 percent, the inaccuracy of the final curve will be considerably less than 0.1 percent.

13. A Method of Removing the Errors of Tooth Spacing to Produce High Precision Worm Gear Wheels by Lapping. DOUGLAS MARLOW AND JESSE W. M. DUMOND, *California Institute of Technology.*—We describe a rapid and cheap method of reducing and distributing the initial errors of tooth spacing in a worm gear wheel by constructing it in two halves with half the width of each tooth in each half. The wheel is lapped with emery using a dummy worm, the two halves of the wheel being shifted relative to each other according to a certain schedule between stages of lapping. We show that the proper angular intervals for such shiftings should be integer powers of $\frac{1}{2}$ a revolution. The method has been tried on the construction of two highly precise worm gear wheels for a two crystal x-ray spectrometer. By precise optical tests we have determined that on the better of these two wheels making abstraction of the slight eccentricity the greatest deviation of teeth (cumulative error) from the mean position was of the order one ten thousandth of an inch. A further application of the method could doubtless have still improved this.

14. Table of Observable Interstellar Lines. R. M. LANGER, *California Institute of Technology.*—Recent advances in technique which have made possible brighter spectra in the ultraviolet regions have led Mt. Wilson astronomers to look for new absorption lines due to atoms in interstellar space. Calculations by the writer of the intensity and spectral distribution of interstellar light together with published tables of term values of atoms and ions permit the determination of all observable lines which can be expected from the interstellar gas. An exhaustive table of this material is being prepared. Approximate relative intensities can be expressed in terms of relative abundances. Absolute abundances can be determined only when the electron concentration is known. This depends mainly on the relative abundance of hydrogen. The relative abundance according to the present theory of the two elements which have long been known, namely sodium and calcium, is about 30 to 1. This figure is about ten times the apparent relative abundance in the sun. The discovery of any new lines will most likely show whether this discrepancy is real.

15. Precision Determination of h/e from the Short Wave-Length Limit of the Continuous X-Ray Spectrum. VERNON L. BOLLMAN AND JESSE W. M. DUMOND, *California Institute of Technology.*—Two precision determinations of the short wave-length limit of the continuous x-ray spectrum have been made in the regions of 10,000 and 20,000 volts, respectively, by the method of isochromats under very steady applied voltage using the two crystal spectrometer as monochromator. The reference lines for setting the monochromator were Mo $K\beta_2$ and W $L\beta_1$. A thin window tube with a nickel target coated with tungsten by evaporation was used. Very careful attention has been given to all corrections.

On the assumption that the ruled grating x-ray wavelengths are correct (Mo $K\beta_2 = 0.6211 \times 10^{-8}$ cm, W $L\beta_1 = 1.2818 \times 10^{-8}$ cm) we get $h/e = 1.3767 \times 10^{-17}$. Making no such assumption but inserting the value of the x-ray wavelengths as a function of e from the data on crystal density, the Faraday constant and x-ray diffraction and solving for e we get $e/h^{3/4} = 2.0715 \times 10^{10}$. The results on this experiment agree with those of previous experimenters much better than they agree with other methods of determining functions of e and h and the present experiment confirms and emphasizes the puzzling discrepancy in these physical constants already emphasized by Birge. It seems well nigh impossible to blame the present experiment for this discrepancy. By elimination we are led to suspect the correctness of accepted values of the Faraday constant.

16. Carrier Mobility Spectra in the Electrification by Spraying and Bubbling of Liquids. SEVILLE CHAPMAN, *University of California* (*Introduced by Leonard B. Loeb*).—Data previously reported on the mobility spectrum of spray electrified salt solutions investigated with an Erickson mobility tube under conditions of high resolving power have been extended to a larger number of substances. Results for these are similar to those previously obtained. Data on the electrification of distilled water by bubbling show that there are carriers of both signs produced although the negative predominate in the ratio of 2.5 to one. Bubbling gives somewhat more sharply defined groups of carriers than spraying, the groups for bubbling occurring at mobilities 1.5 cm/sec. per volt/cm and 0.23 for the negative, and 0.9 and 0.4 for the positive. Preliminary work on the spraying of nonaqueous liquids shows that for benzene there is no electrification. Water free absolute alcohol shows pronounced groups of mobilities at 1.0 and 0.4, the electrification in this case being about 12 times that for distilled water. Nitrobenzene, aniline, and glacial acetic acid do not show pronounced groups, the spectra being more or less continuous, although few carriers of mobility greater than 0.5 were found. For these substances the total amount of electrification is respectively the same as, and six times that for distilled water.

17. On the Continuous β-Ray Spectrum of P^{32}. W. E. LAMB, JR., *University of California* (*Introduced by J. R. Oppenheimer*).—The results of Lyman on the form of the continuous β-ray spectrum of P^{32} are not in agreement with the Konopinski-Uhlenbeck plots. Some improvement in the fit may be obtained if one uses the K. U. ansatz, but applies it to find the distribution for the 3rd Sargent curve, which is probably the correct one for P^{32}, although the discrepancy is still beyond experimental error. One can, however, obtain an almost perfect agreement with experiment by an ansatz for the coupling which depends only on first derivatives of the neutrino wave functions. For this, one may take for the coupling term in the Lagrangian, a sum of two scalars, one of which may be written as the product of heavy and light particle six vectors, and the other as product of one pair of the corresponding pseudovectors.

18. The Radioactive Isotope of Potassium. W. R. SMYTHE AND A. HEMMENDINGER, *California Institute of Technology*.—Using the high intensity mass spectrometer described by Smythe, Rumbaugh, and West,[1] we have separated samples of the three isotopes of potassium, K^{39}, K^{40}, and K^{41}. The radioactivity of the collector bearing the isotopic sample can be compared with that of a dummy collector by swinging them alternately in front of a thin aluminum walled Geiger-Müller counter mounted inside the apparatus and admitting the proper amount of air for counting. The background of the counter is extremely steady at one count per minute. Two complete sets of samples were tested. One sample of K^{40}, probably considerably less than the 20.4/8300 mg estimated from the uncorrected collecting current, doubled the original activity of the collector, whereas the samples of K^{39} and K^{40} showed only the activity to be expected from the known amount of K^{40} present, which was 7 percent of the natural abundance. Comparison with counts made on weighed samples of potassium chloride indicates that K^{40} is responsible certainly for the low energy beta-particles and very probably for those of high energy also.

[1] Smythe, Rumbaugh and West, Phys. Rev. **45**, 724 (1934).

19. Optical Absorption of Fused Germanium Dioxide from 0.185μ to 8.5μ. R. WILLIAM SHAW, *Cornell University*.—Studies by Laubengayer[1] have shown that the values of refractivity and dispersion of fused germanium dioxide in the visible spectrum are both considerably higher than for silicon dioxide in the same chemical family. The ultraviolet transmission, unlike that of quartz, is zero from 0.315μ to 0.185μ for a sample 2 mm thick. Immersion in liquid nitrogen moves the transmission limit 160 angstroms toward shorter wave-lengths. No appreciable absorptions appear from 0.315μ to 2.86μ. At the latter point a characteristic absorption is observed. Between 2.86μ and 4.5μ the transmission is again normal except for a shallow (5 percent) but narrow band at 4.24μ which seems to have an analogue at 2.26μ. From 4.5μ the transmission decreases rapidly to zero at 6.15μ with a characteristic inflexion in the curve at 5.40μ. From 6.15μ to 8.5μ the 2 mm sample is opaque. Fused germanium dioxide exhibits then a uniform transmission from the near ultraviolet to 4.5μ except for one sharp absorption at 2.86μ. This absorption is very nearly symmetrical and might conceivably be suitable for calibration purposes in the near infrared. The Raman spectrum of germanium dioxide, excited by the Hg line λ3650, is a single band. The frequency interval between the band center and the parent line corresponds to the wave-length 2.88μ. Details will be published in the near future.

[1] A. W. Laubengayer, J. Phys. Chem. **30**, 1510 (1926).

20. The Band Spectra of BiF, BiCl, SbF, and SbCl. GEORGE D. ROCHESTER,* *University of California*.—Three new systems of bands, degraded to shorter wave-lengths and forming a triplet system with wide multiplet separations (7300 cm^{-1} and 4800 cm^{-1}), have been found in the spectrum of BiF at 3050–3250A, 2650–2850A, and 2250–2350A. Photographs taken with small dispersion indicate that the ω values for the ground and excited states are approximately 520 cm^{-1} and 620 cm^{-1}. No new band systems have been found in BiCl. The spectrum of SbF has been observed from λ2000–λ5500 and found to have groups of bands in the regions 3600–5200A, 2600–2700A and 2200–2430A. An analysis of the first group shows that 61 out of 69 bands can be placed into two systems with almost the same values of ω_e' and ω_e''; the wave numbers of the bandheads are given by the formulae:

$$\nu_1 = 21887.5 + 411.3(v'+\tfrac{1}{2}) - 1.71(v'+\tfrac{1}{2})^2 - 616.9(v''+\tfrac{1}{2}) + 2.89(v''+\tfrac{1}{2})^2,$$

$$\nu_2 = 23992.5 + 420.0(v'+\tfrac{1}{2}) - 1.75(v'+\tfrac{1}{2})^2 - 612.6(v''+\tfrac{1}{2}) + 2.58(v''+\tfrac{1}{2})^2.$$

The group at 2600–2700A consists of a few isolated bands degraded to shorter wave-lengths and that at 2200–2430A of bands grouped in sequences and also degraded to shorter wave-lengths. A preliminary analysis of this group indicates that most of the bands fit into two systems for which $\omega_e' \sim 700$ cm^{-1}, $\omega_e'' \sim 620$ cm^{-1}, and $\Delta\nu_{12} \sim 1900$ cm^{-1}. A new system has been found in the spectrum of SbCl in the region 4000–5500A.

* Commonwealth Fund Fellow.

21. Analysis of the Linear Amplifier.* H. TATEL, *Stanford University*.—An attempt has been made to improve the empirical linear amplifier used with a Wynn-Williams ionization chamber to detect α-particles. This investigation has been divided into two parts. First the signal to noise ratio was determined analytically by resolving the pulse into a Fourier integrand and multiplying it by an amplifier function $(\omega^n/\omega_0)e^{-n\omega}$ where ω is the circular frequency. Upon integration, the output voltage was compared to the random noise voltage generated in the input stage as given by Johnson† and using the amplifier function above. Neglecting shot noise, $n=2$ and $\alpha=0.577T$ (T is the collection time). The r.m.s. of the signal to noise ratio is

$$\overline{\rho^2}(p^2)^{\frac{1}{2}} = 4.46\times 10^{10} N(R/T)^{\frac{1}{2}}$$

(N is the number of ions collected, R is the input resistance).

The second part of the investigation has been aimed at reducing natural α-particle background. This was achieved by designing the chamber so that any surface at which a detectable α-particle could originate could easily be removed and rinsed in concentrated nitric acid. Experience has shown that this procedure keeps the background consistently below 5 α-particles per 100 cm^2 of brass per hour.

* A large part of this was done at the Massachusetts Institute of Technology.

† J. B. Johnson, Phys. Rev. **32**, 97 (1928).

22. Positive Ion Mobilities in H_2 by the Townsend Deflection Method. ALLEN V. HERSHEY, *University of California* (*Introduced by Leonard B. Loeb*).—The mobility of positive ions at low pressure and at high X/p is being studied as a function of field strength by means of the Townsend deflection method. From preliminary measurements with ions presumably K^+ having a molecular weight of 39, the mobility constant in H_2 was found to be 13.5 at $p=0.7$ and at $X/p=5$ (p = pressure in mm, X = field

strength in volts/cm), in excellent agreement with values obtained by Powell and Brata.[1] At the same pressure and at $X/p=50$ the mobility constant was 30 percent greater.

[1] Powell and Brata, Proc. Roy. Soc. **A138**, 117 (1930).

23. Method for the Production of Metal Single Crystals Between 20μ and 0.2μ. J. RINEHART AND A. GOETZ, *California Institute of Technology.*—In order to measure the dependence of electromagnetic properties of metal crystals upon their size, it is necessary to avoid plastic deformation during the production of the crystal. As the methods used in general for the production of fine single-crystalline powders consisted of the application of mechanical methods such as grinding, etc., a new method was developed by which the metal is sprayed while liquid by the application of a high pressure gas (100–150 atm.) at a temperature above the melting point of the metal. The resulting metal dust crystallizes while hovering in an oil fog. The particles are then separated by sedimentation and centrifuging in order to obtain suspensions of crystals of equal size which are then oriented crystallographically parallel after the method of Goetz and Faessler.

24. The Modified Scattered Spectrum of Characteristic Molybdenum *K* Radiation at Large Scattering Angle with Helium Gas as the Scattering Substance Using a Curved Quartz Crystal Spectrograph. HARRY A. KIRKPATRICK AND JESSE W. M. DUMOND, *Occidental College and California Institute of Technology.*—After an exposure of over two thousand hours with a curved quartz crystal spectrograph and a scattering chamber one meter long with celluloid window containing helium gas under 200 lbs./in.^{2} pressure, we have obtained what we believe to be the first actual spectrum of Compton shifted radiation ever made with a gaseous scatterer. This permits a comparison of the observed breadth and structure of the modified line with the absolute predictions of DuMond's theory for an atom of sufficient simplicity to permit the electron momentum distribution to be computed and this without the uncertainties introduced by the perturbing effects of neighbors (always present in previous work with solid scatterers). A fairly precise measurement of shift is also obtained in which the Ross and Kirkpatrick shift defect is minimized by the choice of He as scatterer. Preliminary measurements support the theoretical expectations.

25. The Effect of Mercury Vapor on the Townsend Coefficient, α, in Pure Nitrogen. WOODFORD E. BOWLS, *University of California* (*Introduced by Leonard B. Loeb*).—In conjunction with an investigation of the apparent effect of cathode material on β, the second Townsend coefficient of ionization by collision, in nitrogen, the values of α, the coefficient of ionization by electrons, have been evaluated. The measurements have been carried out in a carefully baked out, mercury free, chamber. The values of α/p have been determined in a range of X/p from 215 to 1000. (p is the pressure in millimeters of mercury and X, the field strength in volts per centimeter.) The values of α/p obtained were approximately 80 percent of the values obtained by Townsend. Since the original ionization chamber of Townsend contained mercury, it was thought advisable to ascertain whether the presence of mercury could account for the difference in the values of α/p. When mercury was admitted to the chamber, values of α/p approximately 96 percent of the Townsend values were obtained. Outgassing up to 375° centigrade for twenty-four hours did not suffice to restore the low values completely. Removal of the mercury by dismantling of the chamber and chemically treating all the parts nearly restored the low values.

26. Intensities of X-Ray Reflections from Bi Crystals Between 25° and 530° Abs. ALEXANDER GOETZ AND ROBERT B. JACOBS, *California Institute of Technology.*—The temperature variations of the integrated intensities of reflections of Mo $K\alpha$ radiation from Bi crystals on (111) are measured over a range near the boiling point of hydrogen to the melting point by means of the modified Bragg method using the second, third, and fifth order. The temperature functions of the relative values of the intensities (J_T/J_N) were checked with the Debye-Waller relation. By an approximation method the characteristic temperatures of Bi were calculated without (θ) and with (θ^*) consideration of the zero point energy. The values thus obtained are $\theta=92.5°$ and $\theta^*=95.9°$. The latter value is in very close agreement with θ-values determined from specific heat measurements. The measurements support the assumption of the zero point energy.

No indication of a discontinuity of the intensity was found in the regions of pseudo-allotropic transformations.

A deviation from the Debye-Waller relation is noticeable for higher temperatures, especially in a range 50°–80° before the melting point in the direction of an absolute increase of the Debye factor. This increase is reversible if the crystal is kept in thermal equilibrium, shows, however, a hysteresis if this is not the case. This phenomenon can be interpreted as being due to a temperature dependence of the secondary extinction.

27. The Thermal Expansion of the Bi Lattice Between 25° and 530° Abs. ROBERT B. JACOBS AND ALEXANDER GOETZ, *California Institute of Technology.*—The thermal expansion of the lattice of Bi crystals between the boiling point of hydrogen and within 7° of the melting point of the crystal is measured by means of a modified Bragg method along [111] for the 2nd, 3rd and 5th order. The thermal expansion coefficient thus obtained (α_{11}) varies from 8.3×10^{-6} to 17.4×10^{-6} for the temperature range $\theta\geq T$. Beyond 120° α_{11} stays unchanged until the melting point. Only the range between −15°C and +75°C forms an exception where the expansion coefficient drops to 13.8×10^{-6}. This seems to indicate the existence of a separate "phase" not characterized by a change of the lattice configuration and confirms certain previous findings of discontinuities at 75° (Peltier effect, diamagnetic susceptibility, chemical affinity, dilatometric expansion). In qualitative agreement with findings by Goetz and Hergenrother and in disagreement with the measurements of Jay, a definite divergence between the lattice and the integral expansion beginning 30° before the melting point was found. The Grüneisen rule ($\alpha_{11}/c_v=$const.) is found to hold in first approximation for the whole temperature range, except the very lowest temperatures.

28. The Fine Structure of Hα and Dα. WILLIAM V. HOUSTON, *California Institute of Technology.*—By means of the method of analysis described at the Seattle meeting of the Physical Society[1] the interferometer patterns of Hα and Dα have been studied with changes in the conditions of excitation and with different separations of the interferometer plates. The analysis has involved the assumption of four components located at approximately the positions given by the theory for the four strongest components of this pattern. The best fit is obtained when the separation of the two strongest components is about 2 percent less than the theoretical value. The intensity of the third strongest component is always considerably greater than its theoretical value, even at pressures as high as one millimeter. In no case does there seem to be any difference between Hα and Dα except the difference in width due to the temperature motion.

[1] Phys. Rev. **50**, 292 (1936).

29. A New Band of Atmospheric Oxygen. HAROLD D. BABCOCK, *Mount Wilson Observatory.*—With the discovery and measurement of the 1,1 band of ordinary oxygen[1] an accurate determination of the vibrational energy of the normal molecule became possible. This permits the computation of positions of lines in bands, theoretically existent but not previously observed, which arise from the same lower state as the 1,1 band but involve other vibrational levels of the upper state. The band 1,2, having the same upper level as the α band near λ6276, is predicted accurately from the observational data. About twenty lines belonging to it have been measured, λλ6955–6996, with air-paths of about 100 km. The identity of the new band is established by the close agreement between computed and observed positions and by the character of the lines themselves. Known spacings of various energy levels in the molecule are shown by the new band within a few hundredths of a wave number. An improved value of the vibrational constant from 1,1 and 1,2 and full details of these and other bands are being prepared for publication. The strongest lines of 1,2 resemble the sixteenth and seventeenth *P* doublets of the *B* band in intensity.

[1] Babcock, Phys. Rev. **35**, 125 (1930).

30. The Magnetic Scattering of Slow Neutrons. L. JACKSON LASLETT, *University of California (Introduced by E. O. Lawrence).*—To determine whether the large cross sections for the scattering of slow neutrons by iron and nickel[1] arise in part from the ferromagnetic nature of these materials, a comparison of the back scattering at room temperature and above the Curie point was made. In conformity with the methods of earlier workers a thin silver piece was used as a detector of the incident and reflected neutrons, for it was found that with such a detector two thirds of the activity arose from *C*-group neutrons and that the difference in scattering between nickel and copper could be detected easily.

Because no significant change could be found in the scattering by iron and nickel as these elements were raised above their Curie temperatures, it is concluded that the largeness of their scattering cross sections is not of magnetic origin. In view of a calculation by Bloch[2] of the magnetic scattering to be expected in a ferromagnetic substance, however, this result does not preclude the neutron possessing a magnetic moment equal in order of magnitude to a nuclear magneton.

[1] A. C. G. Mitchell, E. J. Murphy and M. D. Whitaker, Phys. Rev. **50**, 133 (1936), and B. Pontecorvo and G. C. Wick, La Ricerca Scientif. II **1**, 134 and 220 (1936).
[2] Bloch, Phys. Rev. **50**, 259 (1936).

31. Fundamental Properties of Light From Distant Nebulae. F. ZWICKY, *California Institute of Technology, Pasadena.*—In order to arrive at a rational explanation of cosmological phenomena, such as the redshift of light from distant nebulae, it is necessary to establish a reference system of physical measurements on a cosmological scale. For this purpose a number of dimensionless ratios between fundamental physical quantities and their dependence on time and location must be investigated. The simplest inquiry of this kind refers to the properties of propagation, diffraction, refraction and absorption of terrestrial light and "nebular" light respectively. Some data are already available on the aberration of light from distant nebulae as well as on the properties of this light when tested with prisms, gratings and suitable absorbing media. From these data we may conclude that the quantities c, hc and h are the same within about five percent for terrestrial light and nebular light respectively. The more fundamental problem of the dependence of a number of dimensionless ratios on the "history" of the universe is still under investigation.

32. Polarization of the Solar Corona. WILLI M. COHN, *Berkeley, California.*—The polarization of the corona was determined from photographic plates taken during the total solar eclipses of 1932 and 1934.[1] The observations were favored by perfectly clear skies. Polarigraphs of 34- and 60-inch focal lengths were used, the quartz Wollaston prisms arranged in front of the objectives. Color screens of narrow transmission ranges were used for obtaining the polarization as a function of the wave-length. Intensity squares were printed on each corona plate right after the eclipses. The plates were measured by means of the Hartmann microphotometer of the Lick Observatory and the Zeiss microphotometer of the Physics Department, University of California. Polarization data are presented for wave-lengths 420, 447, 482, 668 mμ. The results show polarization values increasing, as a rule, from the limb of the sun towards the outer corona. The curves in the violet and green pass through a maximum, then decrease again. The curves for great wave-lengths are considerably steeper than those for small wave-lengths, indicating that electron scattering, alone, cannot be responsible for the light emitted from the corona.

[1] W. M. Cohn, Publ. Astron. Soc. Pacific **46**, 177–185 (1934).

33. The Removal of the Ion Beam of the Cyclotron from the Magnet Field. LUIS W. ALVAREZ, EDWIN MCMILLAN AND ARTHUR H. SNELL, *University of California (Introduced by Ernest O. Lawrence).*—Many obvious advantages can

be obtained if the ion beam produced by the cyclotron is carried to some distance from its source, away from the magnetic field and the background of general radiation due to stray ions striking the inside of the apparatus. The first step in this direction was accomplished when the beam was made to emerge from the wall of the tank.[1] The chief difficulty in bringing it farther arises from the fact that the inhomogeneous field at the edge of the magnet poles causes the beam to diverge very badly. Exploratory experiments showed that, at a distance of 40 cm from the point of emergence, the beam was spread into a horizontal ribbon 10 cm wide, and continued to diverge at greater distances. A partial refocussing has now been accomplished by applying an additional inhomogeneous field, provided by pieces of iron bolted to the magnet poles. The focussed beam of 6 MV deuterons emerges at the end of a six-foot tube, well away from the cyclotron. Twenty-seven percent of the total current arrives at this point, mostly within a focal spot 3×3 cm in area. The beam is nearly parallel, and can be led much farther without much divergence. The rest of the current is not focused by the present field, but can easily be saved by more careful design.

[1] Donald Cooksey and Ernest O. Lawrence, Phys. Rev. **49**, 866(A) (1936).

34. Positive Needle Point Corona Studies at Atmospheric Pressure. LEONARD B. LOEB AND W. LEIGH, *University of California.*—A study of asserted changes in shape and loss of material of positively charged needle points in sustained corona appearing in the literature reveals no real loss of material by sputtering but changes produced by oxidation in air, and the collection of dust etc. was observed in N_2 and in air. No uniform or systematic change in weight could be detected in as much as 1920 microampere hours at 20,000 volts. The fact that positive point corona discharge maintains itself and shows luminosity not only where fields incapable of producing ionization by positive ions, but even where fields incapable of causing electrons to ionize exist, has long required explanation. Studies reveal the corona to consist of many minute but finite transient streamers randomly propagated at great speed from the point and indicating by the blue spark spectrum high field gradients. These are superposed on the general background of arc spectrum. The corona can be explained as consisting of a random emission of minute leader strokes discharges such as observed in lightning probably induced by intense ionization avalanches started by single electrons approaching the point. Cravath and Loeb have given the theory of propagation of such strokes. The arc line glow is emission produced in the space between streamers by the subsequent discharges equalizing the potential gradients caused by space charges left by the extinguished preceding leader strokes.

35. An Anomalous Lightning Discharge. E. J. WORKMAN AND R. E. HOLZER, *University of New Mexico.*—In the execution of a lightning research program initiated by J. W. Beams, L. B. Snoddy and the authors, a photograph of lightning similar in appearance to that photographed by R. J. Spickerman and reported by C. G. Abbot[1] was obtained. The flash occurred near Santa Fe, New Mexico, and was recorded on the films of three rotating cameras. The drums of two of the cameras rotated about a vertical axis and that of the third about a horizontal axis. The analysis of the films, using the horizontal and vertical time sweeps, indicates that the velocity in space is approximately 5×10^8 cm/sec. This velocity is of the order of magnitude of the velocity obtained by Schonland for dart leader strokes.

Assuming a probable distance of four miles, the length of the visible portion of the stroke exceeds sixteen miles with the greatest spread exceeding three miles.

[1] Smithsonian Miscellaneous Collections, Vol. 92, No. 12.

AUTHOR INDEX TO ABSTRACTS OF THE PASADENA MEETING

Alvarez, Luis W., Edwin McMillan and Arthur H. Snell—No. 33

Babcock, Harold—No. 29
Bender, David—No. 12
Bollman, Vernon L. and Jesse W. M. DuMond—No. 15
Bowle, Woodford, E.—No. 25
Bradbury, Norris E.—see Nielsen
Brice, R. T.—No. 1

Chapman, Seville—No. 16
Cohn, Willi M.—No. 32

Delsasso, L. A., W. A. Fowler and C. C. Lauritsen—No. 6
DuMond, Jesse W. M.—see Bollman
——— see Kirkpatrick
——— see Marlow
——— see Youtz

Einarsson, A. W.—see Loeb
Elsasser, W. M.—No. 11

Fowler, W. A.—see Delsasso

Gardner, M. E.—No. 10
Goetz, A.—see Jackson
——— see Jacobs
——— see Rinehart

Hemmendinger, A.—see Smythe
Hershey, Allen V.—No. 22
Holzer, R. E.—see Workman
Houston, William V.—No. 28

Jackson, O. B. and A. Goetz—No. 2
Jacobs, Robert B. and Alexander Goetz—No. 27

Kaplan, Joseph—No. 8
Kip, A. F.—see Loeb
Kirkpatrick, Harry A. and Jesse W. M. DuMond—No. 24

Lamb, W. W., Jr.—No. 17
Langer, R. M.—No. 14
Laslett, L. Jackson—No. 30
Lauritsen, C. C.—see Delsasso
Leigh, W.—see Loeb
Loeb, Leonard B., A. F. Kip and A. W. Einarsson—No. 3
——— **and W. Leigh**—No. 34

Marlow, Douglas and Jesse W. M. DuMond—No. 13
McMillan, Edwin—see Alvarez

Nielsen, Russell A. and Norris E. Bradbury—No. 4

Rinehart, J. and A. Goetz—No. 23
Rochester, George D.—No. 20

Shaw, R. William—No. 19
Smythe, W. R. and A. Hemmendinger—No. 18
Snell, Arthur—see Alvarez
——— No. 5

Tatel, H.—No. 21

Walke, Harold—No. 7
Workman, E. J. and R. E. Holzer—No. 35

Youtz, J. Paul and Jesse W. M. DuMond—No. 9

Zwicky, F.—No. 31